NPS 67-81-015

(2)

NAVAL POSTGRADUATE SCHOOL
Monterey, California

THESIS

AIRBORNE LASER TURRET FLOW CONTROL:
A PARAMETRIC STUDY
OF WIND TUNNEL MODEL CONDITIONS

by

David Allen Rippel

December, 1981

Thesis Advisor: A. E. Fuhs

Approved for public release; distribution unlimited

Prepared for: Captain Richard deJonckheere, USAF
Air Force Weapons Laboratory
AFWL/ARLB
Kirtland AFB
Albuquerque, New Mexico 87117

DISCLAIMER NOTICE

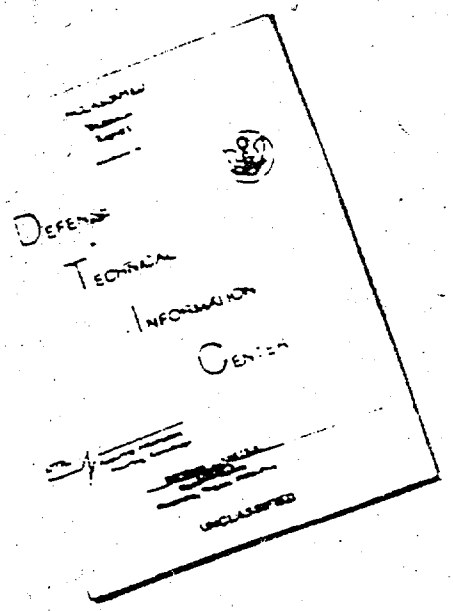

THIS DOCUMENT IS BEST QUALITY AVAILABLE. THE COPY FURNISHED TO DTIC CONTAINED A SIGNIFICANT NUMBER OF PAGES WHICH DO NOT REPRODUCE LEGIBLY.

NAVAL POSTGRADUATE SCHOOL
Monterey, California

Rear Admiral J. J. Ekelund
Superintendent

David Schrady
Acting Provost

This thesis prepared in conjunction with research supported in part by the Air Force Weapons Laboratory.

Released as a
Technical Report by:

William M. Tolles

W. M. Tolles
Dean of Research

UNCLASSIFIED

SECURITY CLASSIFICATION OF THIS PAGE (When Data Entered)

REPORT DOCUMENTATION PAGE		READ INSTRUCTIONS BEFORE COMPLETING FORM
1. REPORT NUMBER NPS 67-81-015	2. GOVT ACCESSION NO. AD-A113 557	3. RECIPIENT'S CATALOG NUMBER
4. TITLE (and Subtitle) Airborne Laser Turret Flow Control: A Parametric Study of Wind Tunnel Model Conditions		5. TYPE OF REPORT & PERIOD COVERED Master's Thesis; December 1981 6. PERFORMING ORG. REPORT NUMBER
7. AUTHOR(s) David Allen Rippel		8. CONTRACT OR GRANT NUMBER(s)
9. PERFORMING ORGANIZATION NAME AND ADDRESS Naval Postgraduate School Monterey, California 93940		10. PROGRAM ELEMENT, PROJECT, TASK AREA & WORK UNIT NUMBERS MIPR 81-MP-071
11. CONTROLLING OFFICE NAME AND ADDRESS Naval Postgraduate School Monterey, California 93940		12. REPORT DATE December 1981 13. NUMBER OF PAGES 141
14. MONITORING AGENCY NAME & ADDRESS(if different from Controlling Office) Air Force Weapons Laboratory AFWL/ARLB Kirtland AFB Albuquerque, New Mexico 87177		15. SECURITY CLASS. (of this report) UNCLASSIFIED 15a. DECLASSIFICATION/DOWNGRADING SCHEDULE

16. DISTRIBUTION STATEMENT (of this Report)

Approved for public release; distribution unlimited

17. DISTRIBUTION STATEMENT (of the abstract entered in Block 20, if different from Report)

18. SUPPLEMENTARY NOTES

19. KEY WORDS (Continue on reverse side if necessary and identify by block number)

AIRFLOW CONTROL
LASER
LASER PROPAGATION
LASER JITTER
LASER TURRET

20. ABSTRACT (Continue on reverse side if necessary and identify by block number)

Wind tunnel tests were conducted on a one-third scale model of the USAF NKC-135 airborne laser turret and aerodynamic fairing. The model was constructed so that six main parameters could be varied as follows: fairing nosepieces, fuselage bleed slot position and condition (porous/non-porous), suction duct throttle position, blower suction throttle position, and the turret-fairing gap. The method of flow control employed to produce quiescent air

DD FORM 1 JAN 73 1473 EDITION OF 1 NOV 65 IS OBSOLETE
S/N 0102-014-6601

UNCLASSIFIED
SECURITY CLASSIFICATION OF THIS PAGE (When Data Entered)

flow about the turret was that of fuselage boundary layer and after-body fairing suction.

Results of the extensive testing indicate that the method is viable for low velocity, incompressible air flow. Additionally, optimum conditions (i.e. minimum suction required and the best combination of other parameters necessary to provide quiescent flow) were determined.

Approved for public release; distribution unlimited

Airborne Laser Turret Flow Control: A Parametric Study of Wind Tunnel Model Conditions

by

David Allen Rippel
Lieutenant Commander, United States Navy
B.A., University of Cincinnati, 1969

Submitted in partial fulfillment of the requirements for the degree of

MASTER OF SCIENCE IN AERONAUTICAL ENGINEERING

from the

NAVAL POSTGRADUATE SCHOOL
December 1981

Author: David A. Rippel

Approved by: Allen E. Fuhs
Thesis Advisor

M. F. Platzer
Chairman, Department of Aeronautics

William M. Tolles
Dean of Science and Engineering

ABSTRACT

Wind tunnel tests were conducted on a one-third scale model of the USAF NKC-135 airborne laser turret and aerodynamic fairing. The model was constructed so that six main parameters could be varied as follows: fairing nosepieces, fuselage bleed slot position and condition (porous/non-porous), suction duct throttle position, blower suction throttle position, and the turret-fairing gap. The method of flow control employed to produce quiescent air flow about the turret was that of fuselage boundary layer and after-body fairing suction.

Results of the extensive testing indicate that the method is viable for low velocity, incompressible air flow. Additionally, optimum conditions (i.e. minimum suction required and the best combination of other parameters necessary to provide quiescent flow) were determined.

COMMENT CONCERNING JOINT RESEARCH

This thesis and Boundary Layer Control of a High Energy Laser Turret Using Suction of Trapped Vortices, a thesis by LT James A. Burd [Ref. 1], were the result of a joint research project begun at the Naval Postgraduate School by LT James Schonberger and LT Alan Mandigo. The flow control concept, experimental apparatus, and the instrumentation were common to both theses. This thesis involves extensive testing of fairing nosepieces designed by Schonberger and Mandigo while Ref. 1 involves the design and testing of a nosepiece based on the trapped vortex concept.

TABLE OF CONTENTS

LIST OF FIGURES

LIST OF TABLES

LIST OF SYMBOLS

A	Aft
C	Closed throttle position
C_p	Pressure coefficient
CPD	Cylindrical pressure distribution
C-SPD	Cylindrical-spherical pressure distribution
CYL	Cylindrical
CYL-SPH	Cylindrical-spherical
F	Forward
FBS	Fuselage bleed slot
$\dot{m}$	Mass flow rate
MAX	Maximum
MIN	Minimum
NP	Non-porous
O	Open throttle position
P	Porous; Static pressure
P_∞	Freestream static pressure
q	Dynamic pressure
S	Side
SPH	Spherical
SPD	Spherical pressure distribution
T-F	Turret-to-fairing
TSN	Tapered symmetric nosepiece
UCN	Uniform conformal nosepiece

V_∞	Freestream velocity
X	Suction duct voltage
Y	Suction duct velocity
θ	Position angle about the laser turret in horizontal plane
ρ	Density
ϕ	Position angle on sphere of laser turret in vertical plane

ACKNOWLEDGMENTS

I would like to express my appreciation to Dr. Allen E. Fuhs, Distinguished Professor of Aeronautics, and to Mr. Ted Dunton, Aerospace Engineering Technician. Dr. Fuhs provided the necessary theoretical expertise and Mr. Dunton offered invaluable guidance on the technical operation of the wind tunnels and data acquisition systems. Without the welcomed advice of both gentlemen this project could not have been completed.

I. INTRODUCTION

A. BACKGROUND

A high energy laser destroys targets by concentrating large amounts of radiant thermal energy onto a small area. Any distortion or jitter of the optical beam tends to smear the beam footprint on the target, thus resulting in a lower power to area ratio and decreasing the likelihood of target destruction. Beam distortion can result when the laser beam propagates through air with varying density caused by turbulence. Beam jitter can be caused by the unsteady aerodynamic effects on the laser test platform.

The test bed aircraft for the airborne gas dynamic high energy laser (HEL) is operating from the Air Force Weapons Laboratory, Kirtland Air Force Base, New Mexico. Experiments are being conducted using two NKC-135 aircraft (one containing a carbon dioxide HEL with external turret-fairing and the other containing extensive data collection instruments).

Testing of a one-third scale turret-fairing model was started at the Naval Postgraduate School (NPS) in 1980. Using fuselage boundary layer suction and suction applied through the fairing behind the turret, flow control was established around the HEL turret. Two fairing nosepieces were designed and preliminary testing conducted by

Schonberger [Ref. 2] and Mandigo [Ref. 3]. Results of these tests indicate that attached quiescent flow can exist to a turret azimuth angle of at least 150°. This larger rearward angle is favorable in that the coverage of the airborne laser turret pointer tracker is enhanced.

B. THEORETICAL FLOW

The airborne laser turret is essentially a hemisphere mounted on top of a finite cylinder (Fig. 1). Schlichting [Ref. 4], among others, gives the theoretical surface pressure distribution as follows:

$$\text{Cylinder:} \quad C_p = \frac{P - P_\infty}{q} = 1 - 4 \sin^2 \theta \tag{1}$$

$$\text{Sphere:} \quad C_p = \frac{P - P_\infty}{q} = 1 - \frac{9}{4} \sin^2 \theta \tag{2}$$

where $q = \frac{\rho V_\infty^2}{2}$ or free-stream dynamic pressure, P_∞ is free-stream static pressure, P is static pressure at a specific station, and θ is the angular location of the specific station referenced to $\theta = 0^{\circ}$ or forward (Fig. 2). These distributions are presented graphically (Fig. 3, 4 and 5). Notice that from the forward stagnation point $\theta = 0^{\circ}$, to $\theta = 90^{\circ}$, the pressure decreases, indicating attached laminar flow. However, from $\theta = 90^{\circ}$ to $\theta = 180^{\circ}$, or the rear stagnation point, the pressure increases, indicating an adverse pressure gradient. This results in flow separation,

which consists of shed vortices and recirculation over both the sphere and the cylinder. Such turbulent flow, with associated density variation, severely affects laser beam propagation in addition to causing turret vibration problems.

Equations (1) and (2) deal with two dimensional flow. For the flow around the turret, a pressure distribution somewhere between that of a sphere and a cylinder can be expected. This is due to the three dimensional effects of sphere-cylinder interaction.

Thus, any method of flow control that permits a neutral or decreasing pressure gradient between $\theta = 90^{o}$ and $\theta = 180^{o}$ is desirable. Furthermore, a favorable pressure gradient that extends further aft permits larger aft look-back angles for the laser beam. This would be an important consideration for tactical applications.

C. FLOW CONTROL METHODS

Various methods to control the turbulence around aircraft turrets have been proposed and include: porous standpipe, slot blowing, trapped vortices [Ref. 1], and base suction. The method selected for testing involves suction applied at both the turret base and through an aerodynamic fairing mounted aft of the turret [Ref. 2 and 3]. Quiescent flow can then be obtained around the turret by applying suction. This method is advantageous in that no modifications to the turret are required and aircraft

structural modifications are minimized. However, the fairing limits laser look-back angle.

D. THESIS OBJECTIVE

Table 1 lists the variables associated with flow control about the laser turret and their ranges. Clearly, the number of possible combinations of setting could number in the thousands and would prove to be an insurmountable data collection and interpretation task. However, it would be expected that by logical selection, trends can be established that would eliminate the majority of these cases.

The goal of this thesis is to determine the minimum amount of suction required to achieve quiescent flow around the turret. The parameter settings with this minimum suction will be considered optimum conditions for the system.

II. EXPERIMENTAL APPARATUS

A. PHYSICAL COMPONENTS

The major experimental components were a one-third scale turret and aerodynamic fairing (Fig. 1) mounted on the floor of the NPS 5x5 wind tunnel, a five section suction duct housing, and an aerovent centrifugal blower with drive motor (Fig. 6). Two interchangeable fairing nosepieces were employed: uniform ~ iformal nosepiece (UCN) (Fig. 7) and tapered symmetric nosepiece (TSN) (Fig. 8). The physical apparatus was essentially that described in References 2 and 3 except as noted below.

The turret base plate was modified to accept a covering of perforated metal sheeting. With this sheet attached to the fuselage bleed slot (Fig. 1), a porous condition could be simulated and with it removed, a non-porous condition resulted. Figure 9 illustrates a full scale view of the perforated sheeting pattern. The 5/16 in. octagons and 1/8 in. circles equate closely to 15/16 in. and 3/8 in. holes that could be used on full-scale applications for porous bleed slots.

Due to the unreliable fluctuating velocity readings in the suction ducts with pitot-static tubes, a different method using propeller anemometers was employed. These devices consisted of low friction, low torque precision DC

motors on which model aircraft or boat propellers were mounted according to suction duct size (Fig. 10). The motors were mounted on stainless steel tubing at the same location as the pitot-static probes. The propeller anemometers were calibrated in the NPS 32 x 45 wind tunnel over the range of expected velocities. Using the Hewlett-Packard 9830 calculator/plotter, this data could be curve fitted to second degree equations expressing velocity as a function of voltage. A blockage factor due to duct size was applied and the resulting equations are given in Appendix A.

Voltage readings from the propeller anemometers were favorably steady with the exception of Duct #3. An aluminum frame surrounding honeycomb material was constructed and inserted into Duct #3. This straightened the air flow sufficiently to permit that propeller anemometer to function properly.

B. INSTRUMENTATION

Pressure taps located on the turret (Fig. 2) and along the wind tunnel wall were renumbered to ease the data acquisition process. Tygon tubing connected these locations to a forty-eight port scanivalve/pressure transducer. The locations of these ports are presented in Table 2. This pressure transducer was then connected to an Intel 80/10 computer system from which a voltage readout could be obtained that was linear with pressure. A teletypewriter set

AN/UGC-59A was used to record this data. Appendix B offers an example of calculating the pressure coefficient using these numbers from two sets of sample data (Tables 3 and 4).

The propeller anemometers were connected via a wiring harness to a five position switch which in turn was connected to a digital multimeter. Voltage measurements could then be recorded manually and converted to velocities with a programmable handheld calculator.

Yarn tufts were affixed strategically to the turret to visually observe locations of turbulence and quiescent flow. Qualitative comments could be made for each case based on the motion or lack of motion of these tufts.

III. EXPERIMENTAL METHOD

A. CONDITION CODES AND GRAPH KEYS

A bookkeeping system was needed to maintain order among the various parameters for each trial run. Consequently, a code was developed listing the fixed and the variable conditions as follows:

A / B / C / D / E / F / G where

A = type of nosepiece (UCN or TSN)

B = fuselage bleed slot position (F--forward, S--side, A--Aft)

C = F.B.S. porous (P) or non-porous (NP)

D = duct throttles #1 - #5 position (O--open, $\frac{1}{2}$--half open, C--closed)

E = turret-fairing gap (in inches)

F = blower suction throttle (% as indicated on throttle lever)

G = TSN inlet door position (TSN only) (O--open, $\frac{1}{4}$C--1/4 closed, $\frac{1}{2}$C--1/2 closed, $\frac{3}{4}$C--3/4 closed)

For example, UCN/A/P/C,O,O,O,$\frac{1}{2}$/1$\frac{1}{4}$/10% would represent the following condition: UCN, FBS located aft and with porous material, duct throttle #1 closed, #2, 3, 4 open, and #5 half open, turret located 1 1/4 in. forward of the fairing and 10% blower suction.

This condition code is affixed on each set of graphed data. Where the effects of one parameter is being studied, that parameter is replaced in the condition code by "*". This variable parameter * then is represented graphically with different line symbols which are also keyed on each graph.

An "X" was placed on the pressure distribution graphs to represent the point where turbulence begins, based on the tuft motion. This eyeball interpretation was, of course, quite subjective.

For selected trials the pressure coefficients were presented on a profile view of the turret, and lines of equal pressure were sketched between the pressure ports. With these figures another approach to pressure variation over the turret could be presented.

B. PRESSURE DISTRIBUTION CUT LINES

It was decided to study three pressure distributions for each trial, namely spherical, cylindrical, and cylindrical-spherical. The spherical cut was taken over the top of the turret. With the FBS aft, this consisted of Ports #28, 20, 19, 24 and 32 representing $\theta = 0^{\circ}$ to 180°. The cylindrical cut was taken over the section C-C (Fig. 2) with Ports #36, 43, 42, 41 and 40 representing $\theta = 0^{\circ}$ to 180°. For the cylindrical-spherical interface distribution, the cut was taken over section B-B (Fig. 2) with Ports #28, 35, 34, 33

and 32 representing $\theta = 0^{\circ}$ to 180°. The ports were selected on the side opposite any tufts to preclude unnecessary turbulence. Other corresponding ports were used with the FBS in the side or forward position since rotating this slot also resulted in the turret rotating.

IV. DATA INTERPRETATION

Table 5 summarizes the conditions of the various runs and Figures 12 through 89 present pressure distributions for these runs.

To arrive at optimum (minimum) suction conditions, it was necessary to compare spherical, cylindrical-spherical, and cylindrical pressure distributions for appropriate runs. To determine which run is "better", three points should be considered:

1. Any pressure rise is undesirable
2. The pressure need only fall to a minimum required
3. Delayed pressure rise is desirable.

From Table 6, the use of a porous material over the FBS produced superior pressure distributions when compared to non-porous. Increasing turret-fairing gap produced worse pressure distribution (Table 7). Thus, it was determined best to butt the turret against the nosepiece fairing splitter plate. The actual suction opening measured between the UCN outer wall lip and turret was 2 inches. While not as clear-cut as other parameters, FBS location was judged best in the forward position (Table 8). Table 9 concluded the optimum suction duct throttle setting was to fully close #1 and open #2, 3, 4, and 5. Fifteen percent blower suction was judged to be the minimum acceptable (Table 10). TSN

door position had negligible effect (Table 11). Furthermore, when compared to the TSN, better pressure distributions were produced with the UCN.

Runs #71 (Fig. 87), #79 (Fig. 88), and #18 (Fig. 89) were selected to illustrate lines of equal C_p along a turret profile view. Constant C_p lines on Run #71 (optimum conditions) constantly decrease across the turret except in the area around $\theta = 135^{\circ}$ and $\phi = 45^{\circ}$ on the sphere. This area produced a curious tuft pattern on all runs near optimum conditions. Run #79 with the TSN and Run #18 (randomly selected) produced rising pressures across the turret.

V. RESULTS

The Reynold's number for these runs at a nominal wind tunnel velocity of 40.8 ft/sec was calculated:

$$Re = \frac{\rho \cdot V \cdot \ell}{\mu}$$

$$= \frac{.23769 \times 10^{-2} \ \frac{\text{lbf-sec}^2}{\text{ft}^4} \cdot 40.8 \text{ ft/sec} \cdot 16.8 \text{ in} \left(\frac{1 \text{ ft}}{12 \text{ in}}\right)}{3.8 \times 10^{-7} \ \frac{\text{lbf-sec}}{\text{ft}^2}}$$

$$= 3.57 \times 10^5$$

From Schlichting [Ref. 4], this value is in the critical range and turbulent flow could be expected around the turret. The method of flow control by boundary layer suction was shown to be a viable method. Optimum flow conditions (minimum required suction) were found and illustrated in Runs #61 and #71.

The tuft motion proved to be an accurate indicator of flow separation when compared to the rising pressure distribution curves. For nearly all figures the X's, or flow separation points, occurred slightly aft of the point where the pressures began to rise.

The blower mass flow rates, $\dot{m}$, as shown on Table 5, are reasonably constant as one would expect by the continuity law. The mass flow rates are in excellent agreement for different runs in which the blower throttle was not changed.

Those runs for which there are differences can best be explained by inaccuracies in throttle settings. From Runs #61 and #71 $\dot{m}_{total}$ = 4.16 lbm/sec. This suction was distributed over the turret as shown in Figure 11. The mass flow rate of streamlines between the turret capture area was calculated to be 5.90 lbm/sec using turret frontal area equal to 1.89 ft^2. Thus, the minimum amount of suction required to obtain quiescent flow at optimum conditions was 70.5% of the turret capture area mass flow rate. Furthermore, since the maximum blower air flow capacity was 7700 ft^3/min, or 9.81 lbm/sec, the 15% blower suction setting actually was 42.4%. Consequently, the blower suction throttle settings should only be considered as an arbitrary scale and not a true indication of blower suction capacity.

VI. CONCLUSIONS

The concept of using fuselage bleed slot and after-body fairing suction as a method of flow control about an airborne laser turret was demonstrated to be effective in low velocity, incompressible flow. The optimum conditions for quiescent flow about the turret were determined to be as follows:

1. A fairing nosepiece shaped like the UCN;
2. The crescent shaped fuselage bleed slot placed forward at the turret base;
3. Porous sheeting covering the FBS;
4. Suction Duct #1 closed; Ducts #2 - #5 open;
5. The turret moved back against the fairing to provide zero gap;
6. Blower suction set at 42.4% of maximum capacity. (Note: Max. blower capacity was 7700 ft^3/min. The minimum required suction was, therefore, 3280 ft^3/min. This corresponded to the arbitrary throttle scale setting of 15%).

Item #4 implies that the fairing height may be reduced to two-thirds of the turret height. This would permit a high aft laser shot from the turret.

Item #6 equates to a suction $\dot{m}$ that is 70.5% of the turret capture area $\dot{m}$. As a proposal, a small turbojet engine such as the YJ69-T-406 or J85 GE-7 with mass flow rates of 30 lbm/sec and 42 lbm/sec (sea level static) respectively, could serve as a source of adequate suction at low

velocity flight. However, the flow control method and suction source in compressible flow remains to be tested.

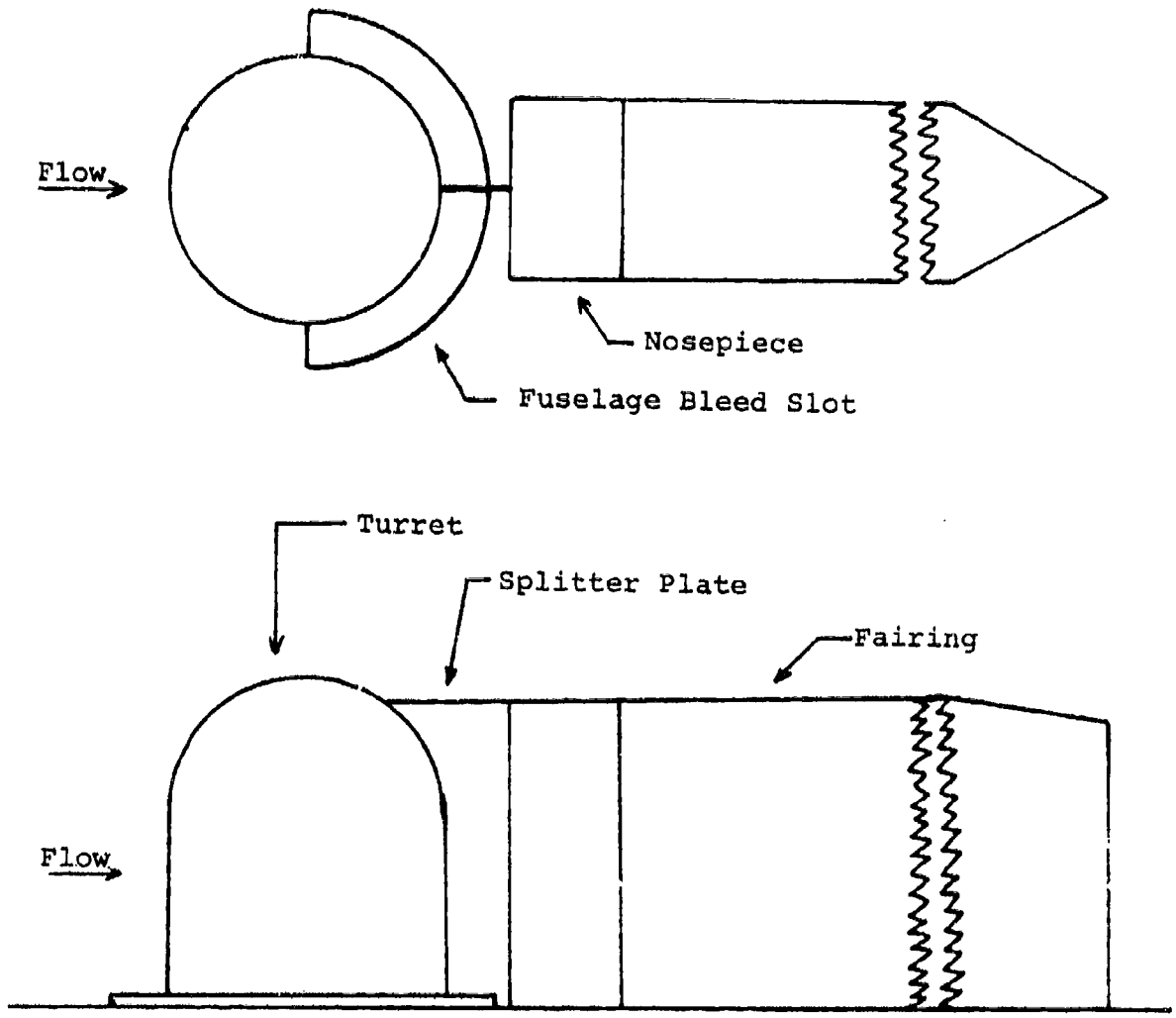

Figure 1. Laser Turret and Fairing Model

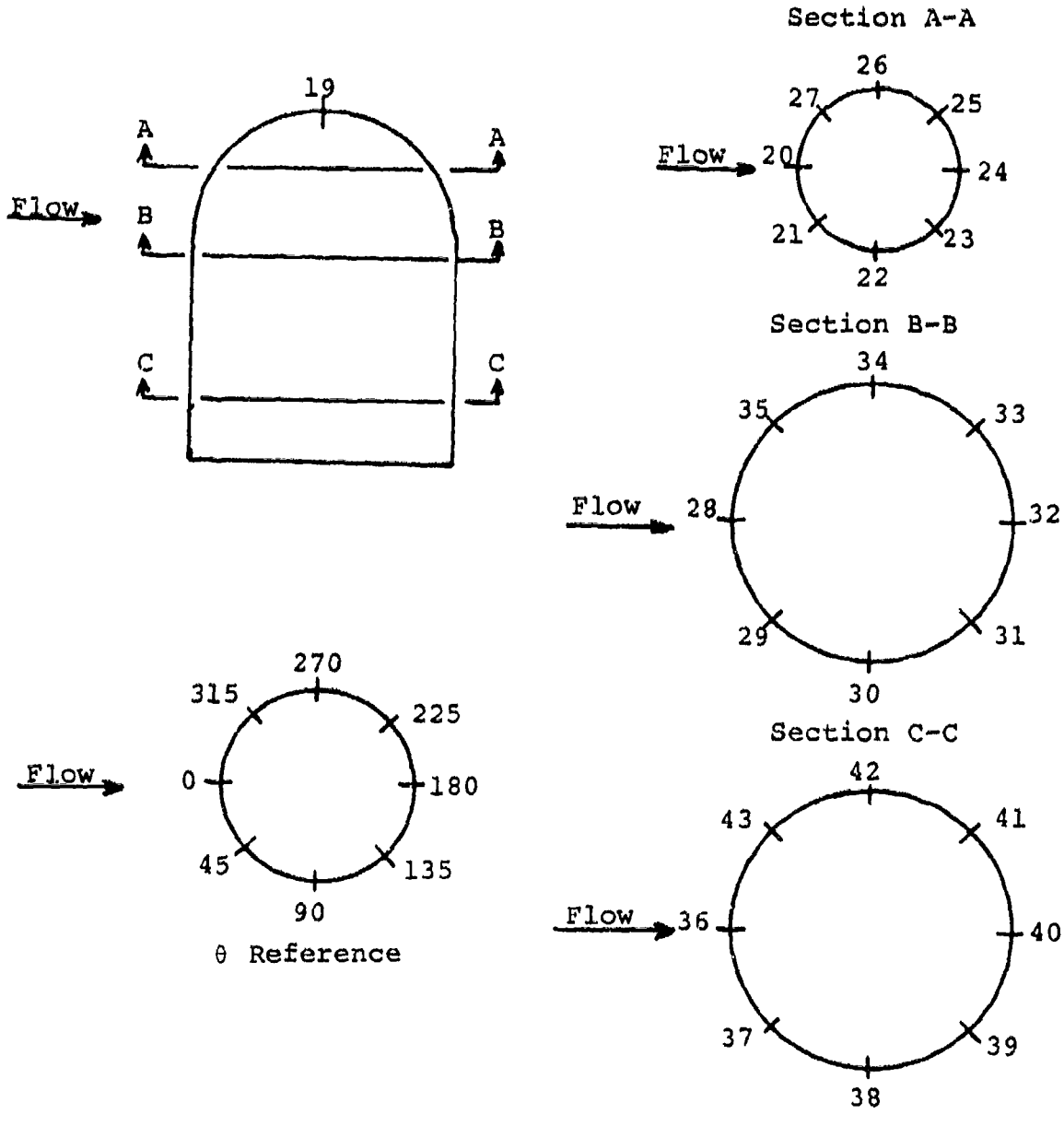

Figure 2. Turret Pressure Tap Locations

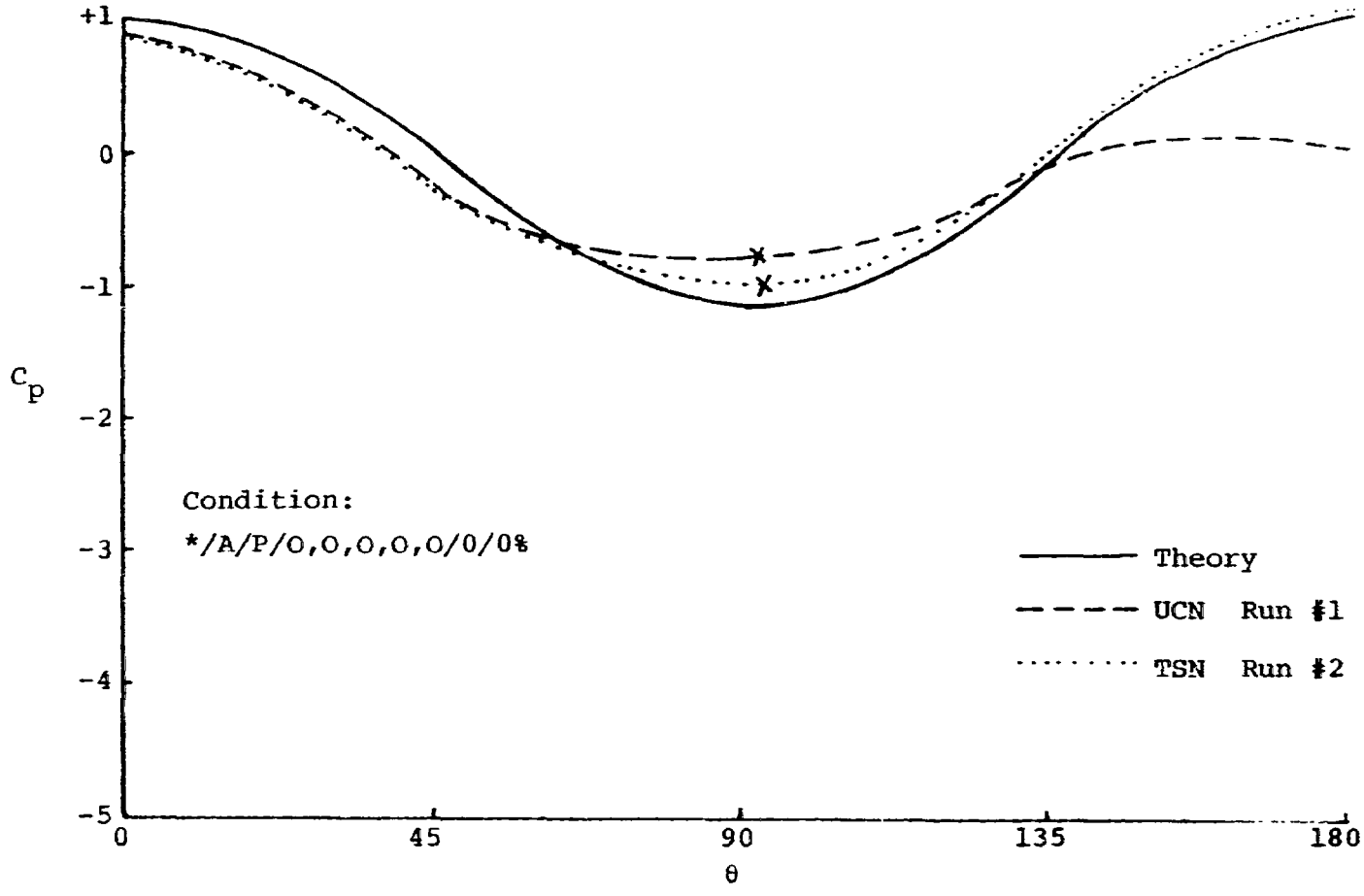

Figure 3. Baseline Spherical Pressure Distribution

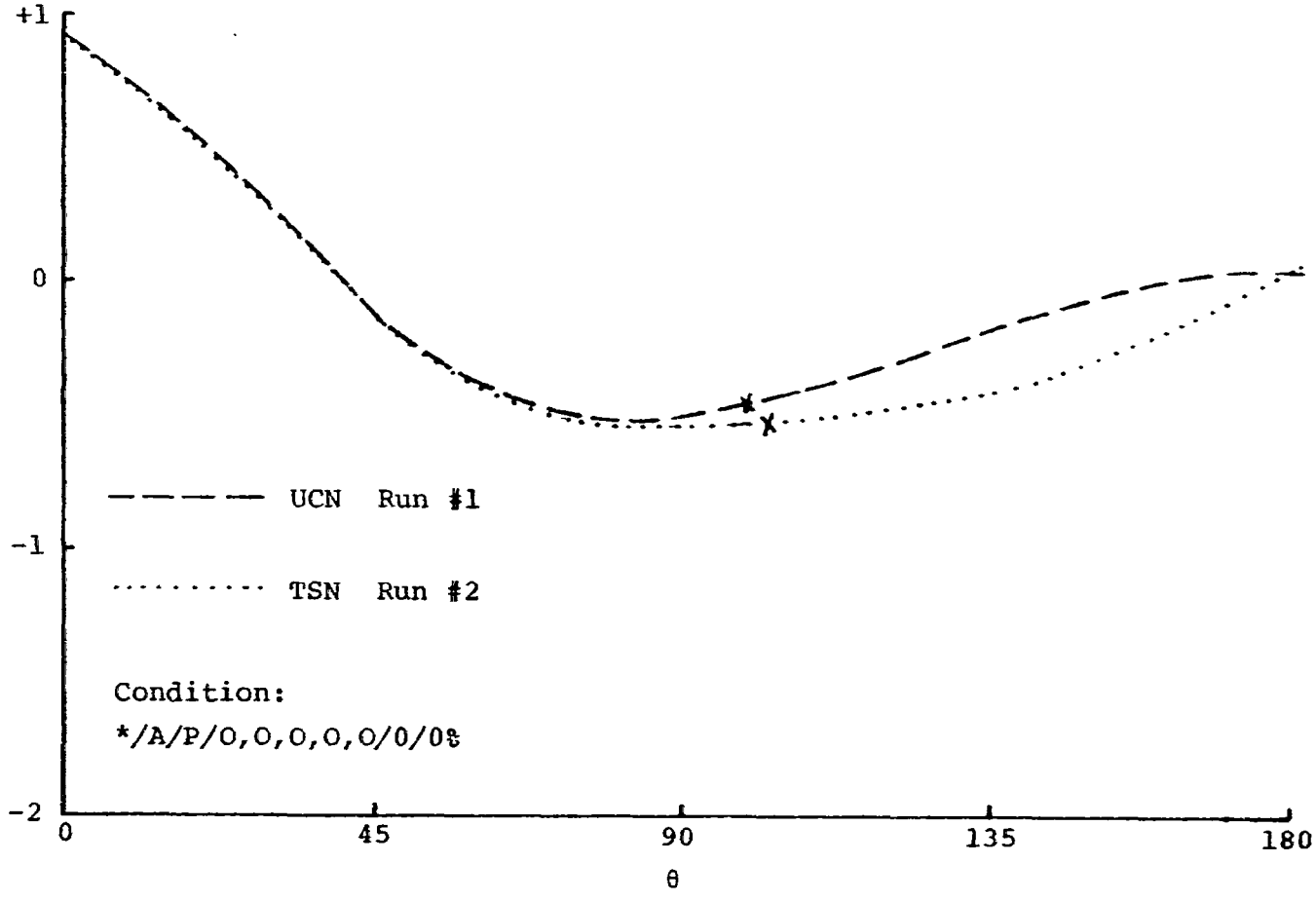

Figure 4. Baseline Cylindrical-Spherical Pressure Distribution

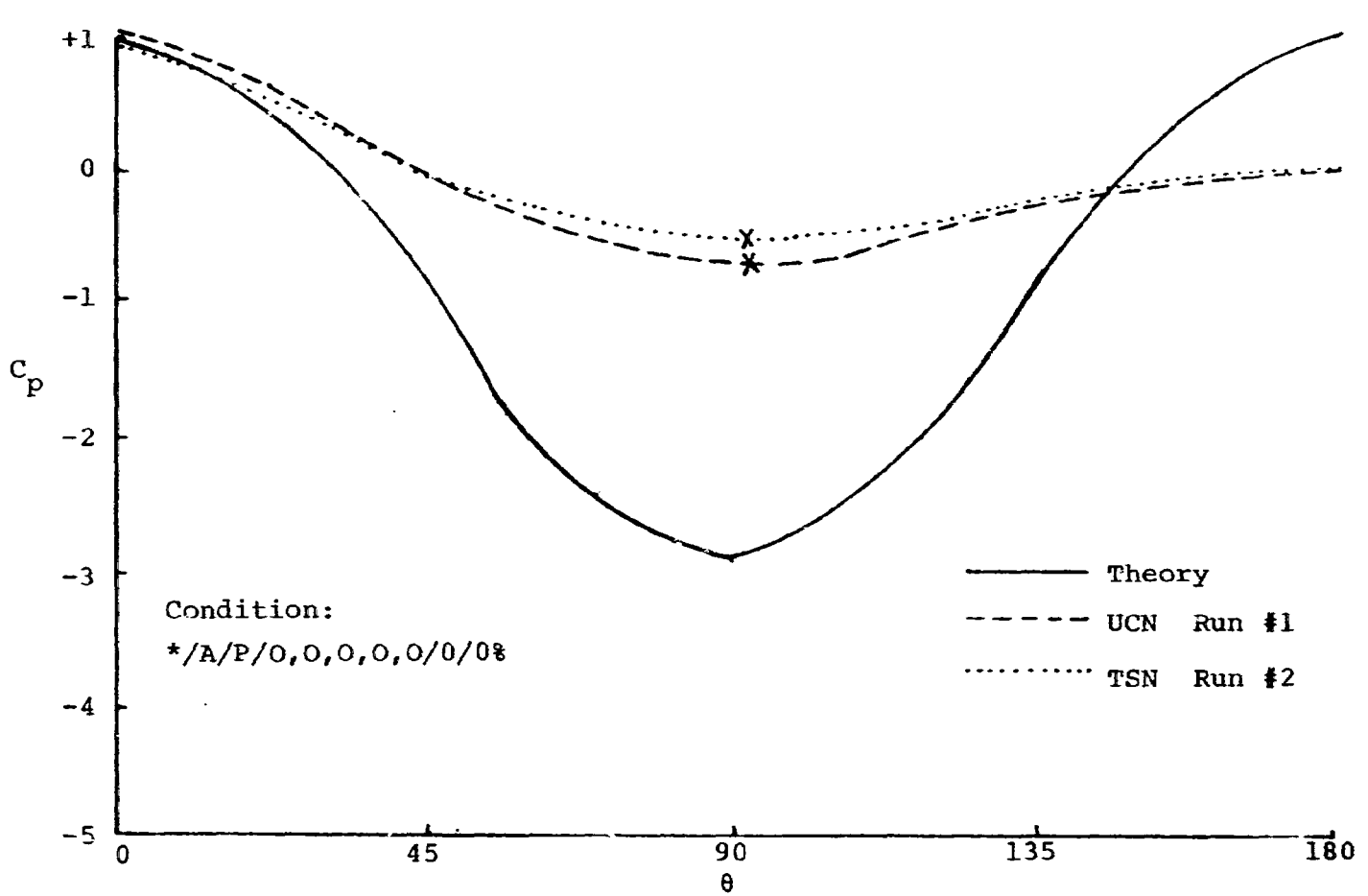

Figure 5. Baseline Cylindrical Pressure Distribution

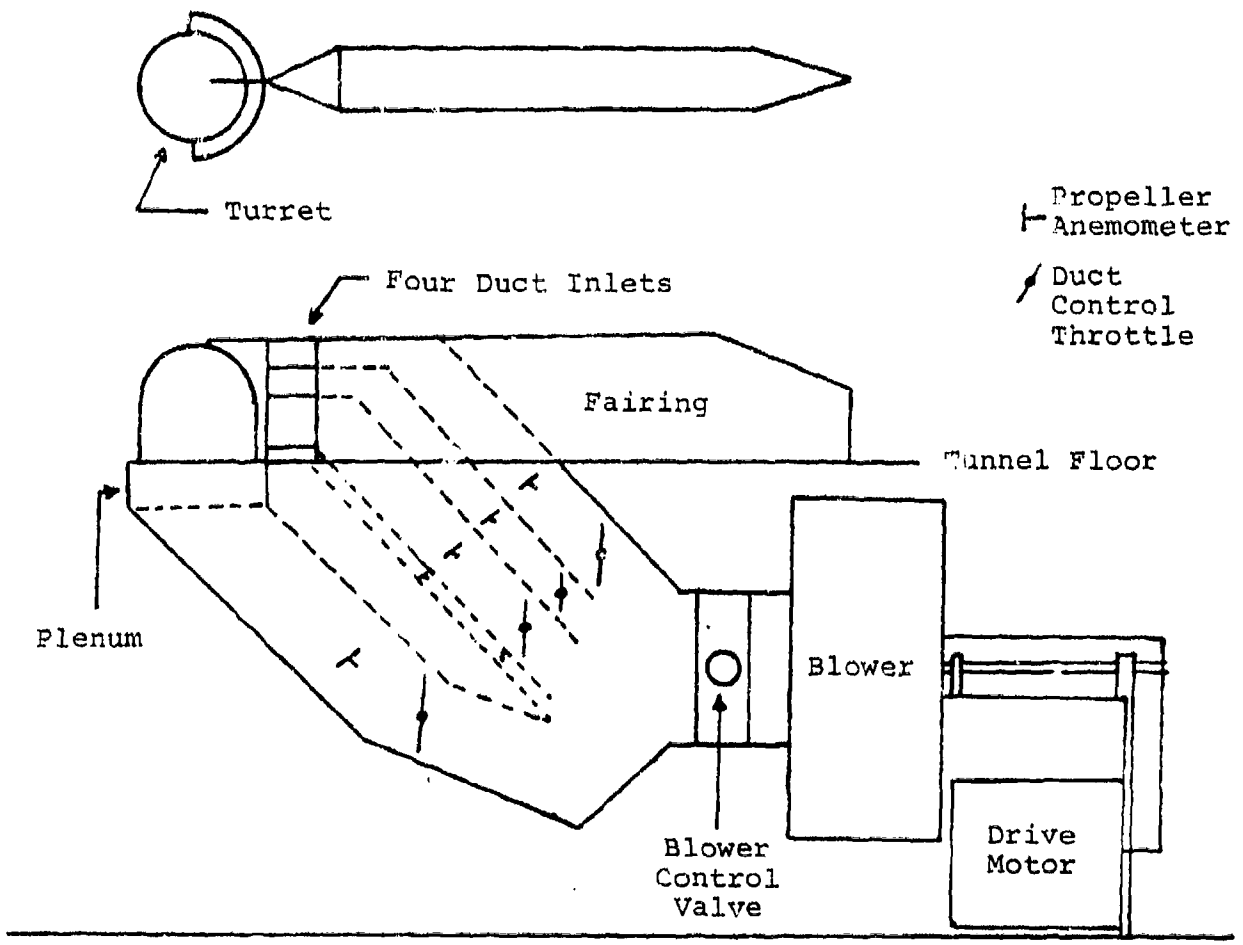

Figure 6. Laser Turret Wind Tunnel Installation

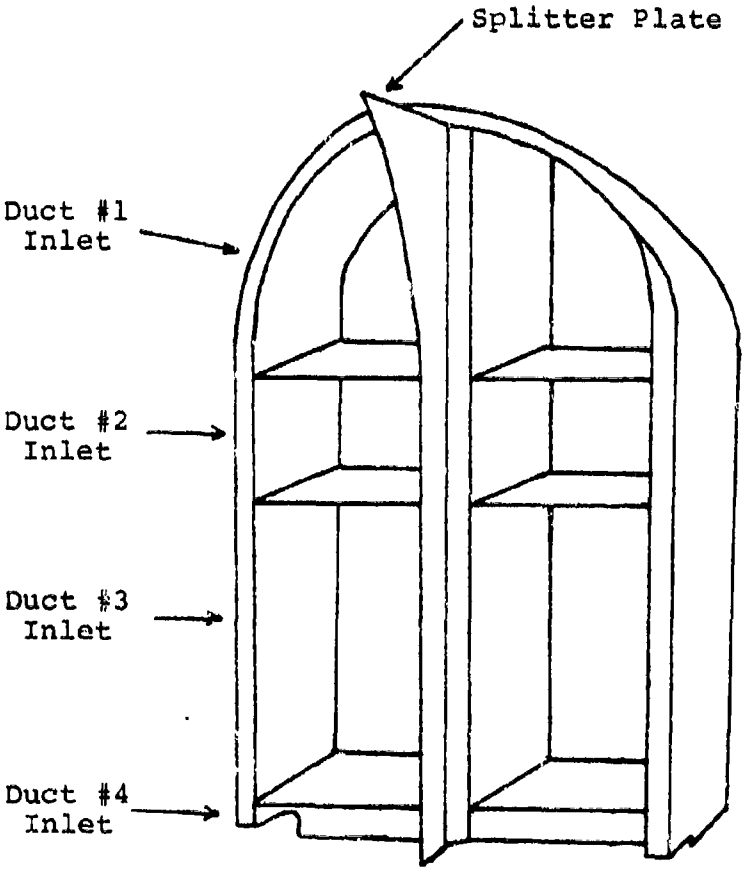

Figure 7. Uniform Conformal Nosepiece (UCN)

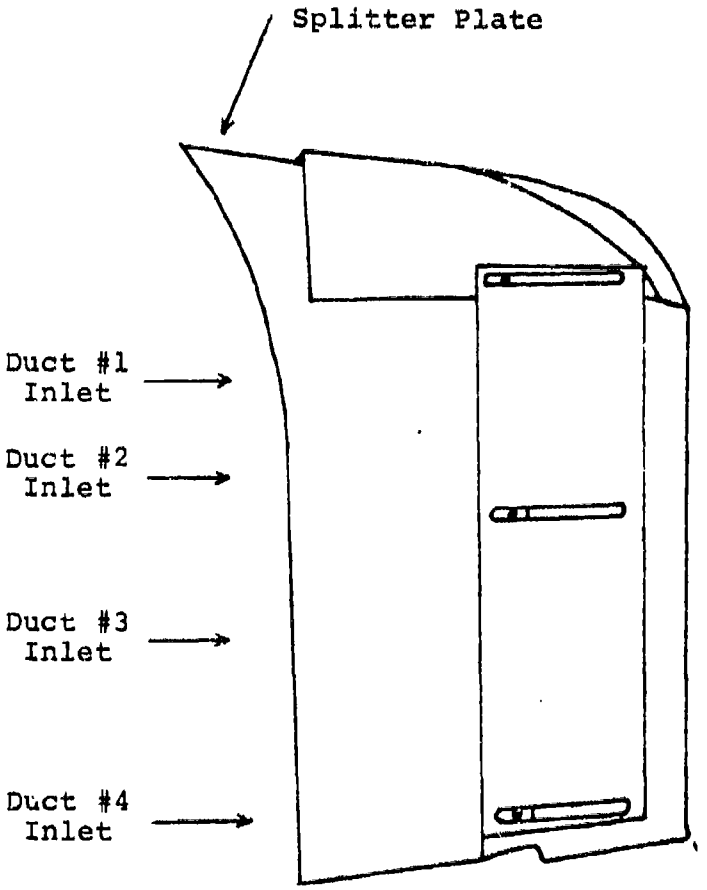

Figure 8. Tapered Symmetric Nosepiece (TSN)

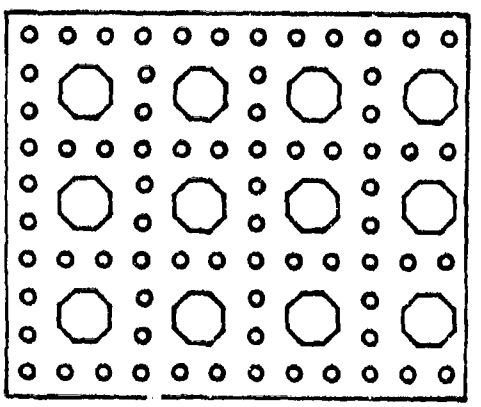

Figure 9. Fuselage Bleed Slot Sheeting

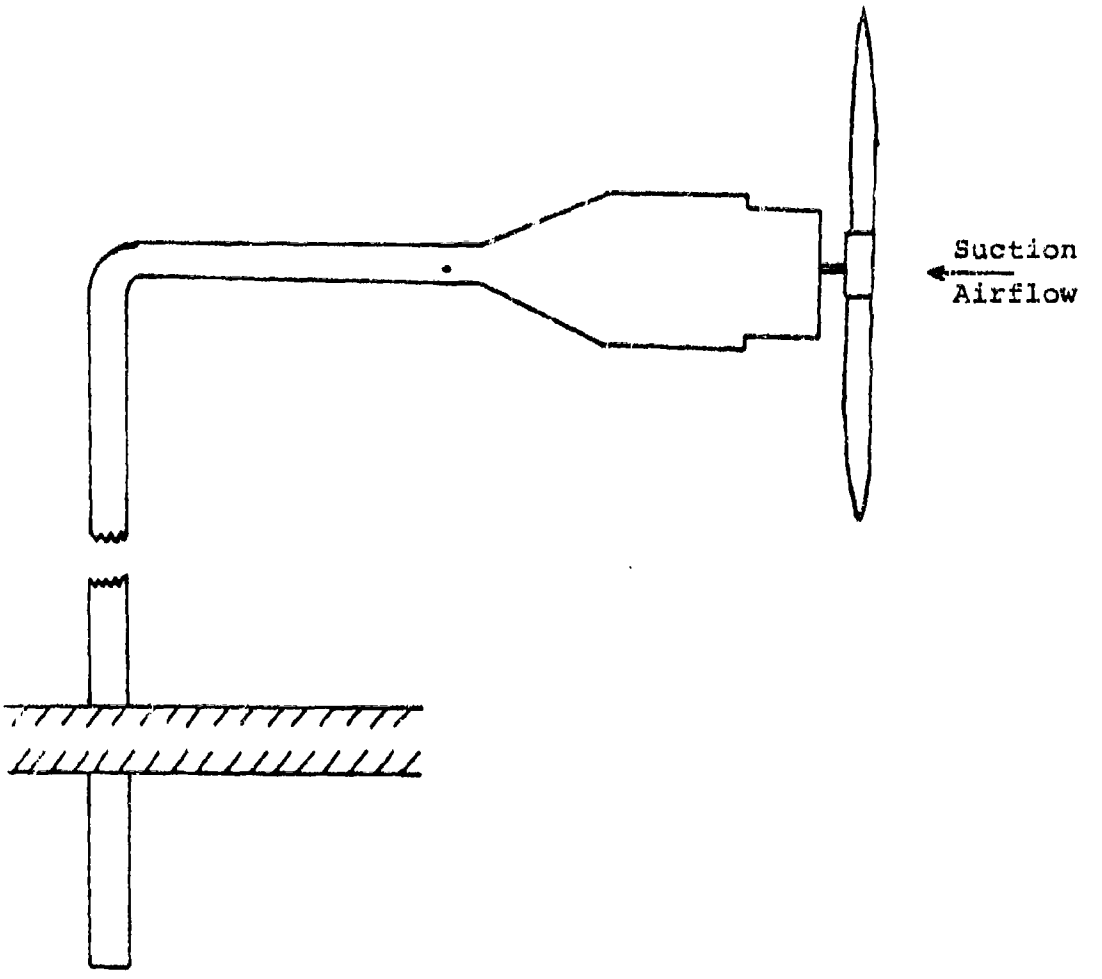

Figure 10. Typical Propeller Anemometer

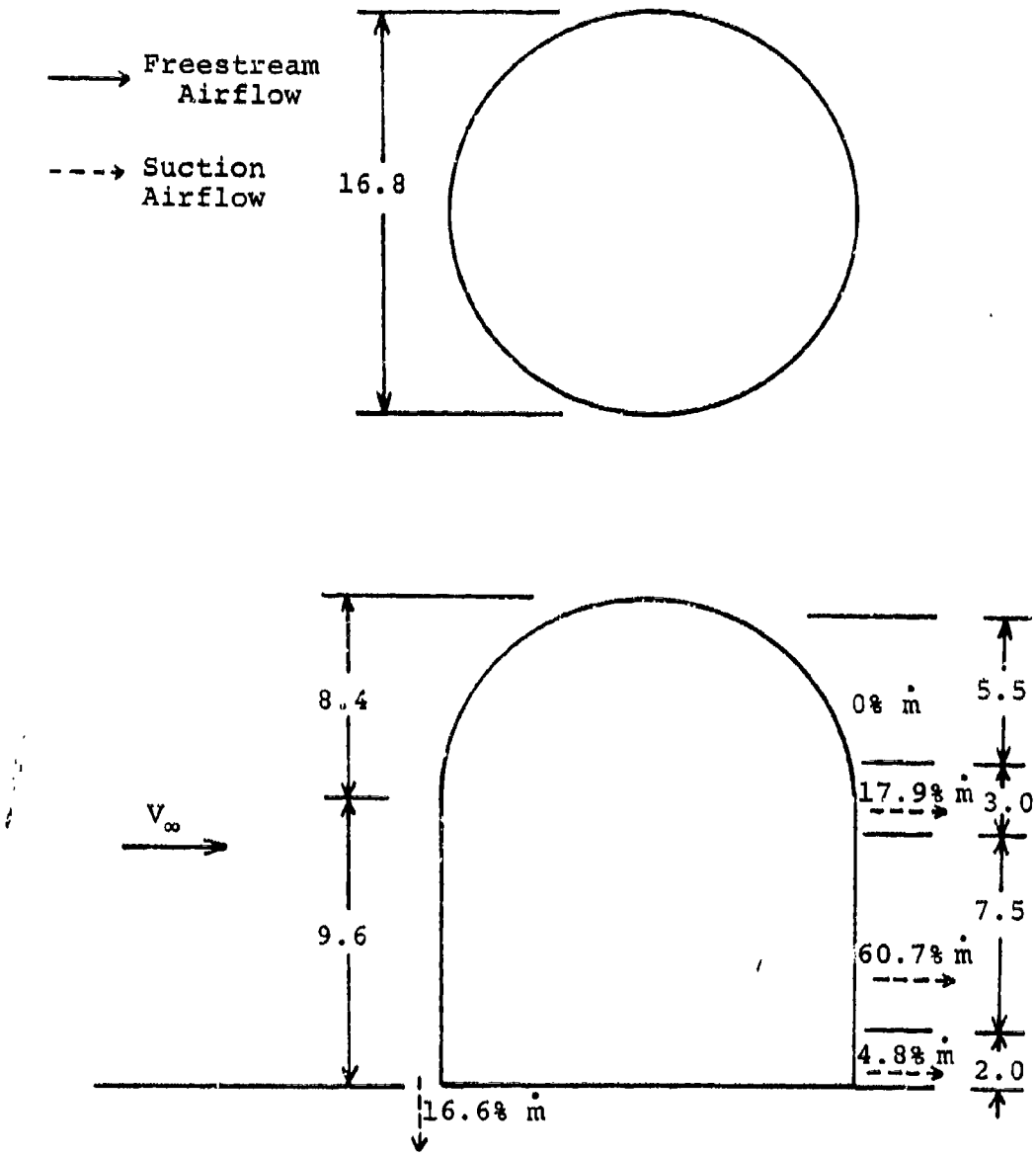

Figure 11. Laser Turret Model Suction Distribution (Dimensions in Inches)

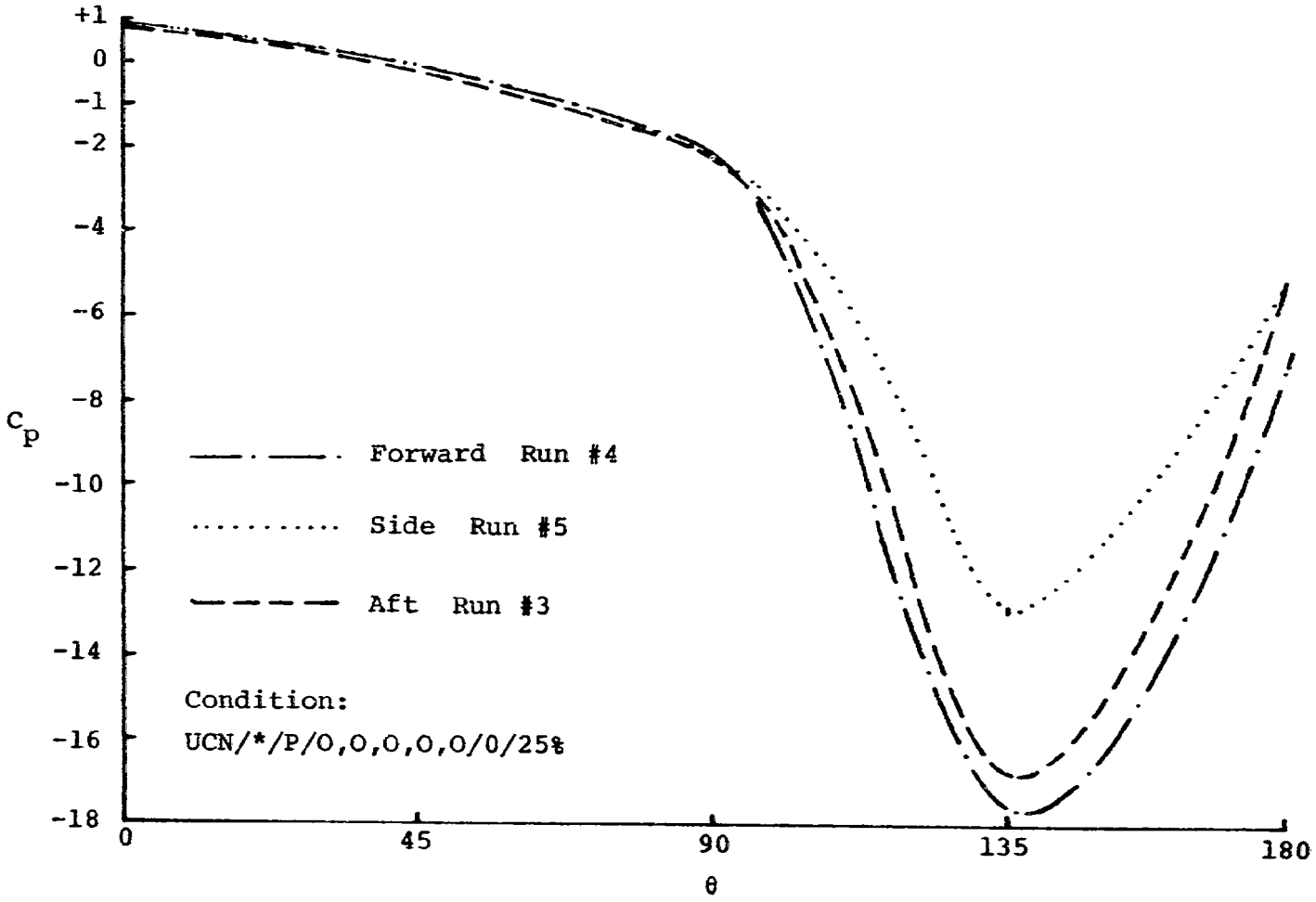

Figure 12. Spherical Pressure Distribution--
Effect of Porous Fuselage Bleed Slot
Location at 25% Suction

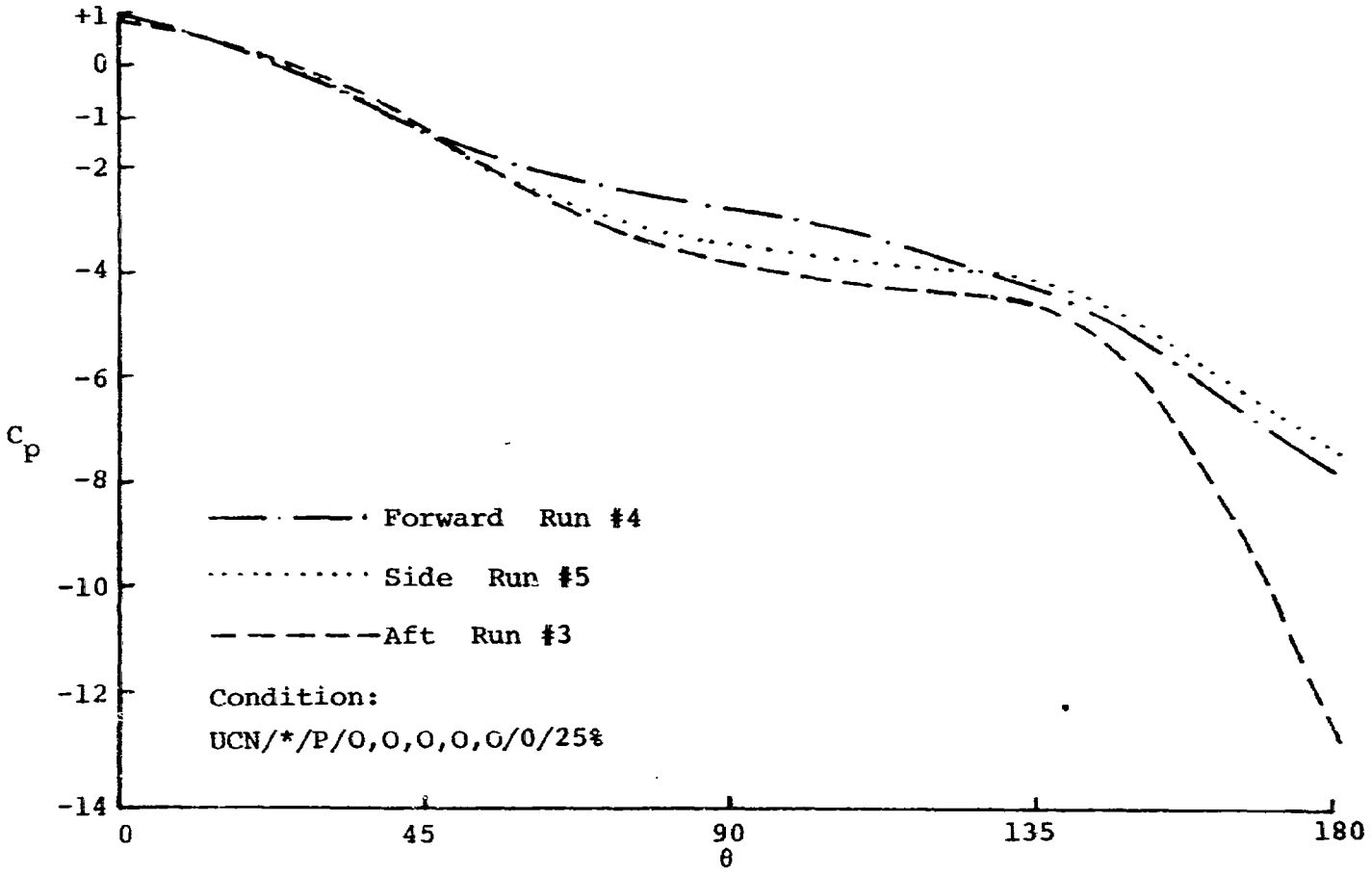

Figure 13. Cylindrical Pressure Distribution-- Effect of Porous Fuselage Bleed Slot Location at 25% Suction

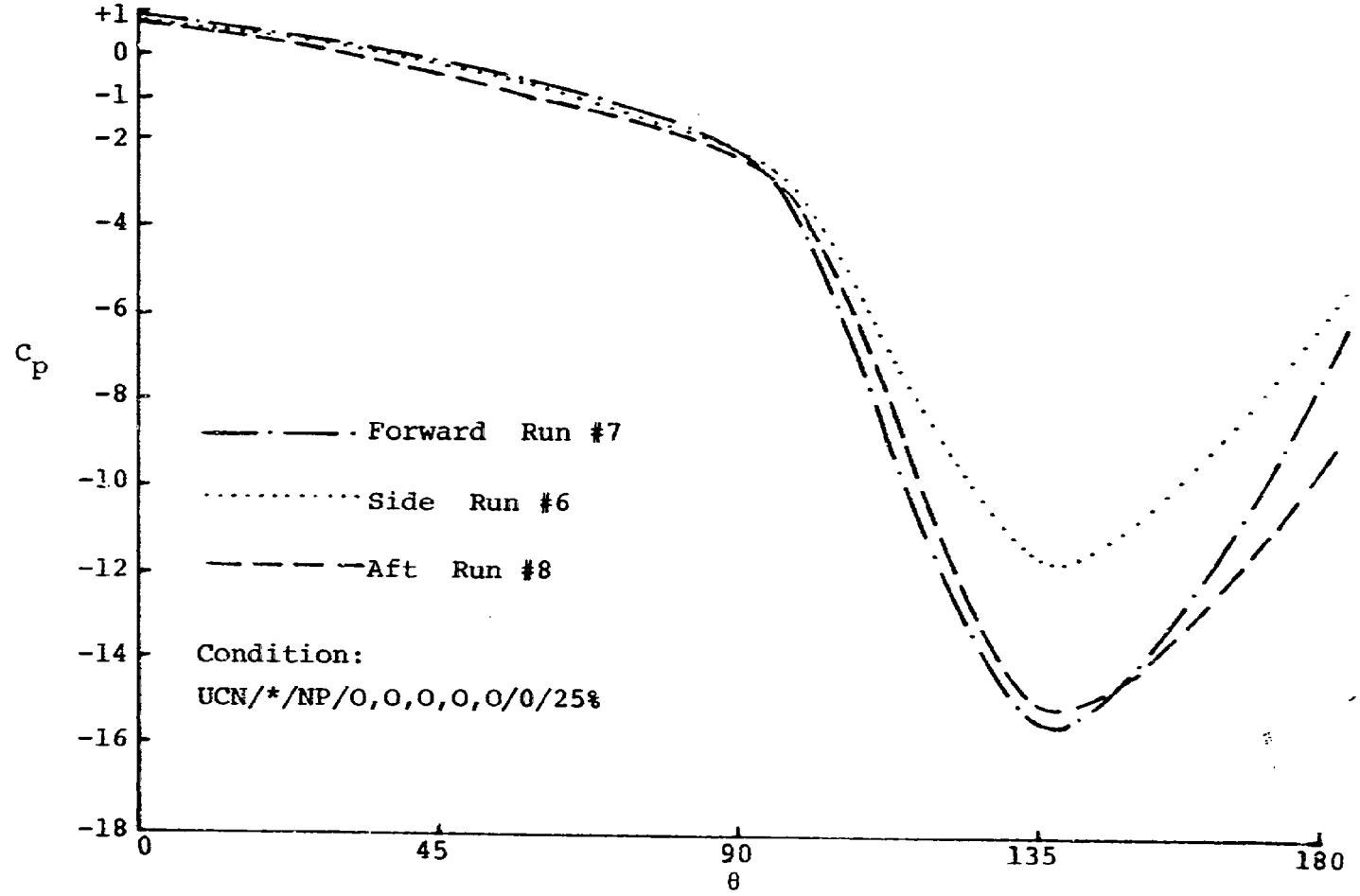

Figure 14. Spherical Pressure Distribution--
Effect of Non-Porous Fuselage Bleed Slot
Location at 25% Suction

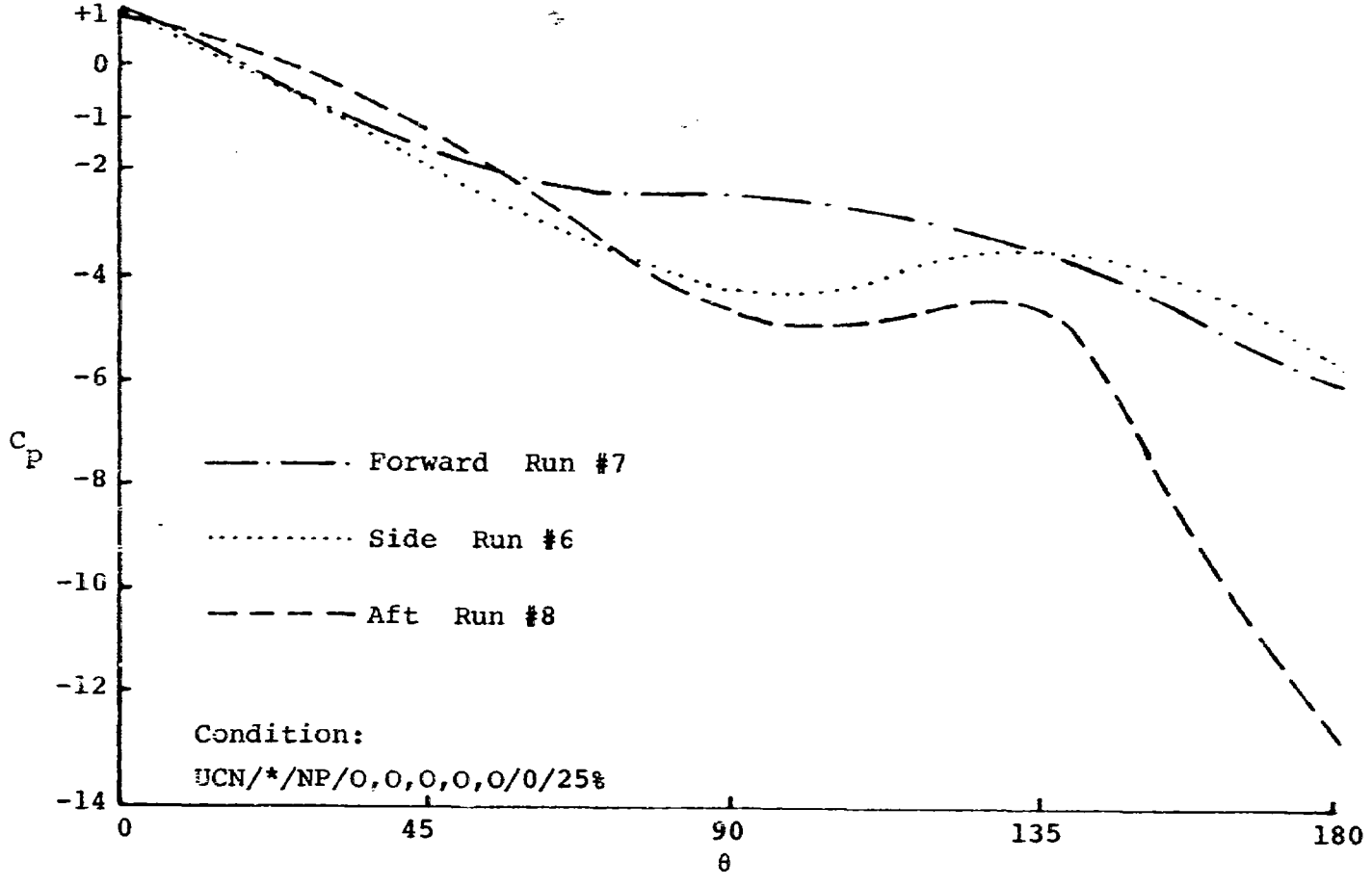

Figure 15. Cylindrical Pressure Distribution--
Effect of Non-Porous Fuselage Bleed Slot
Location at 25% Suction

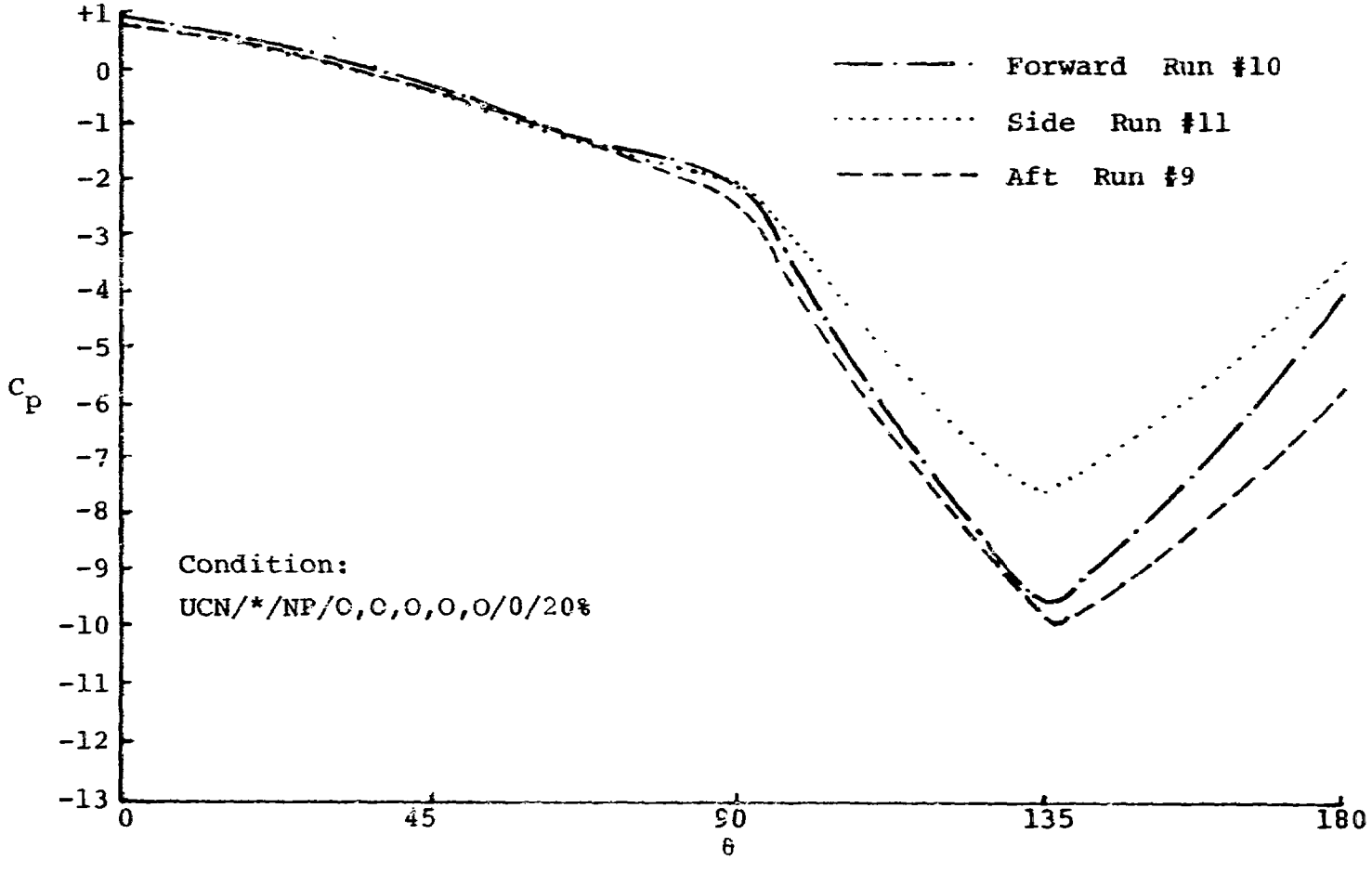

Figure 16. Spherical Pressure Distribution--
Effect of Non-Porous Fuselage Bleed Slot
Location at 20% Suction

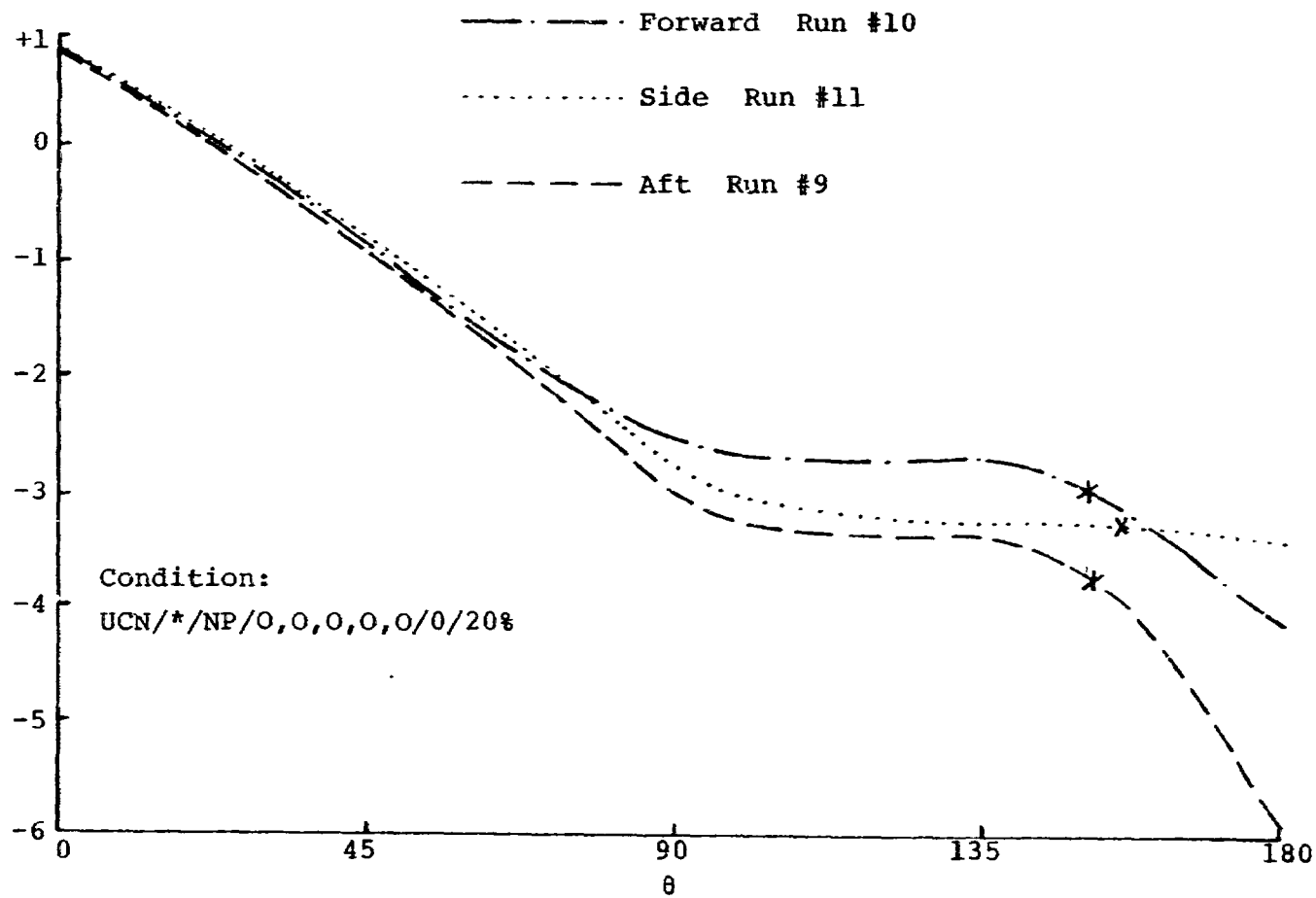

Figure 17. Cylindrical-Spherical Pressure Distribution--
Effect of Non-Porous Fuselage Bleed Slot
Location at 20% Suction

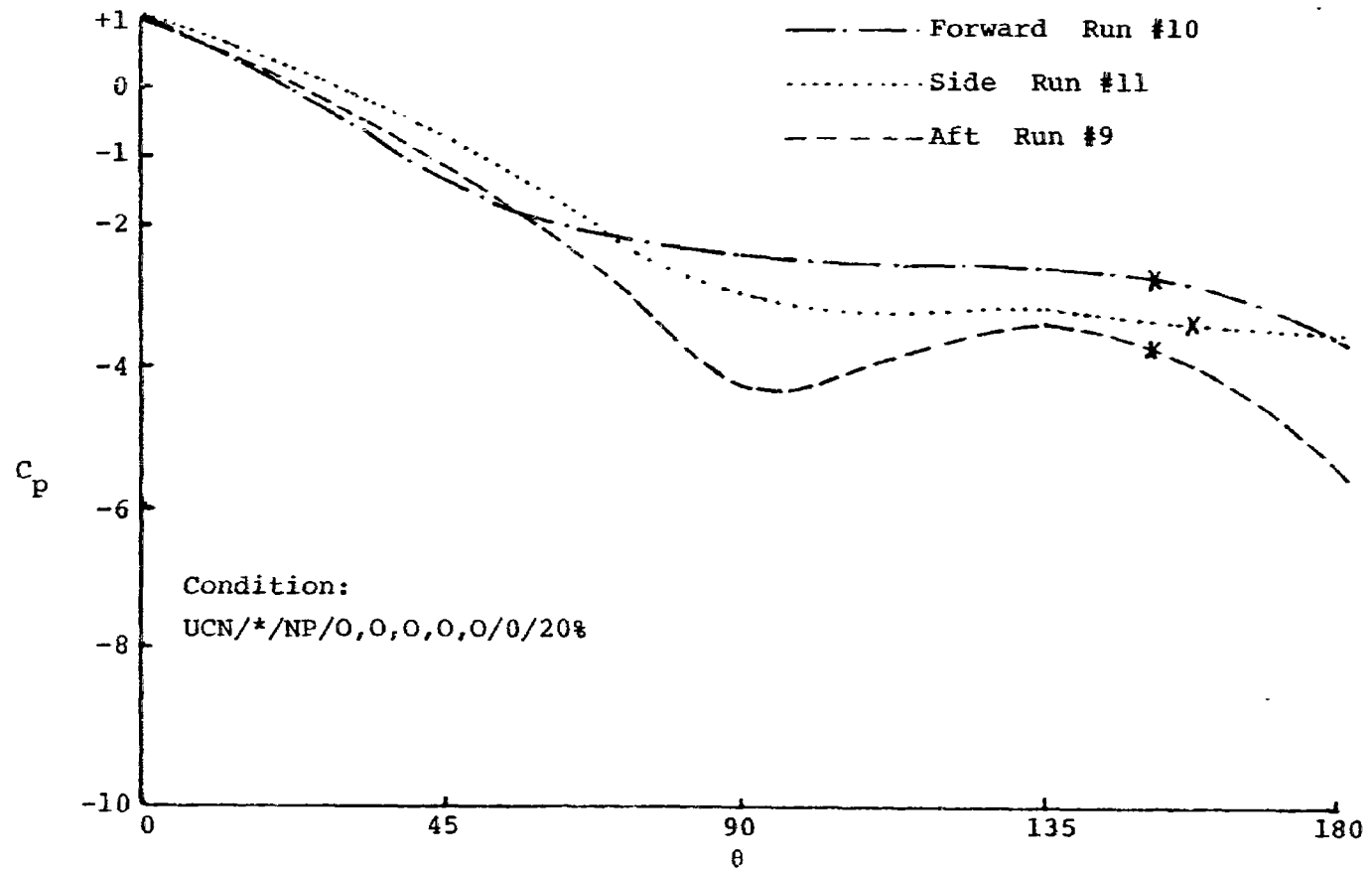

Figure 18. Cylindrical Pressure Distribution--
Effect of Non-Porous Fuselage Bleed Slot
Location at 20% Suction

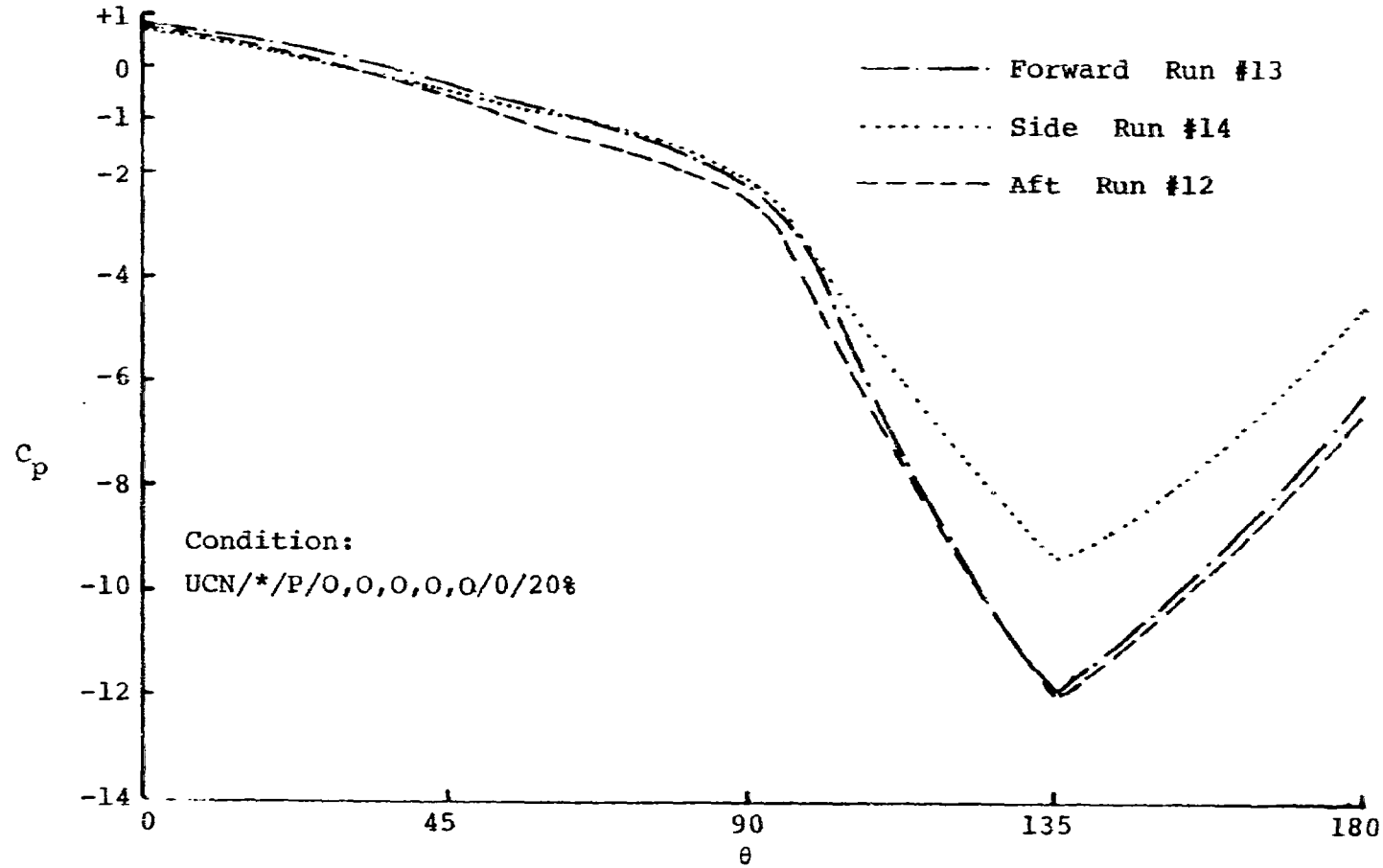

Figure 19. Spherical Pressure Distribution--
Effect of Porous Fuselage Bleed Slot
Location at 20% Suction

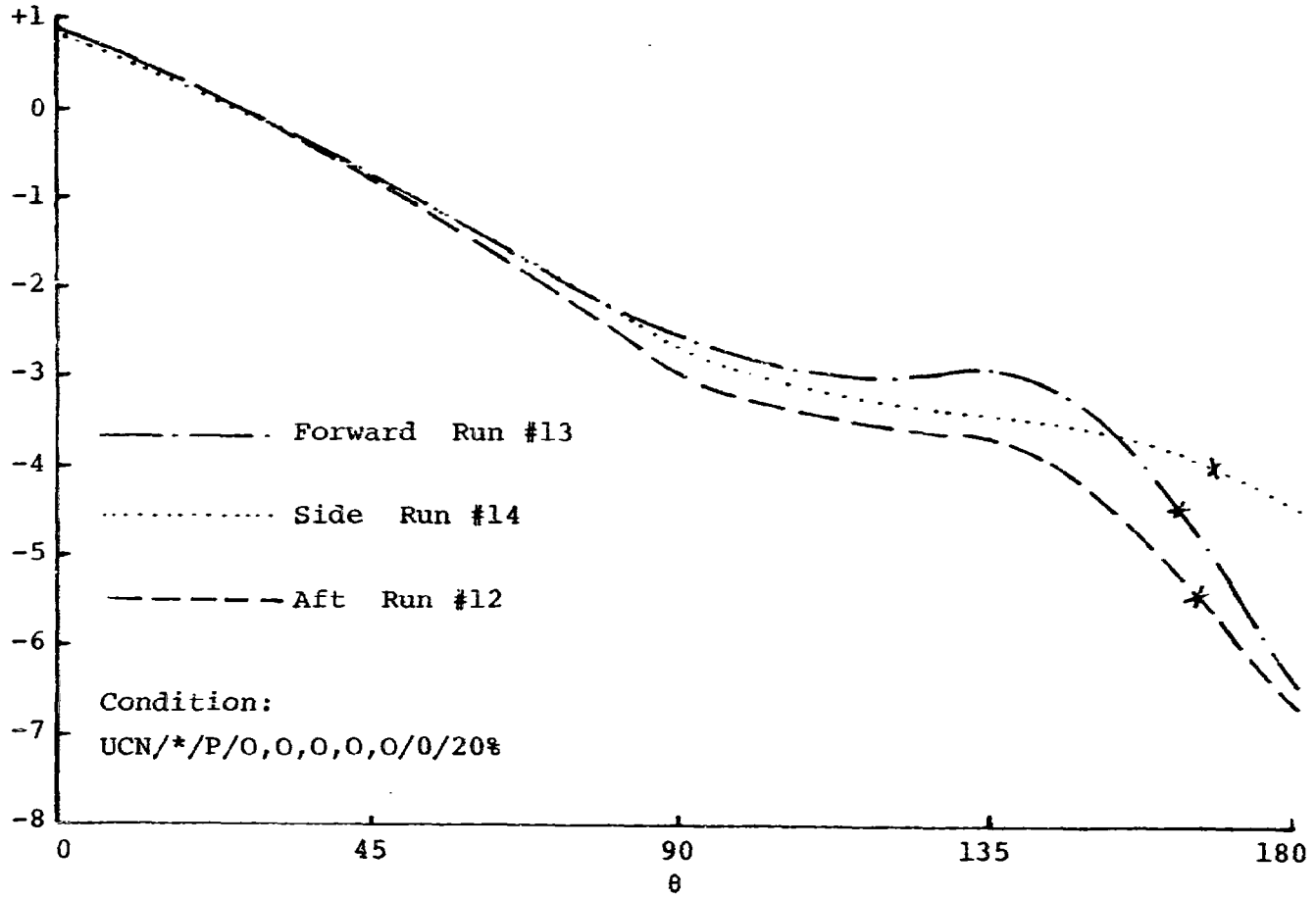

Figure 20. Cylindrical-Spherical Pressure Distribution--
Effect of Porous Fuselage Bleed Slot
Location at 20% Suction

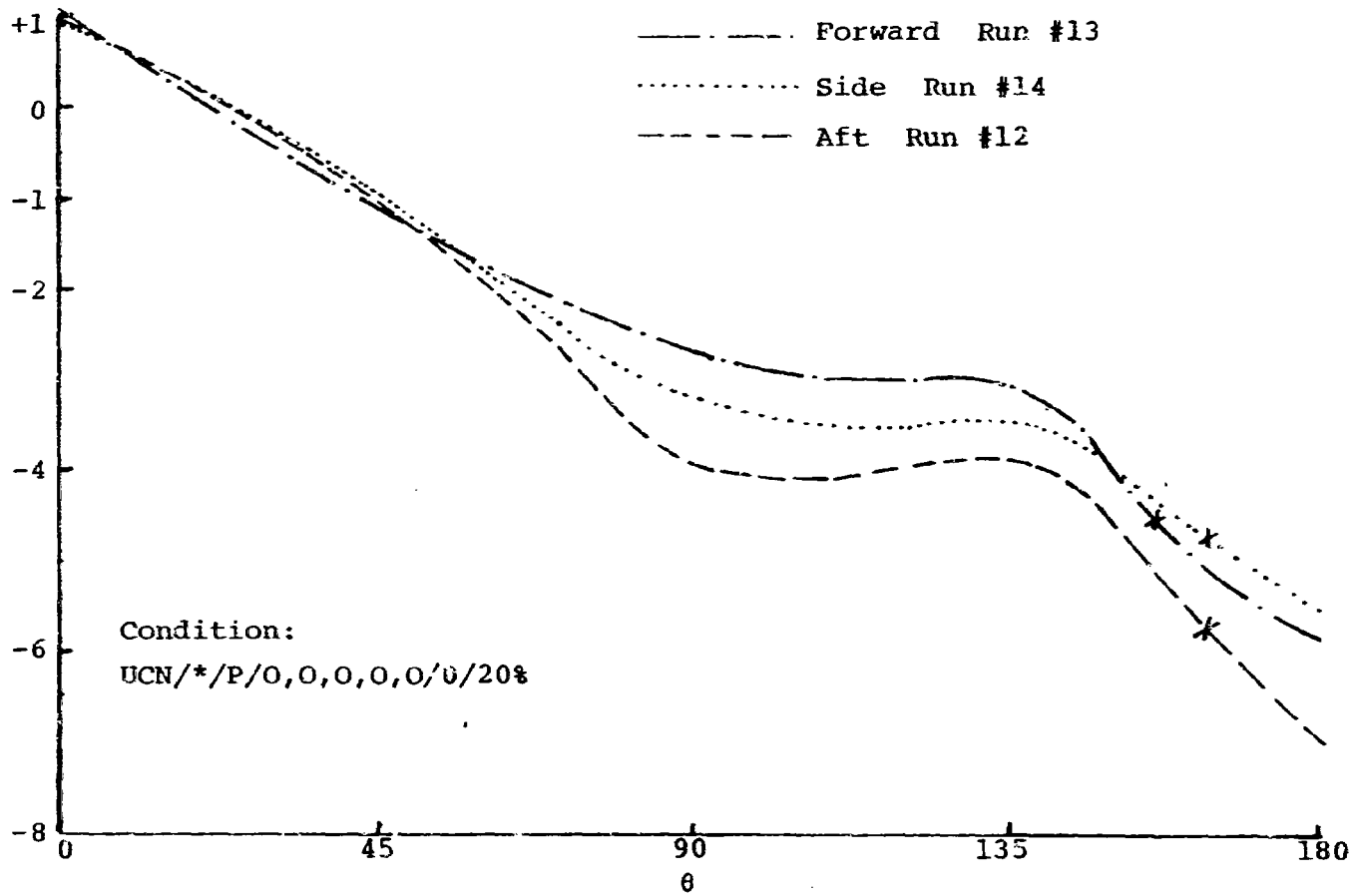

Figure 21. Cylindrical Pressure Distribution--
Effect of Porous Fuselage Bleed Slot
Location at 20% Suction

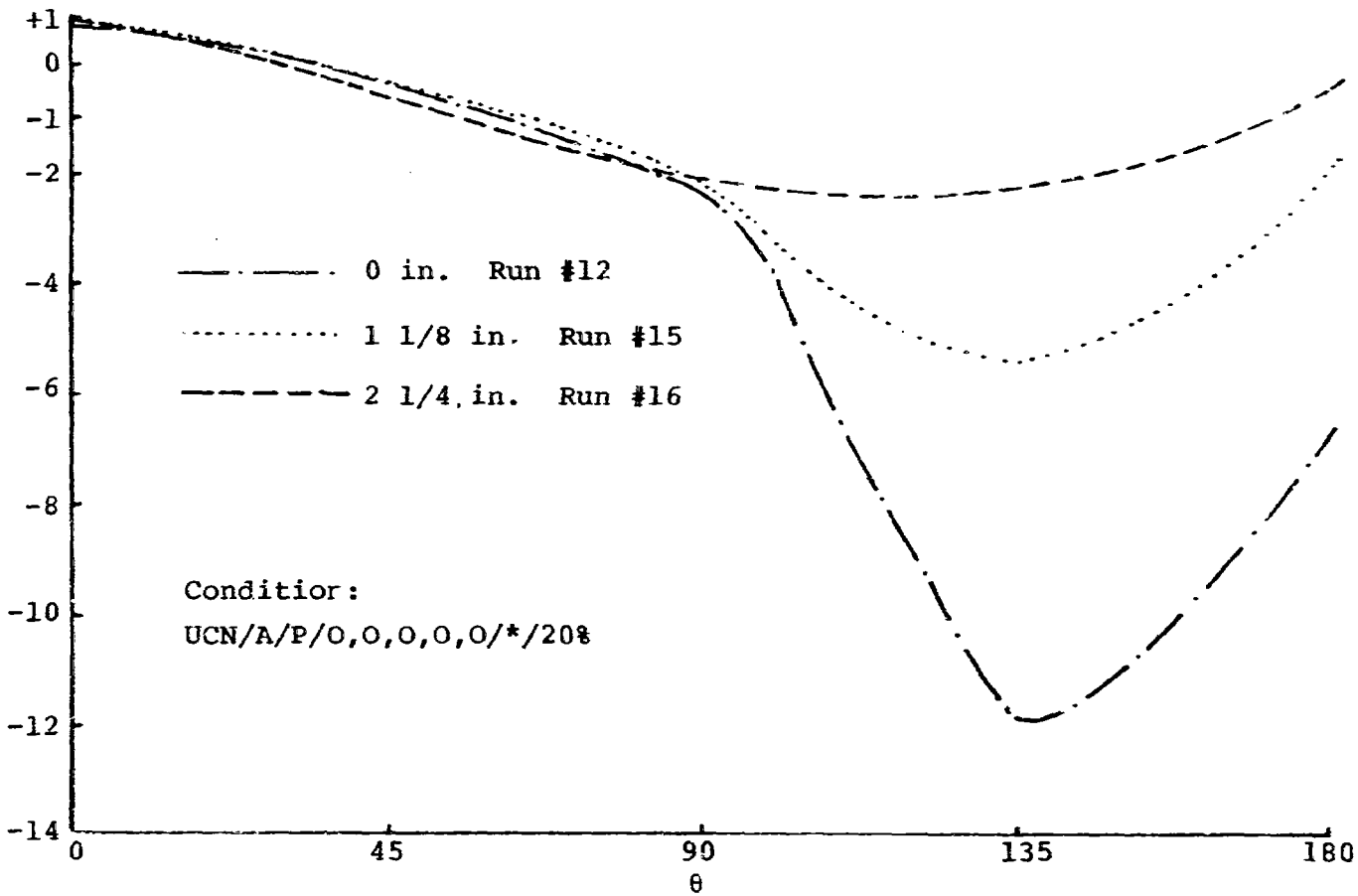

Figure 22. Spherical Pressure Distribution--
Effect of Turret-Fairing Gap
with Porous FBS

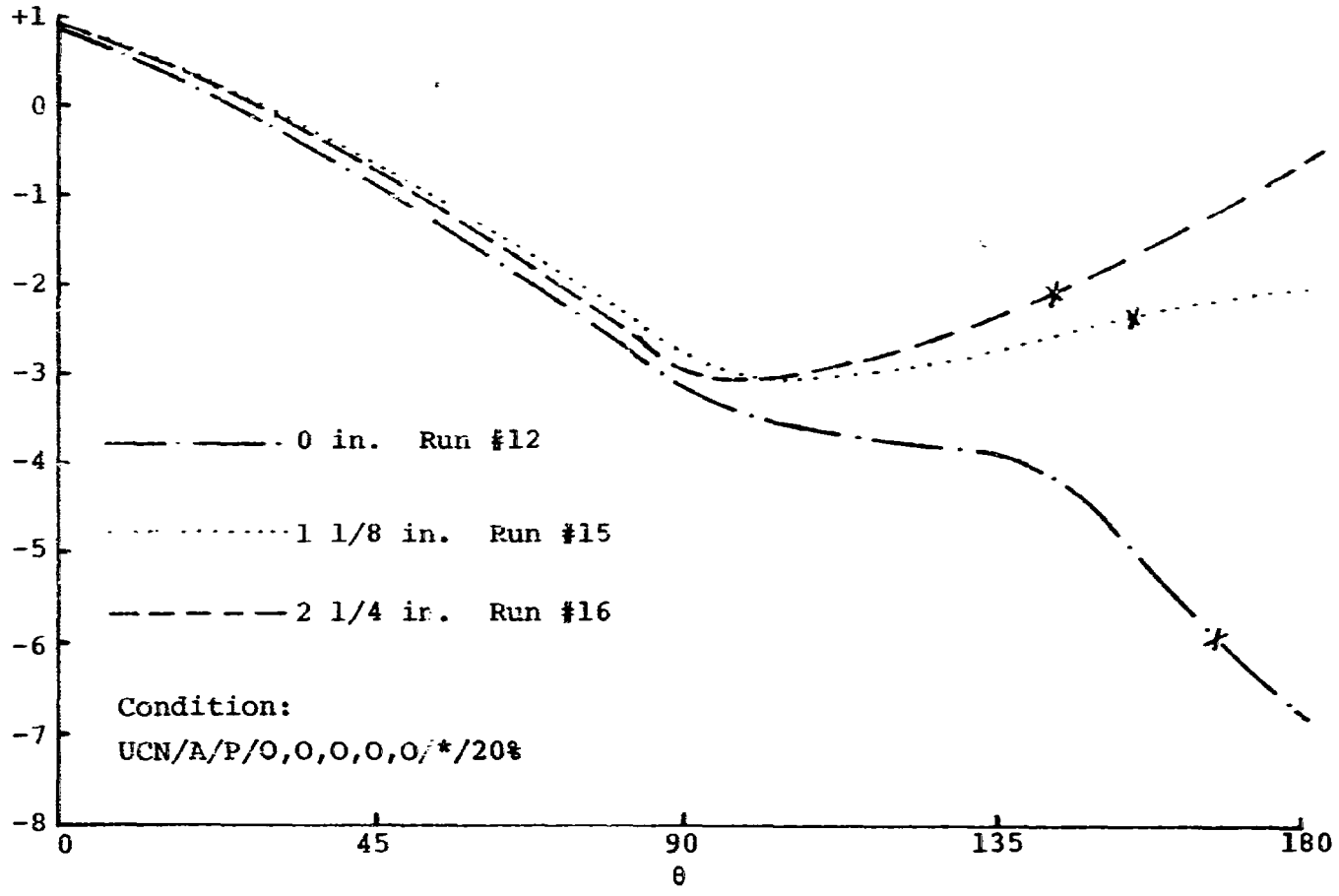

Figure 23. Cylindrical-Spherical Pressure Distribution--
Effect of Turret-Fairing Gap with Porous FBS

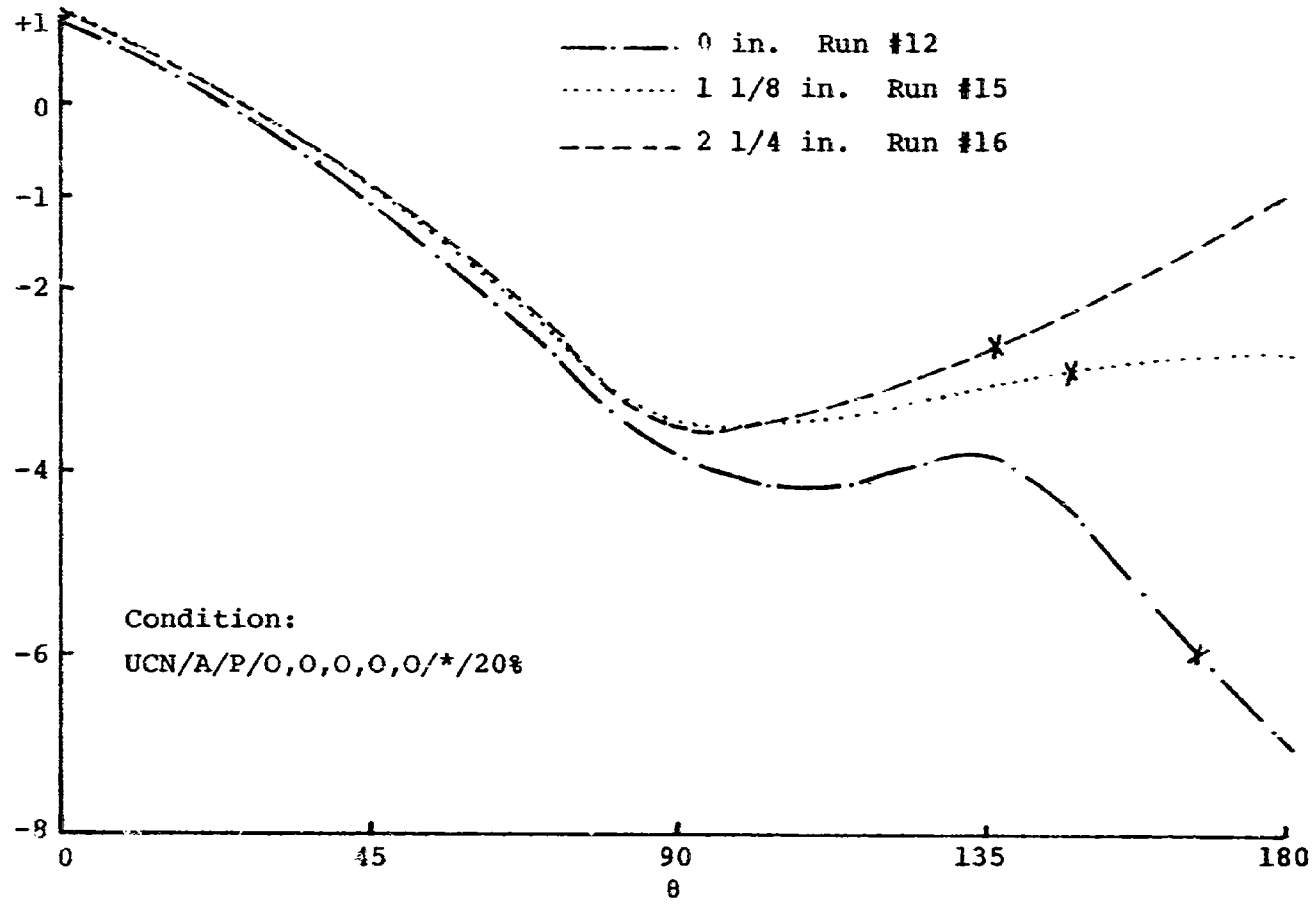

Figure 24. Cylindrical Pressure Distribution--
Effect of Turret-Fairing Gap
with Porous FBS

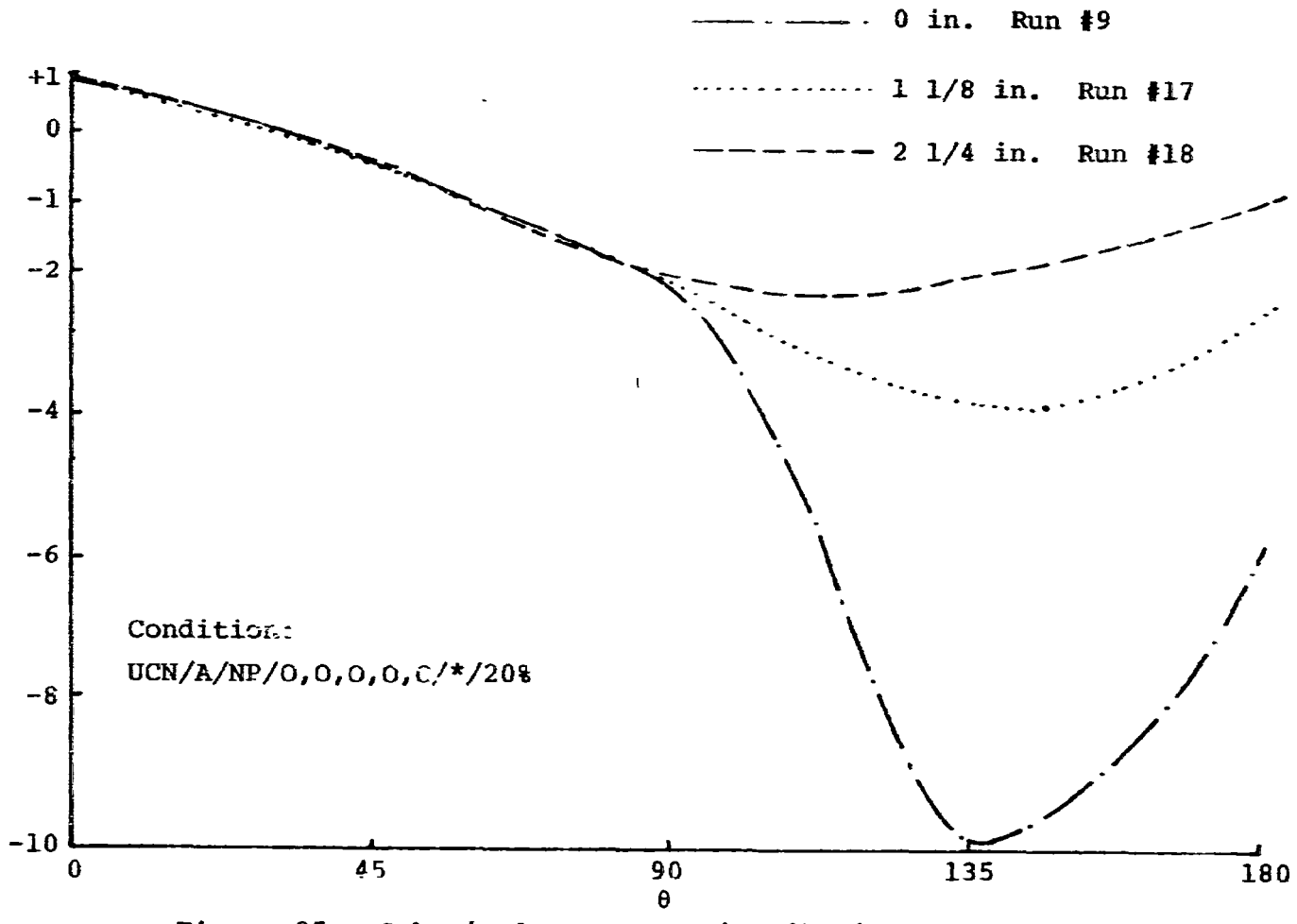

Figure 25. Spherical Pressure Distribution--
Effect of Turret-Fairing Gap
with Non-Porous FBS

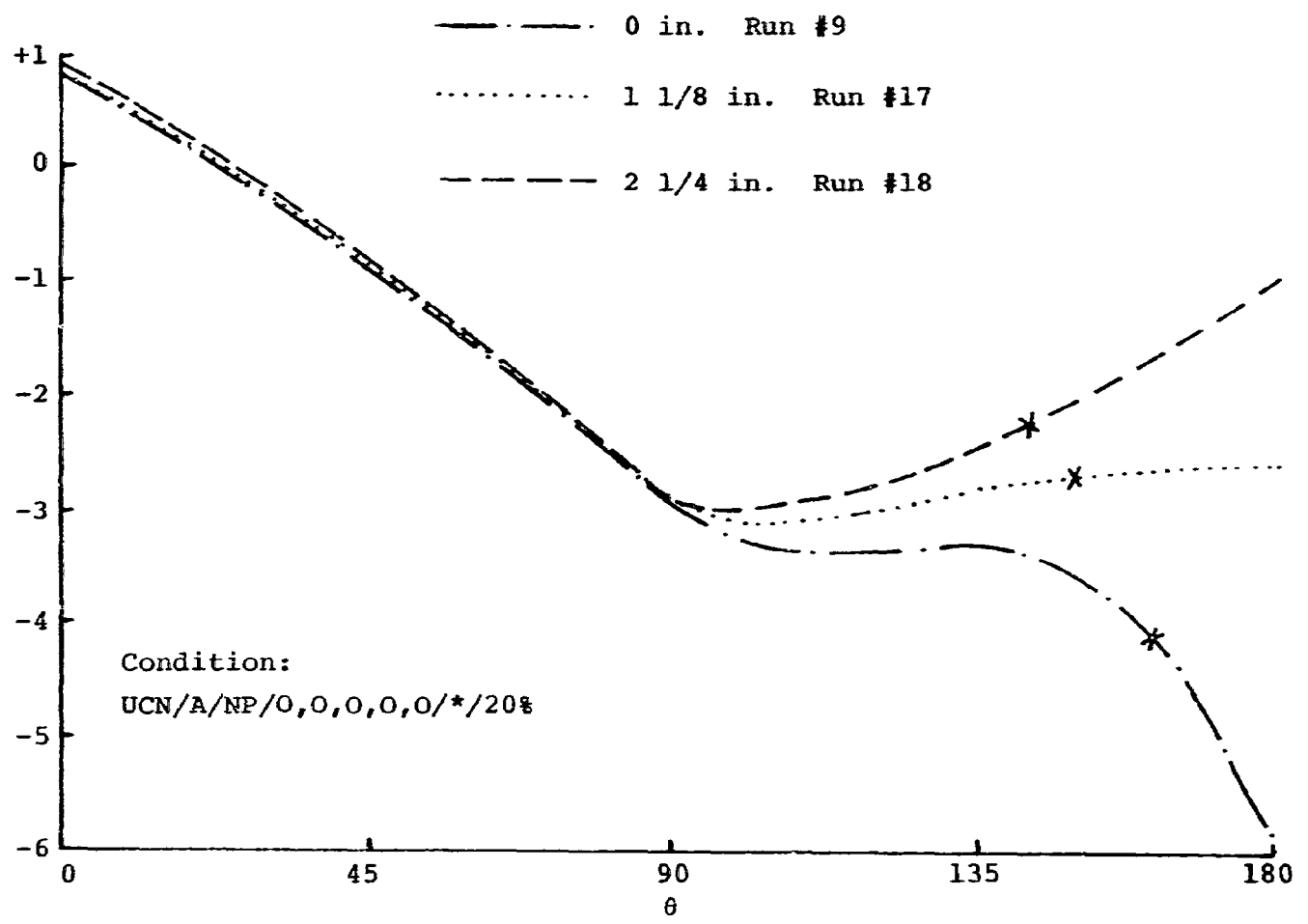

Figure 26. Cylindrical-Spherical Pressure Distribution--
Effect of Turret-Fairing Gap with Non-Porous FBS

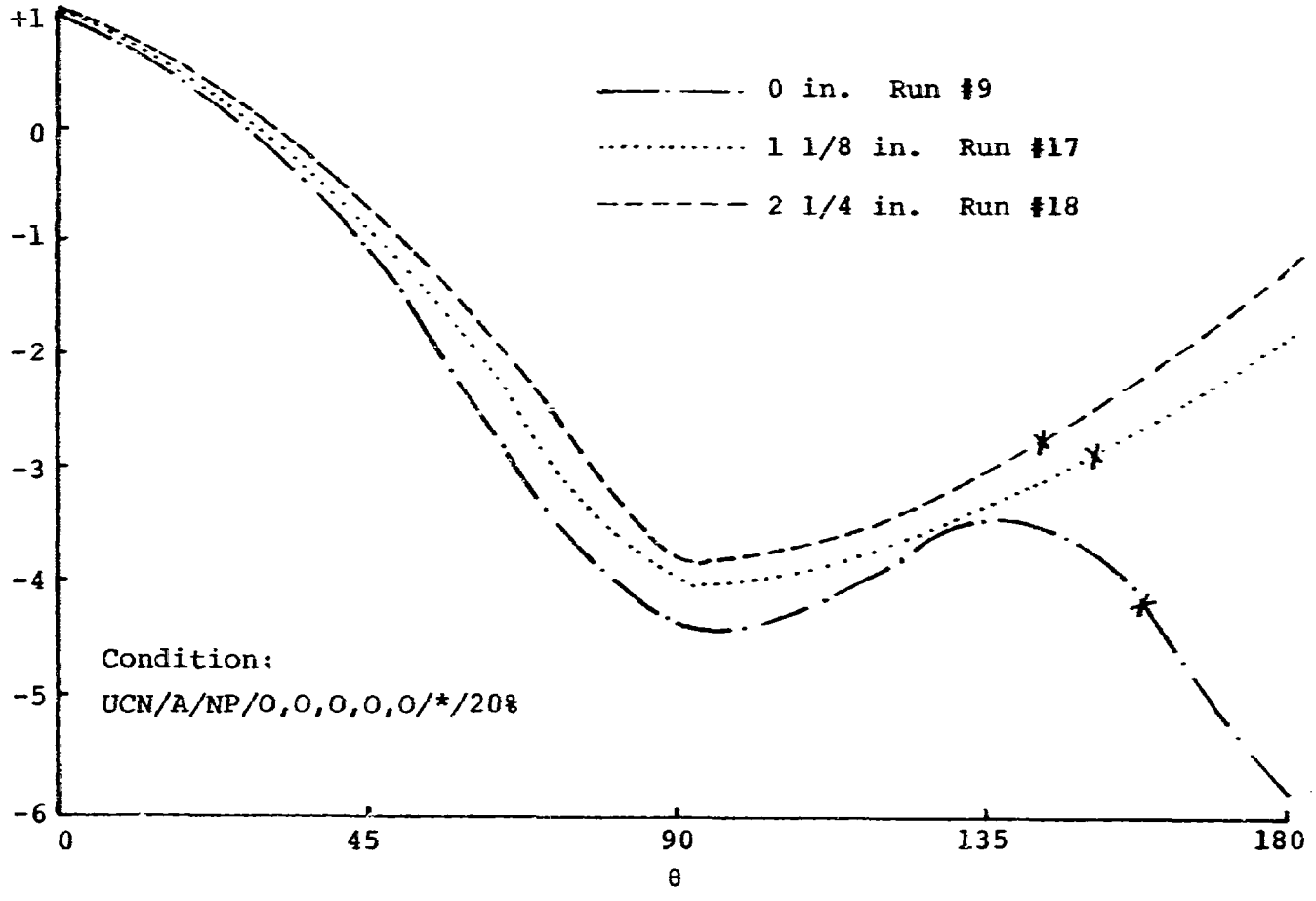

Figure 27. Cylindrical Pressure Distribution--
Effect of Turret-Fairing Gap
with Non-Porous FBS

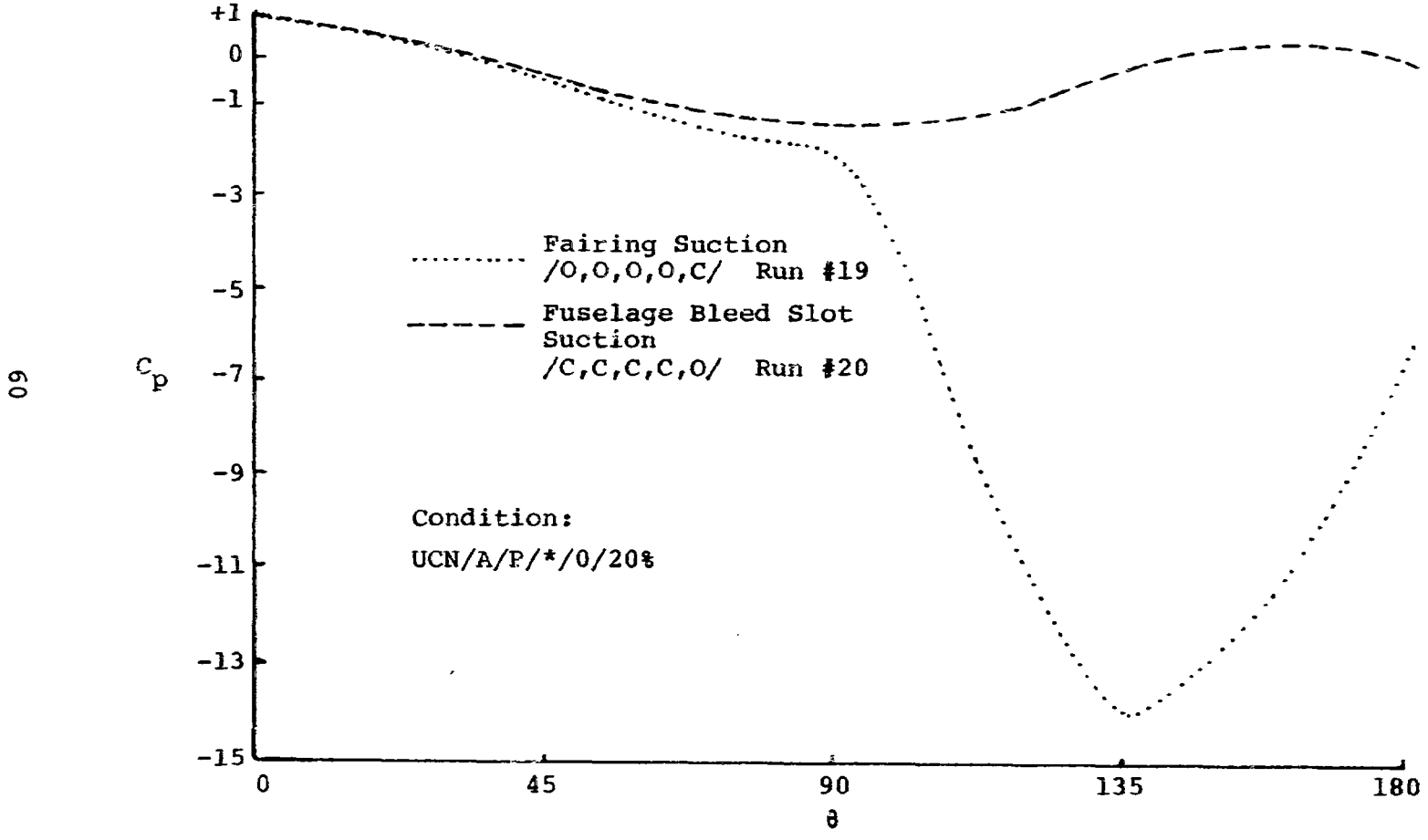

Figure 28. Spherical Pressure Distribution--
Effect of Fairing and FBS Suction

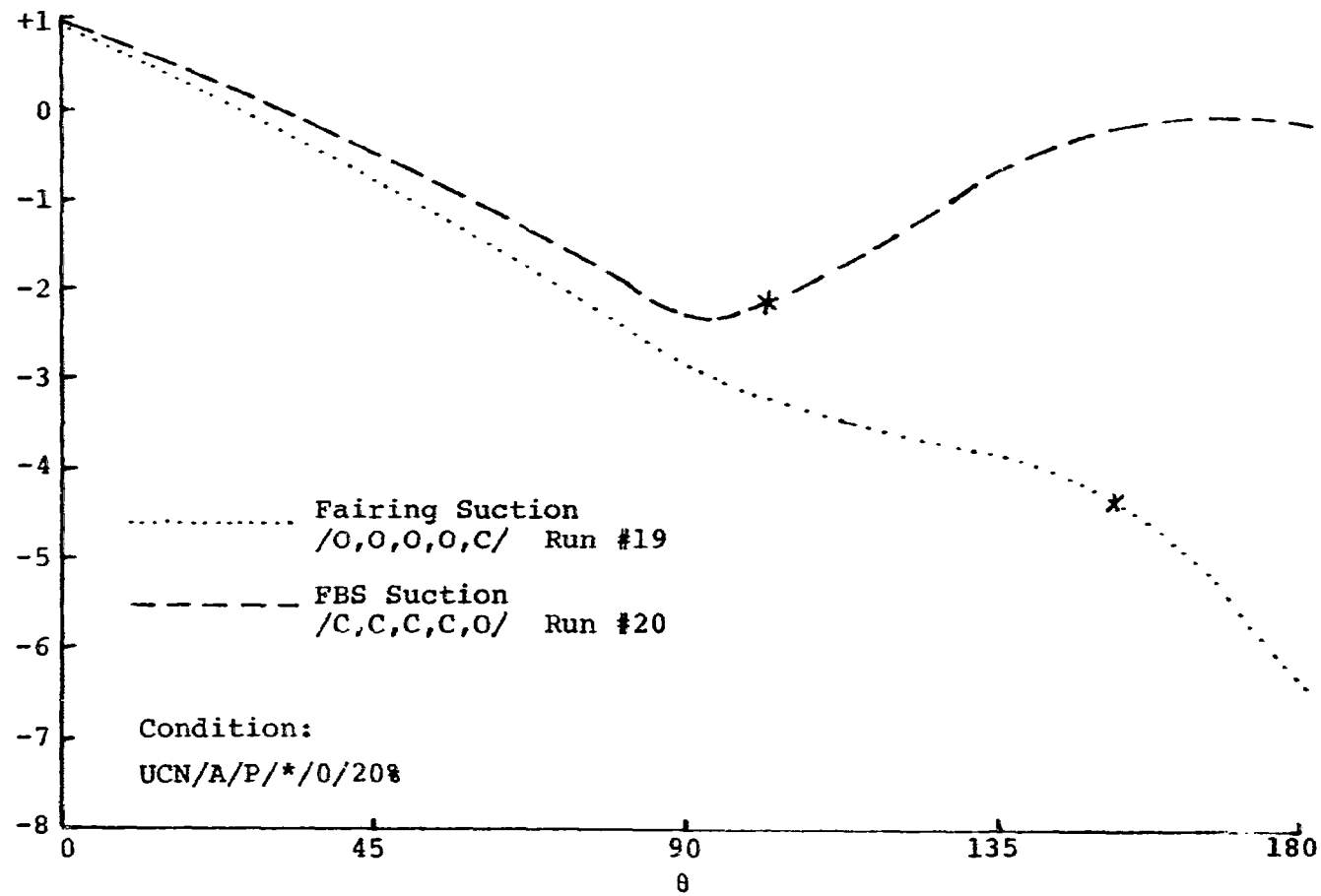

Figure 29. Cylindrical-Spherical Pressure Distribution-Effect of Fairing and FBS Suction

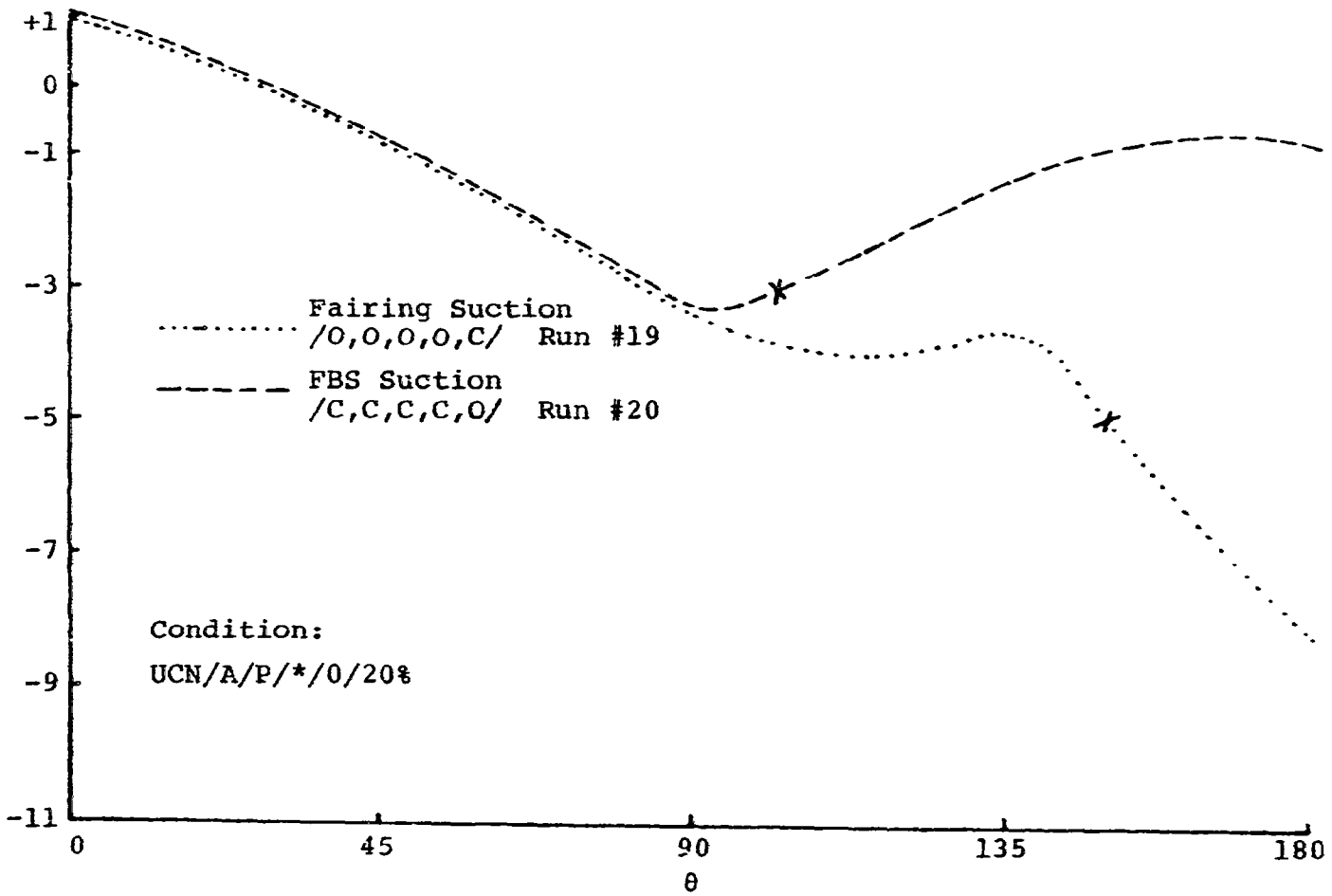

Figure 30. Cylindrical Pressure Distribution--
Effect of Fairing and FBS Suction

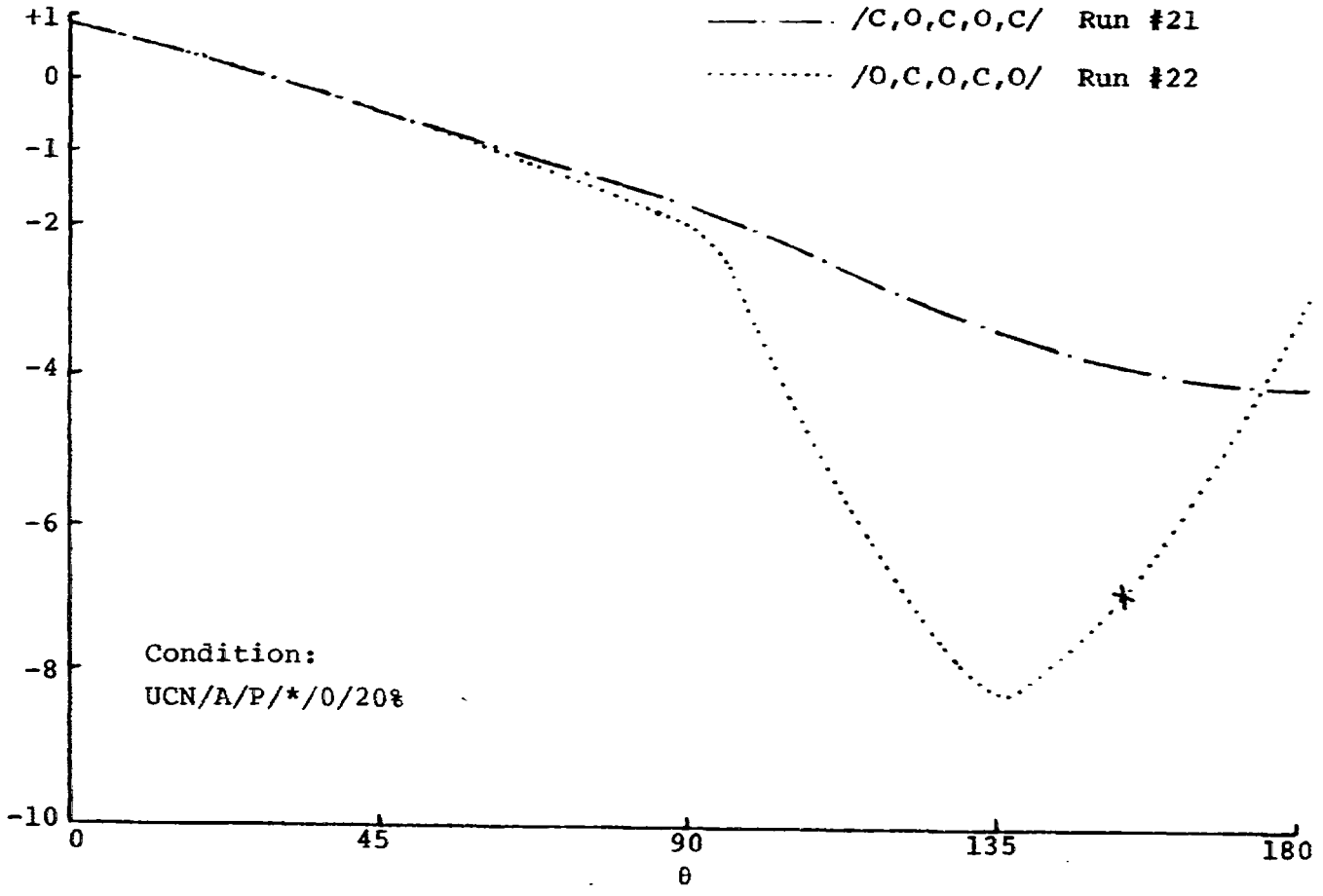

Figure 31. Spherical Pressure Distribution--
Effect of Alternate Throttle Closing

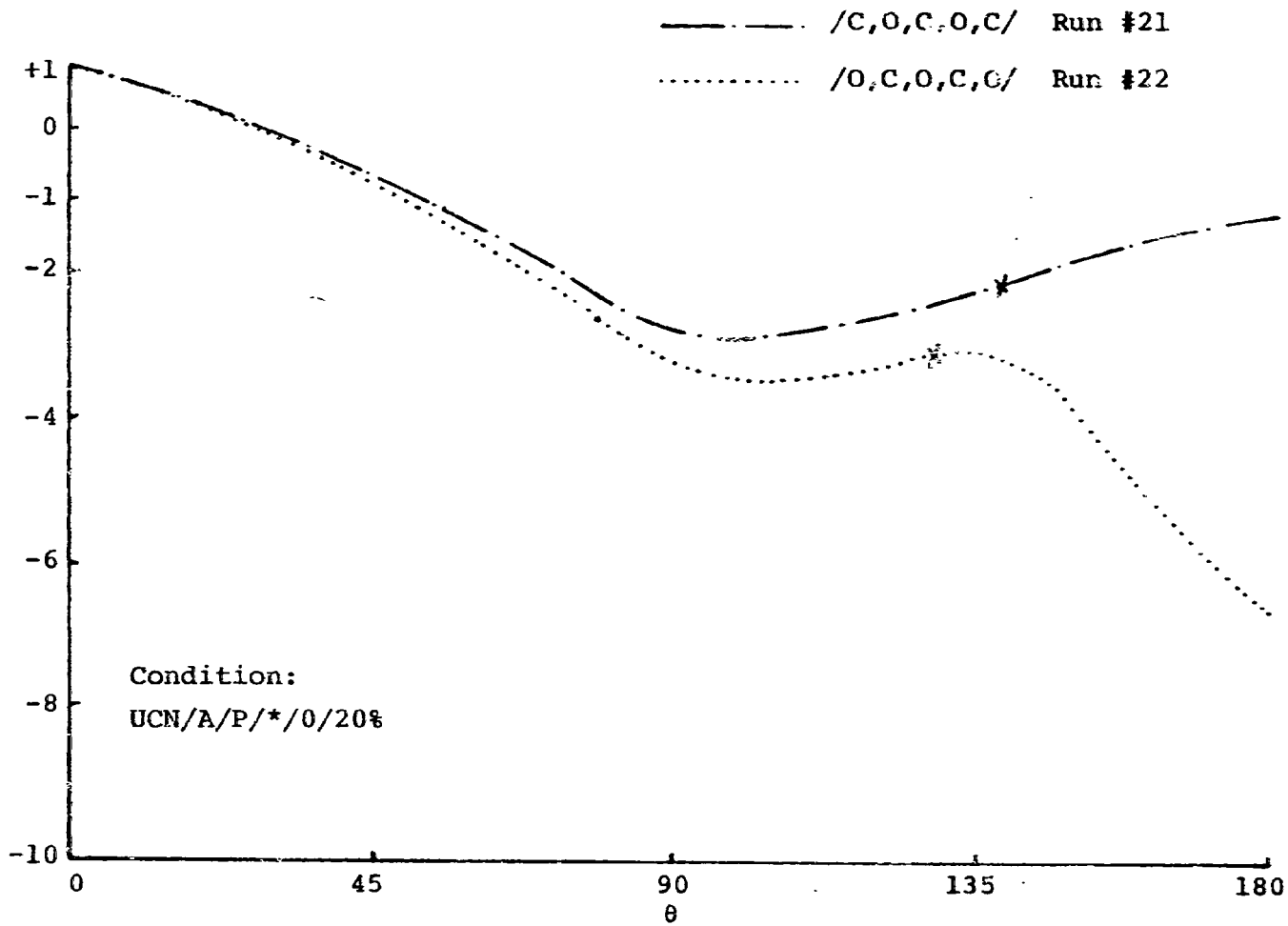

Figure 32. Cylindrical Pressure Distribution--
Effect of Alternate Throttle Closing

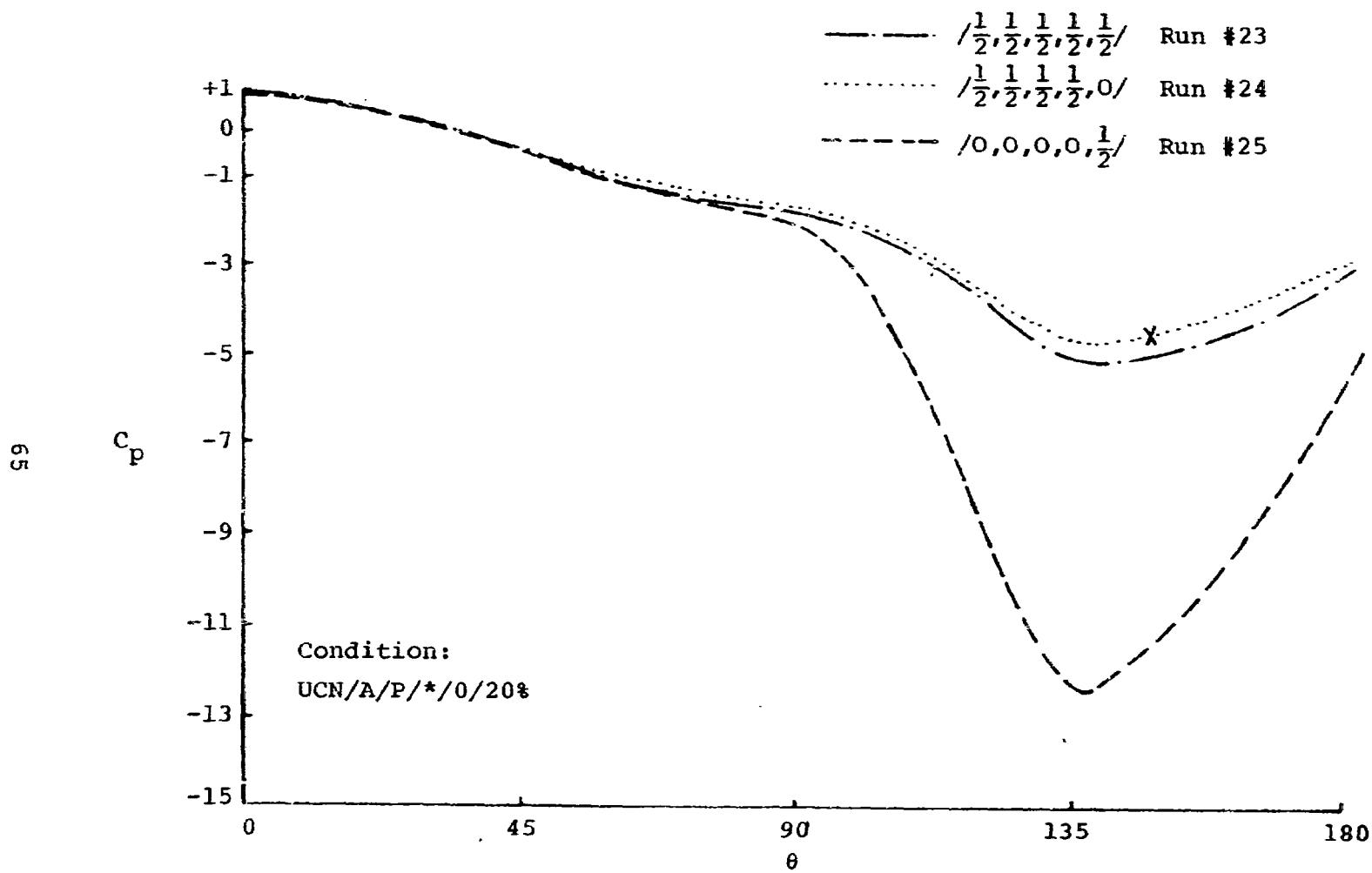

Figure 33. Spherical Pressure Distribution--
Effect of Half Throttle Settings

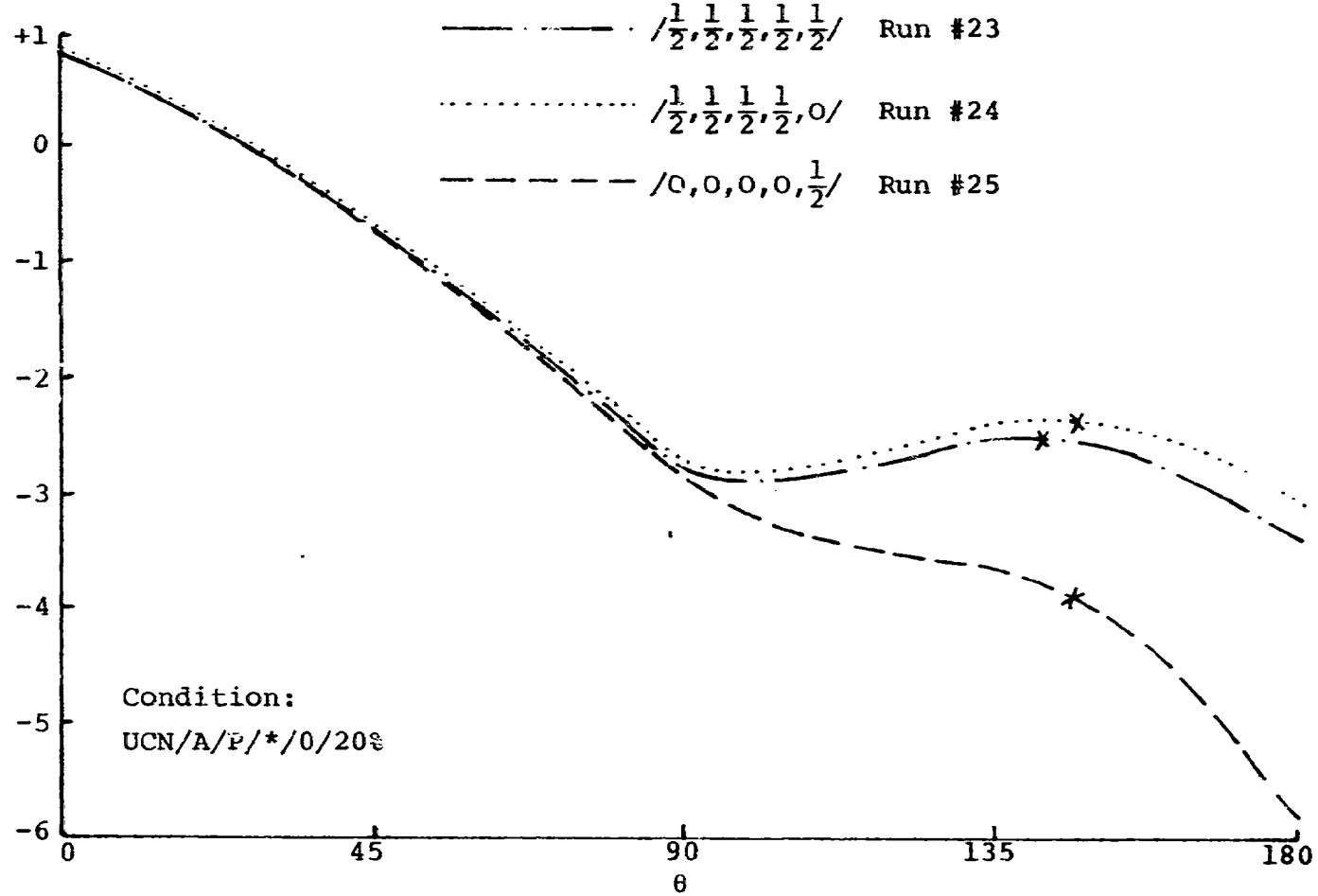

Figure 34. Cylindrical-Spherical Pressure Distribution--
Effect of Half Throttle Settings

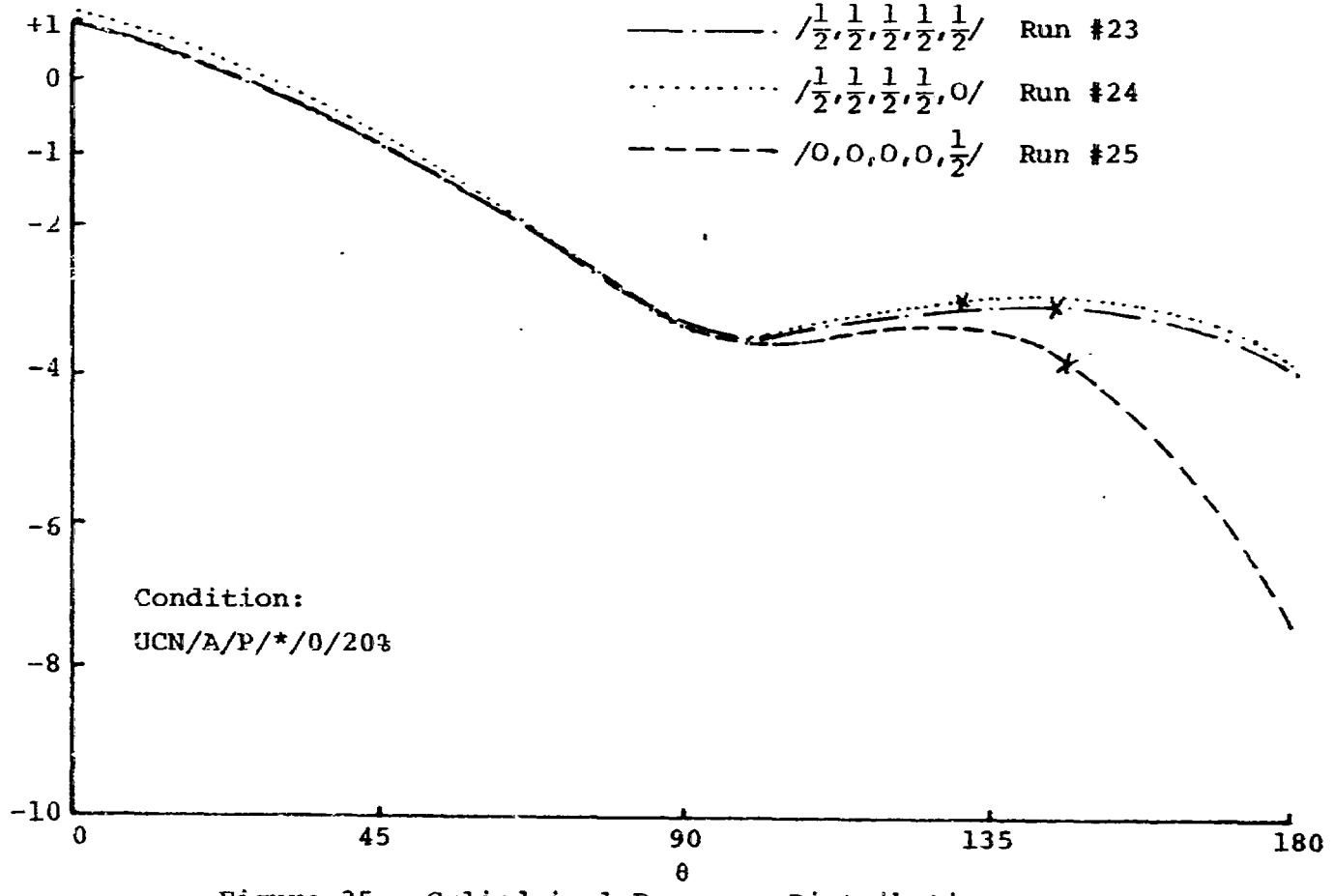

Figure 35. Cylindrical Pressure Distribution--
Effect of Half Throttle Settings

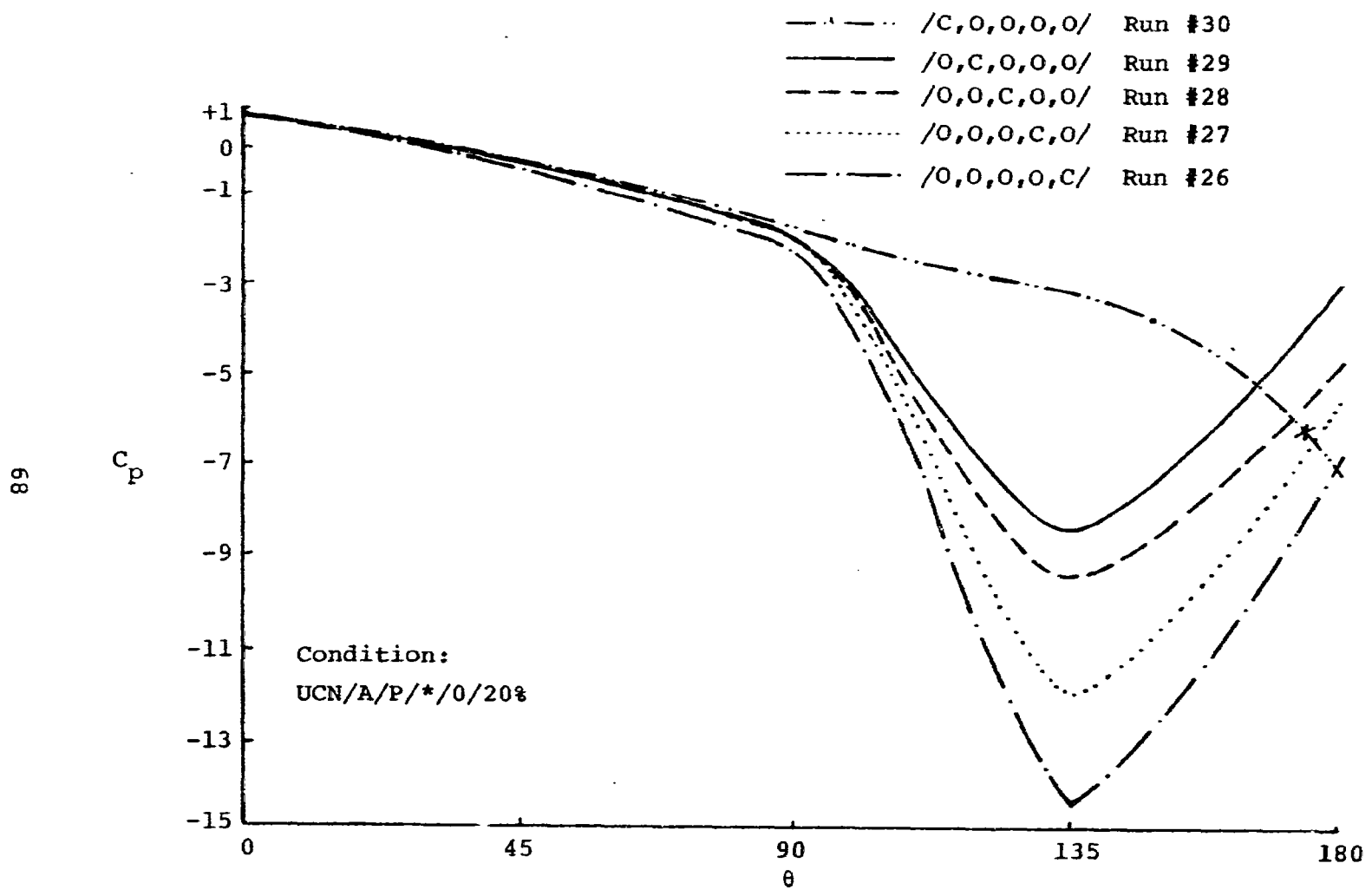

Figure 36. Spherical Pressure Distribution--
Effect of Selectively Closing One Throttle

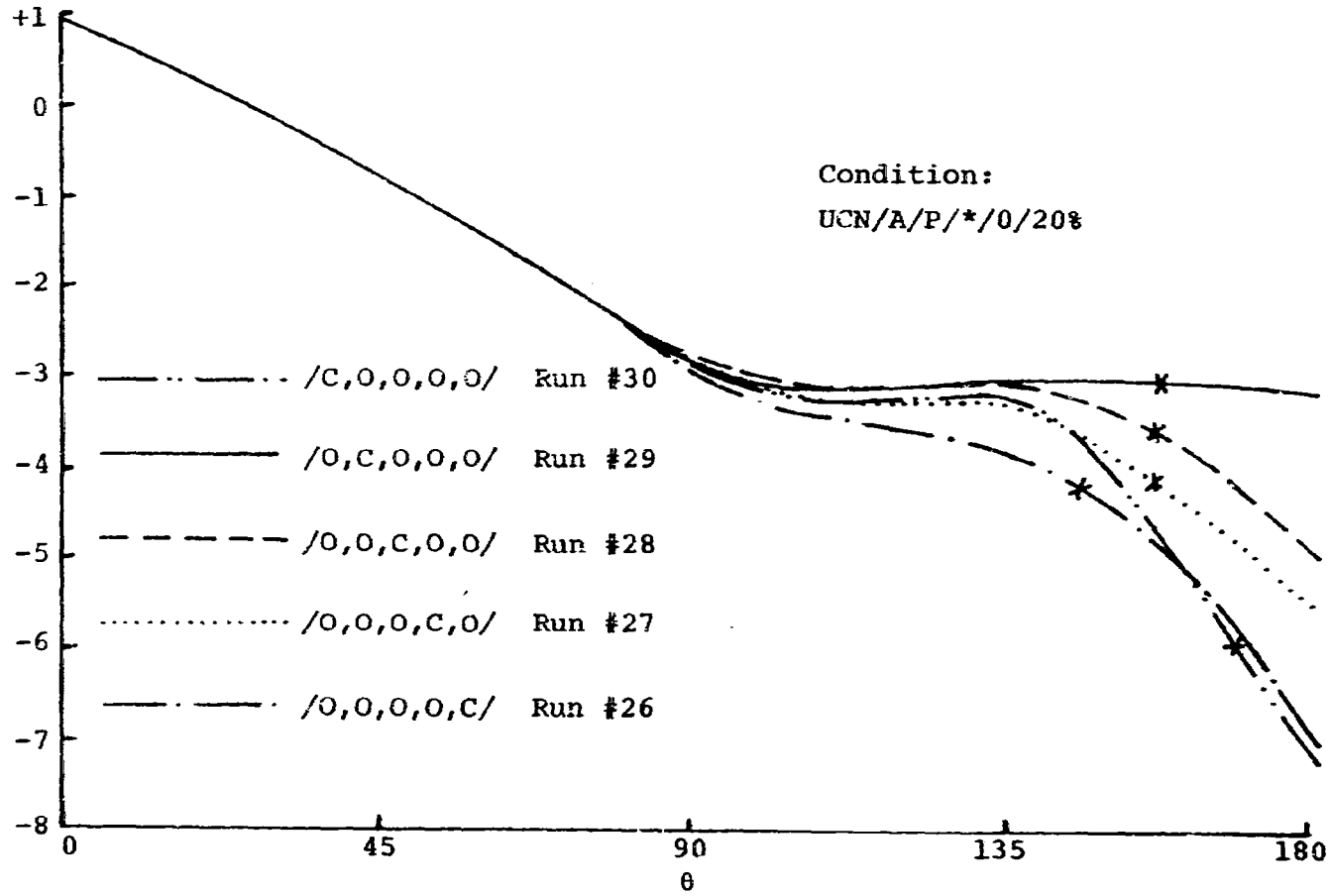

Figure 37. Cylindrical-Spherical Pressure Distribution--
Effect of Selectively Closing One Throttle

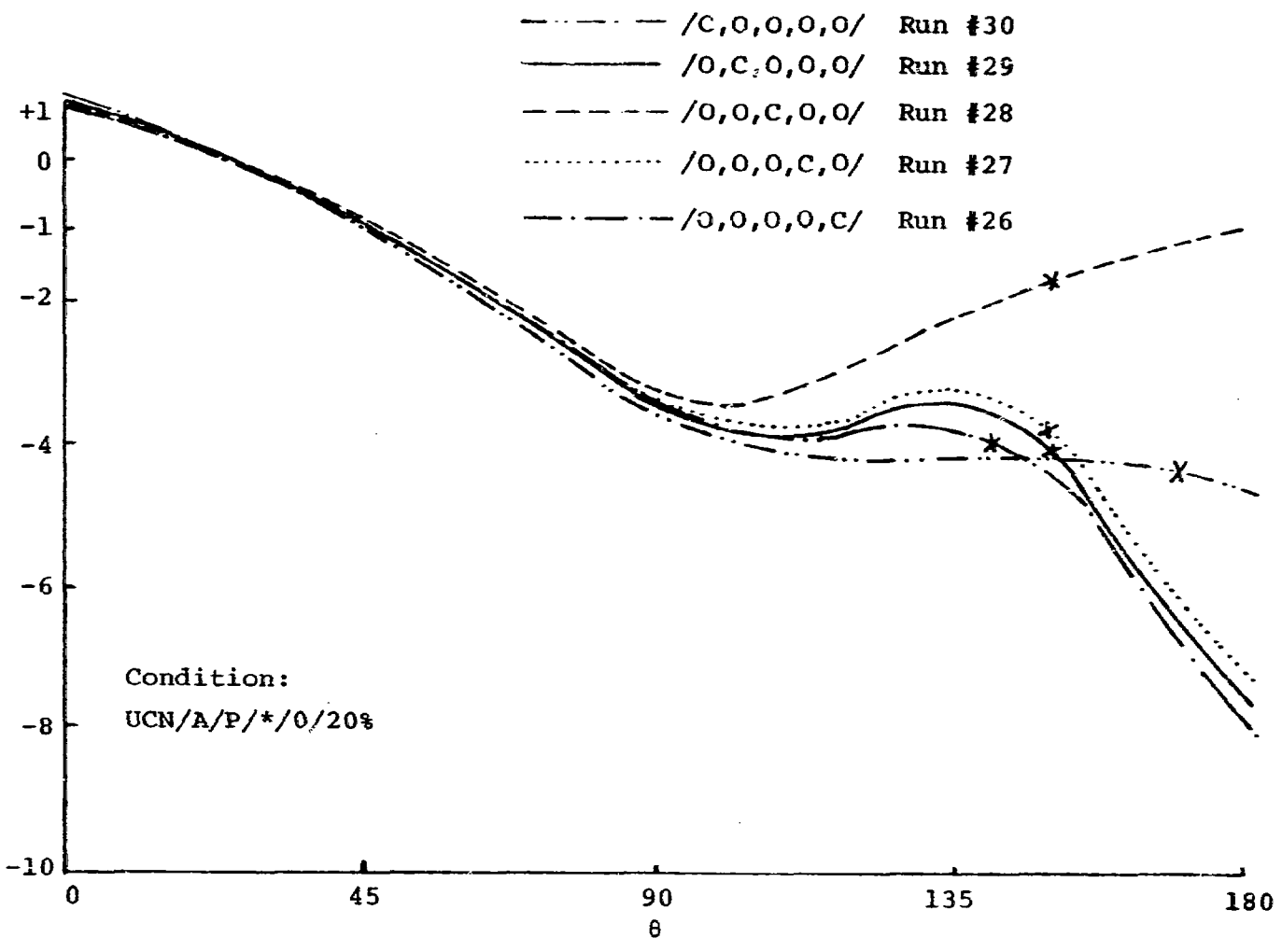

Figure 38. Cylindrical Pressure Distribution--
Effect of Selectively Closing One Throttle

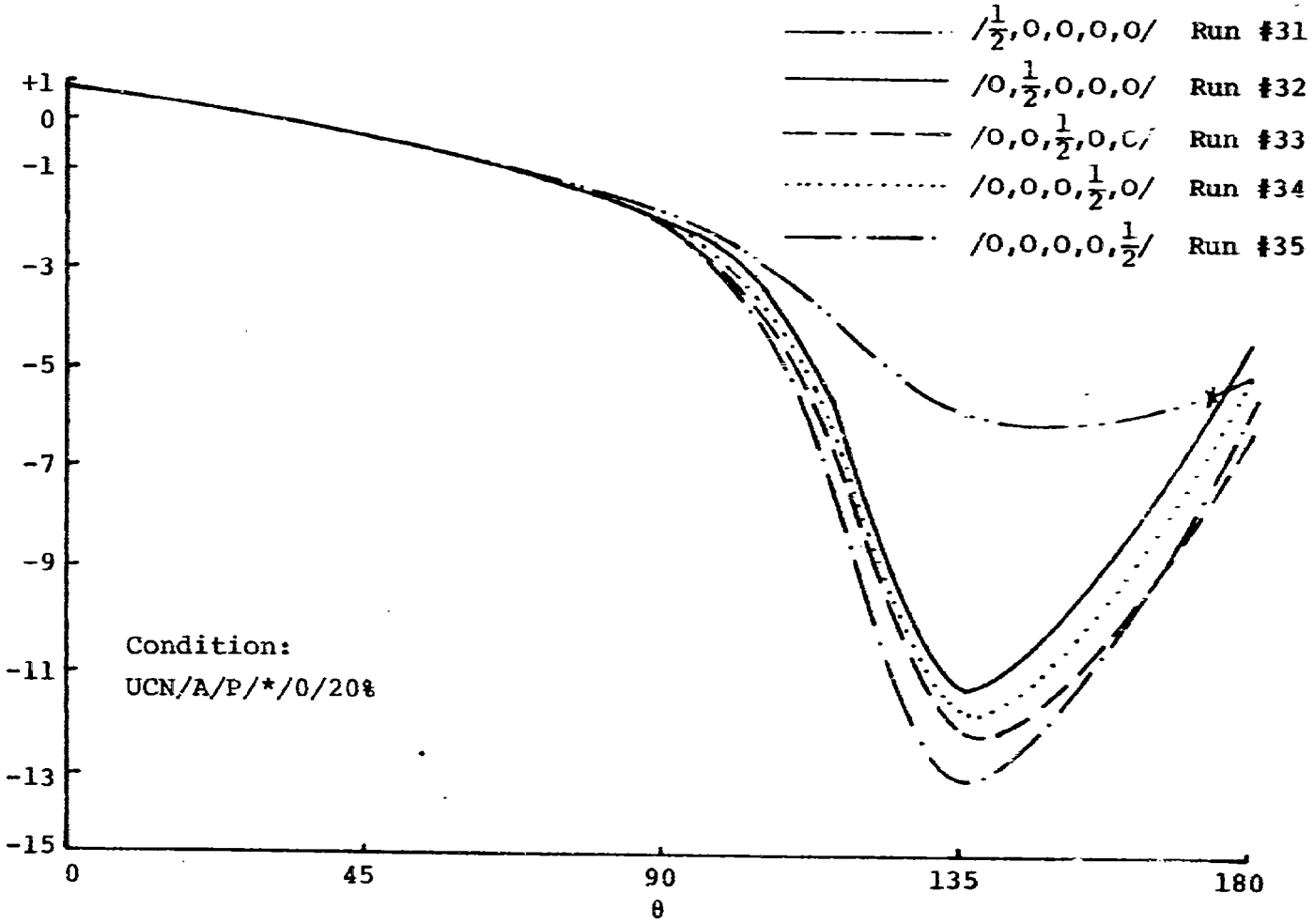

Figure 39. Spherical Pressure Distribution--
Effect of Selectively Half-Closing One Throttle

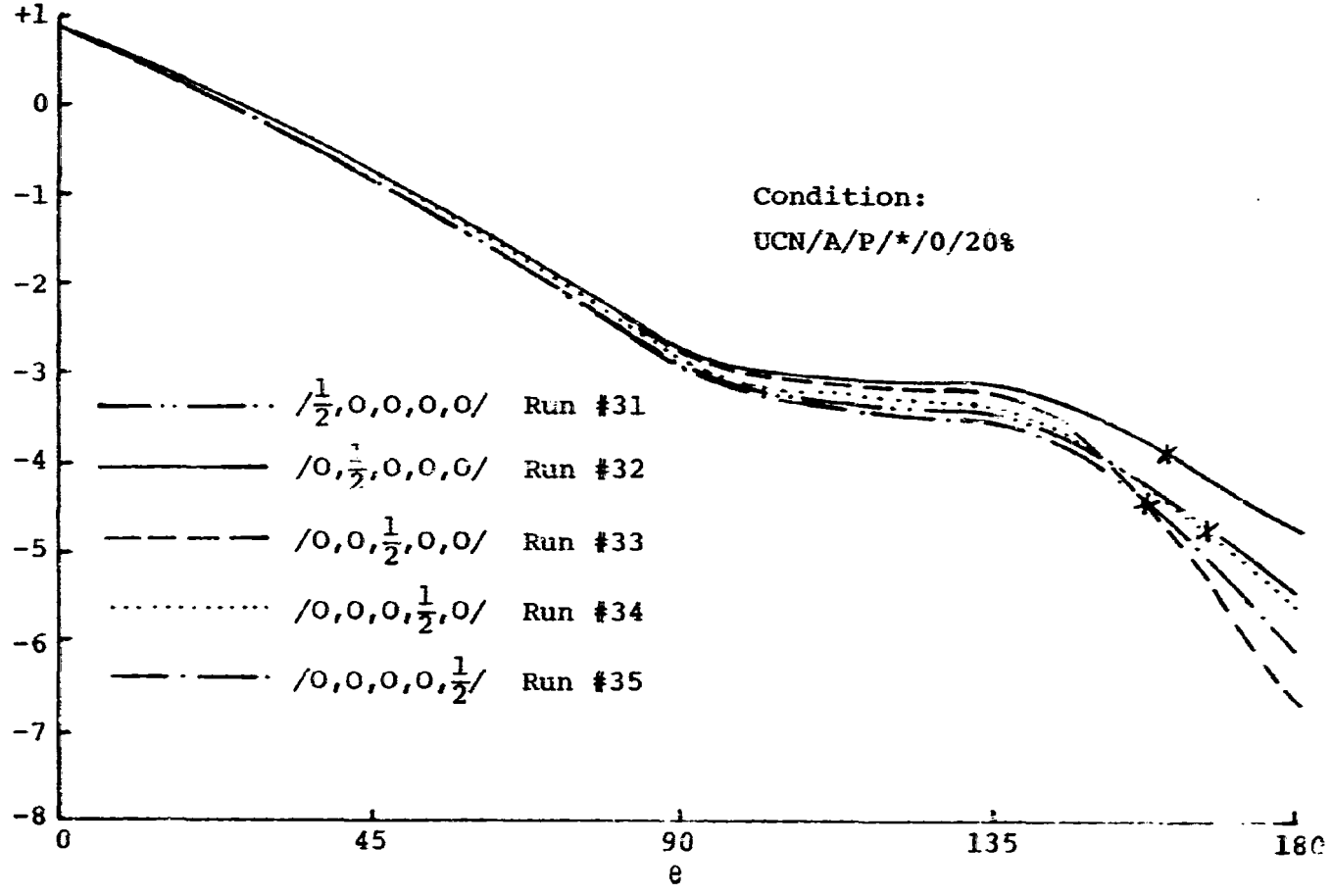

Figure 40. Cylindrical-Spherical Pressure Distribution--
Effect of Selectively Half-Closing One Throttle

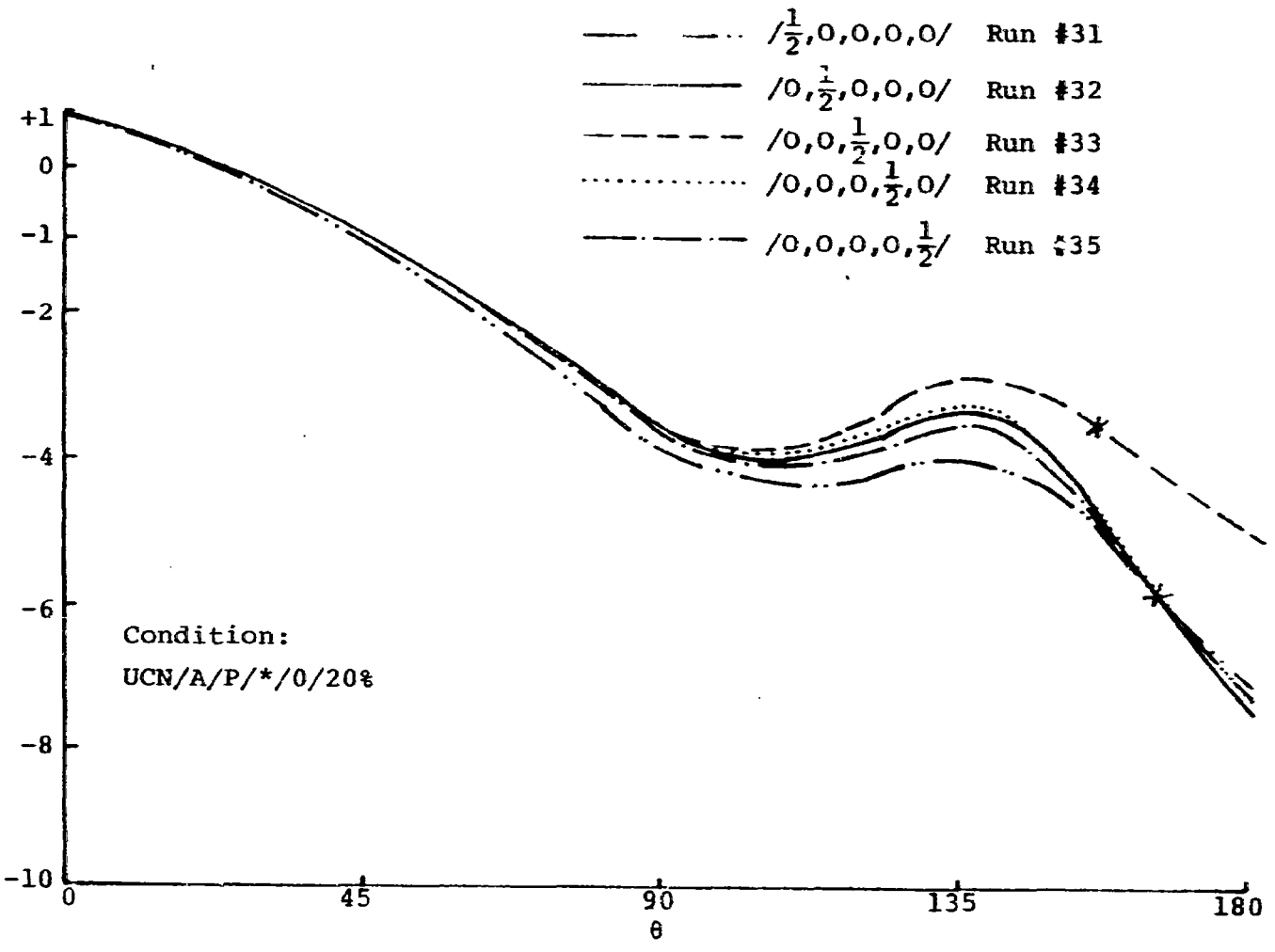

Figure 41. Cylindrical Pressure Distribution--
Effect of Selectively Half-Closing One Throttle

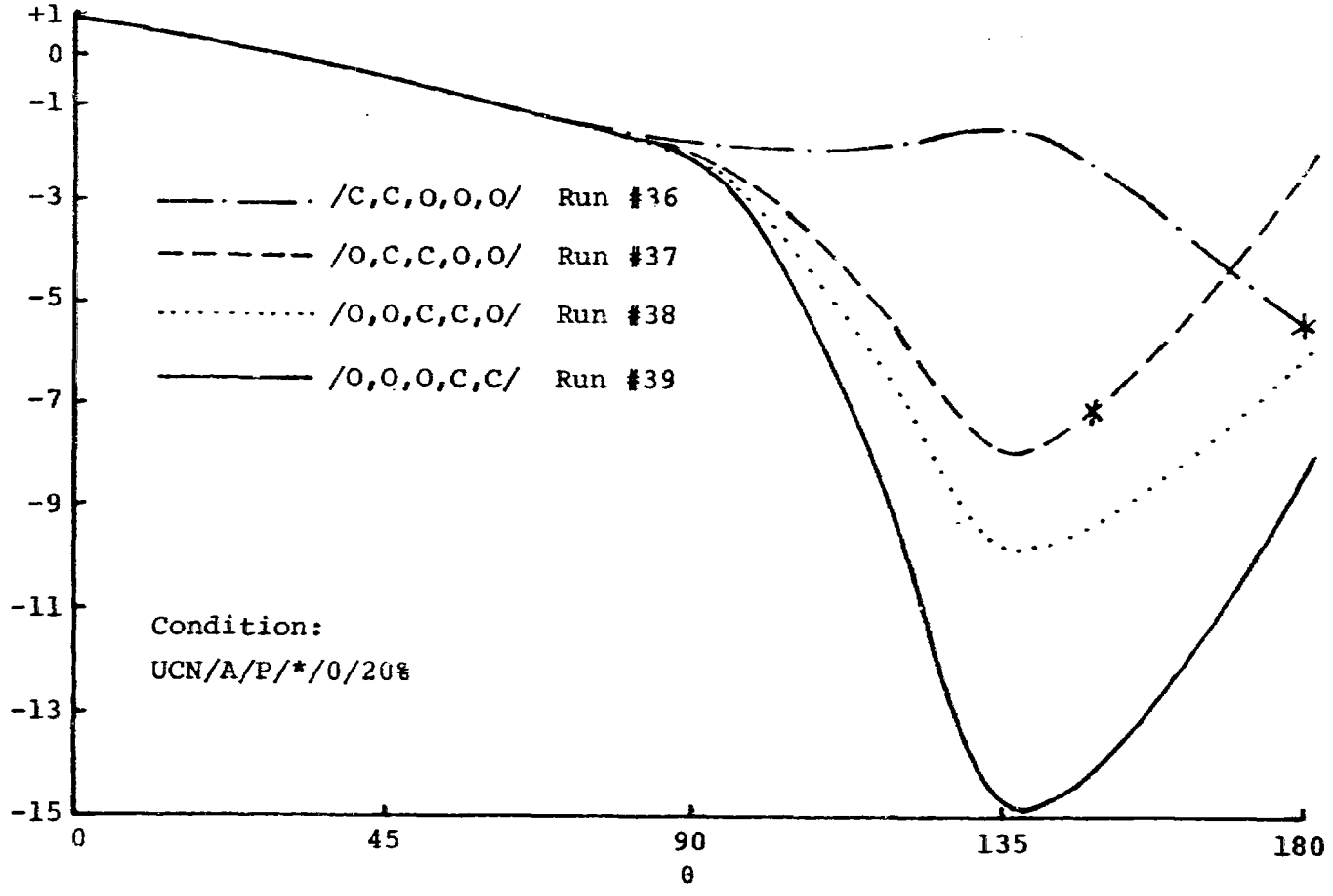

Figure 42. Spherical Pressure Distribution--
Effect of Closing Two Adjacent Throttles

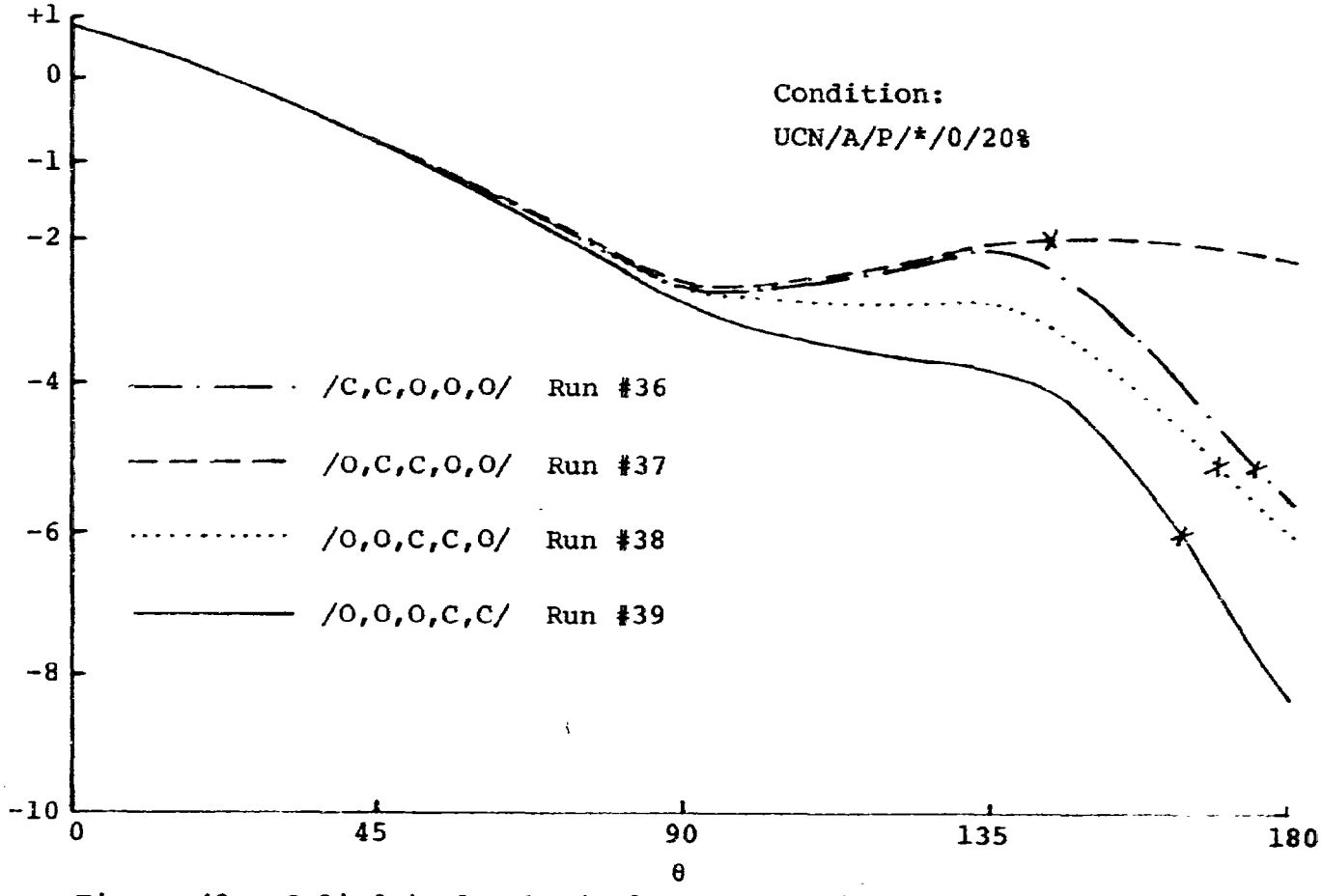

Figure 43. Cylindrical-Spherical Pressure Distribution--
Effect of Closing Two Adjacent Throttles

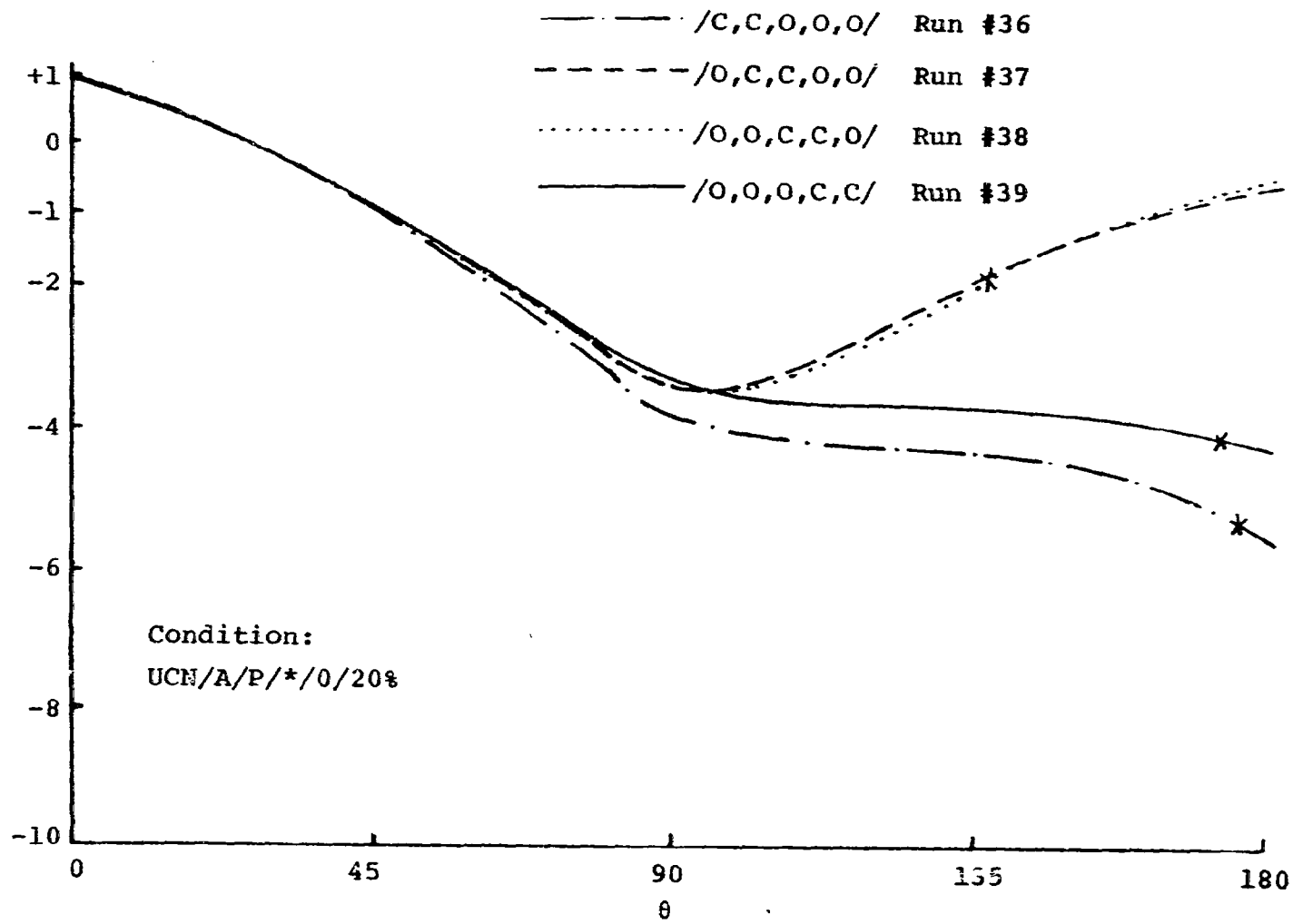

Figure 44. Cylindrical Pressure Distribution--
Effect of Closing Two Adjacent Throttles

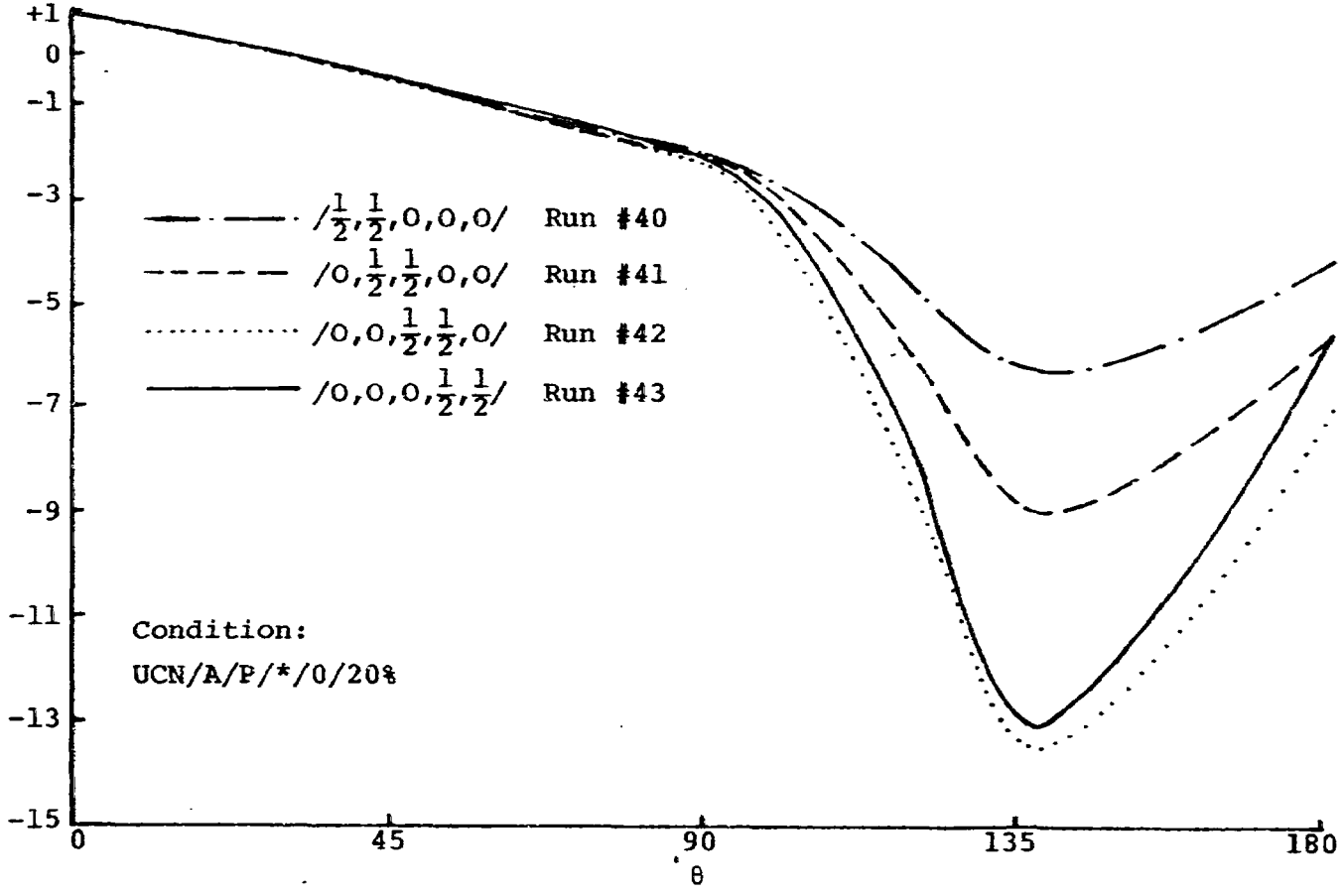

Figure 45. Spherical Pressure Distribution--
Effect of Half Closing Two Adjacent Throttles

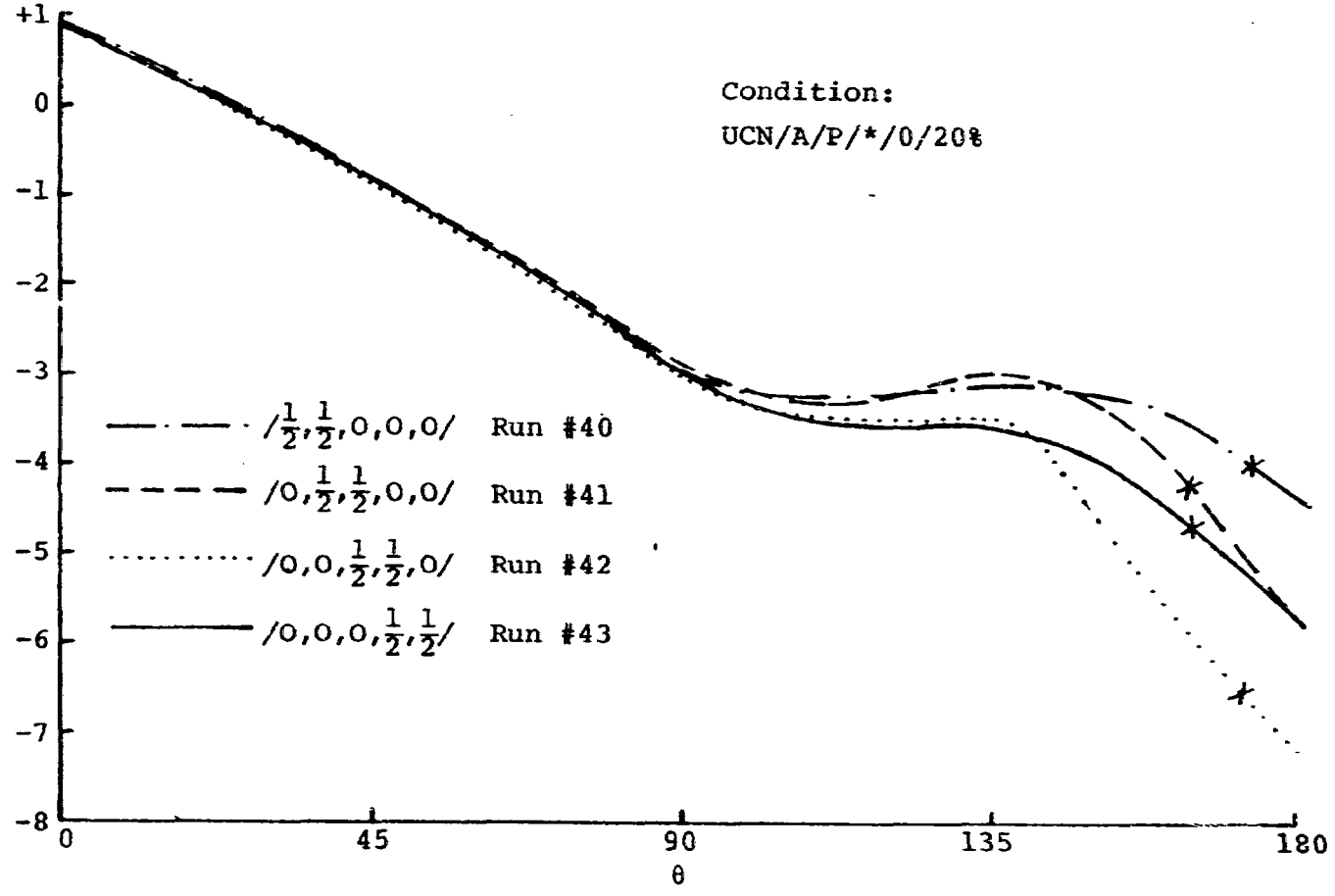

Figure 46. Cylindrical-Spherical Pressure Distribution--
Effect of Half-Closing Two Adjacent Throttles

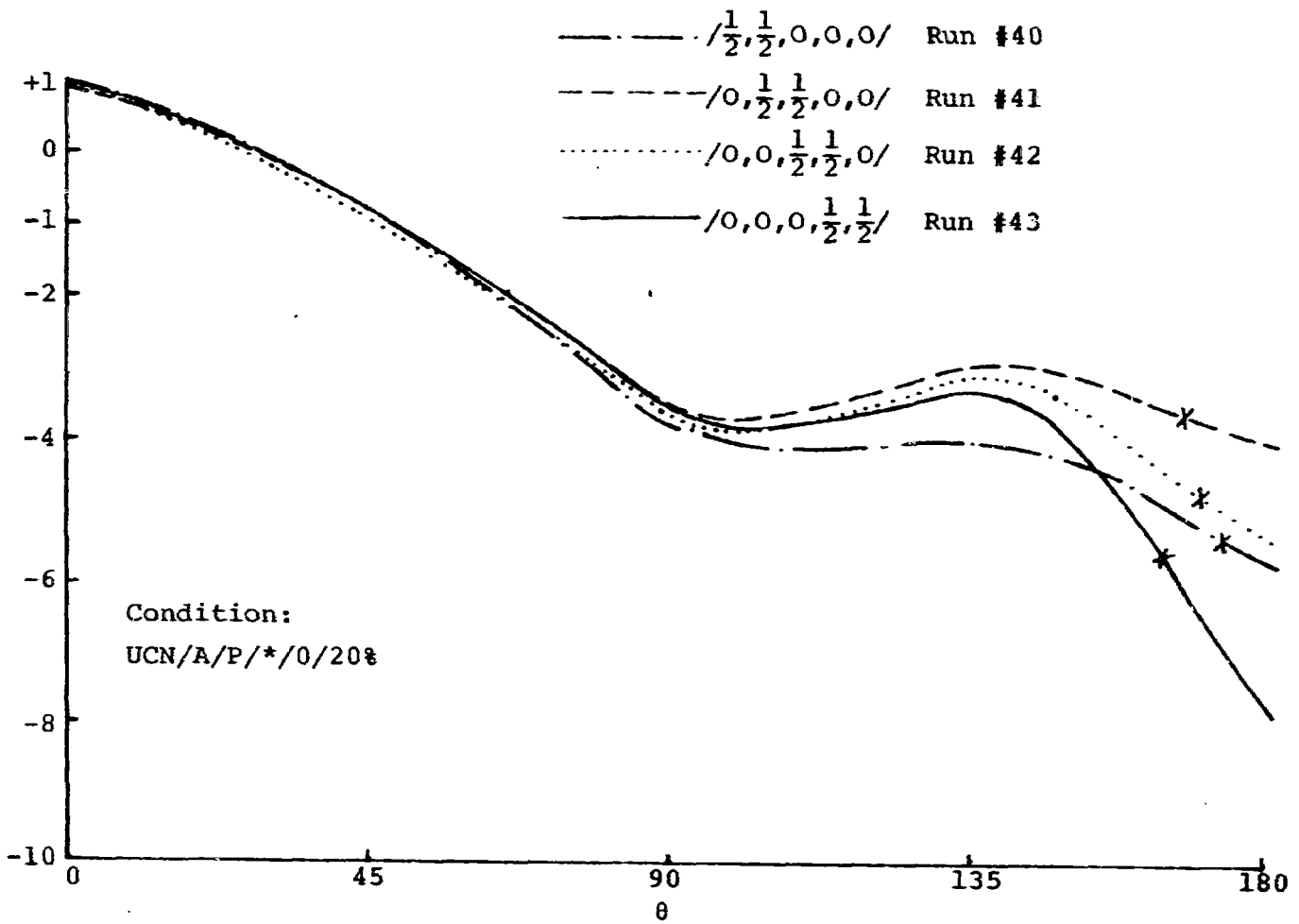

Figure 47. Cylindrical Pressure Distribution--
Effect of Half Closing Two Adjacent Throttles

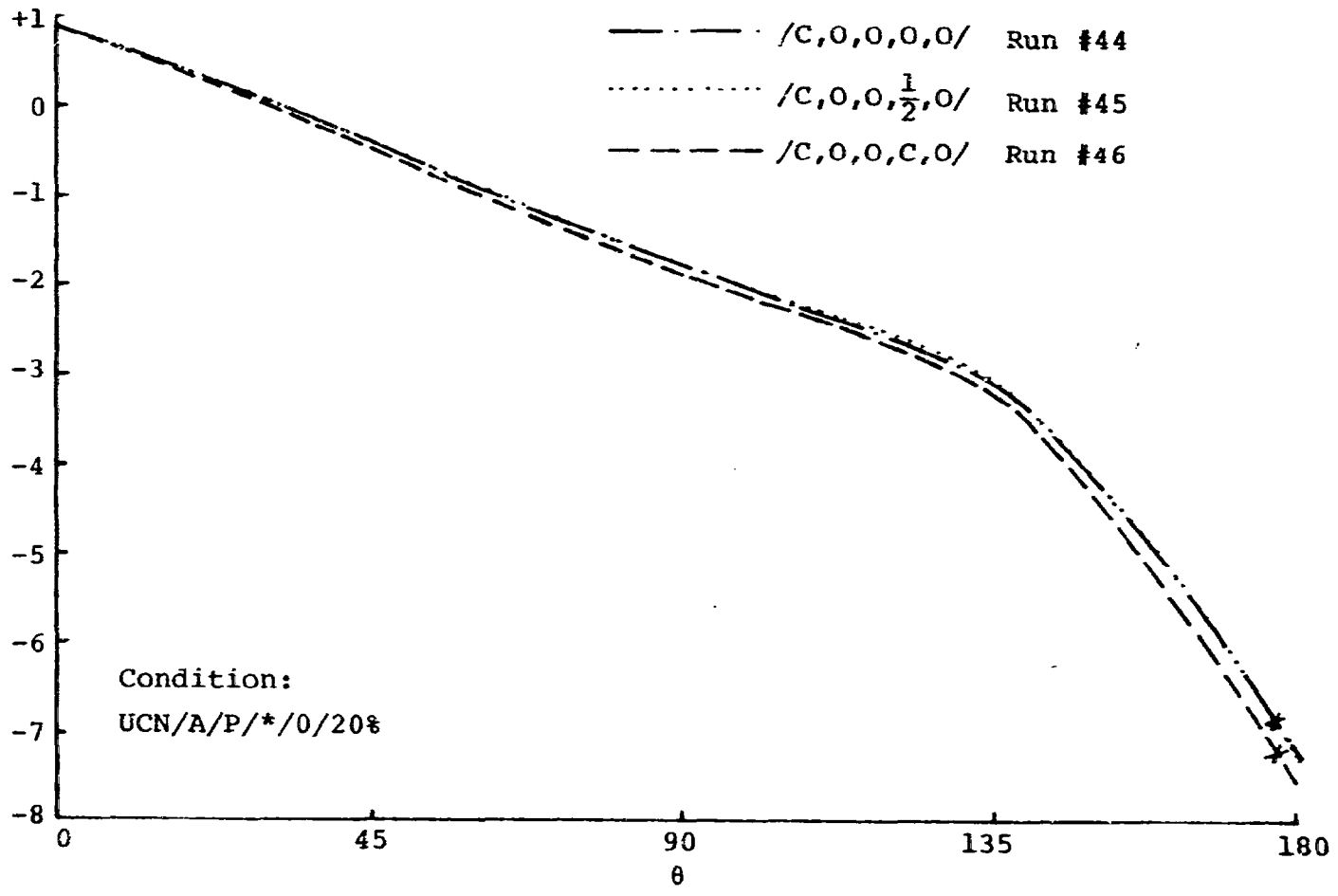

Figure 48. Spherical Pressure Distribution--
Effect of Throttle #4

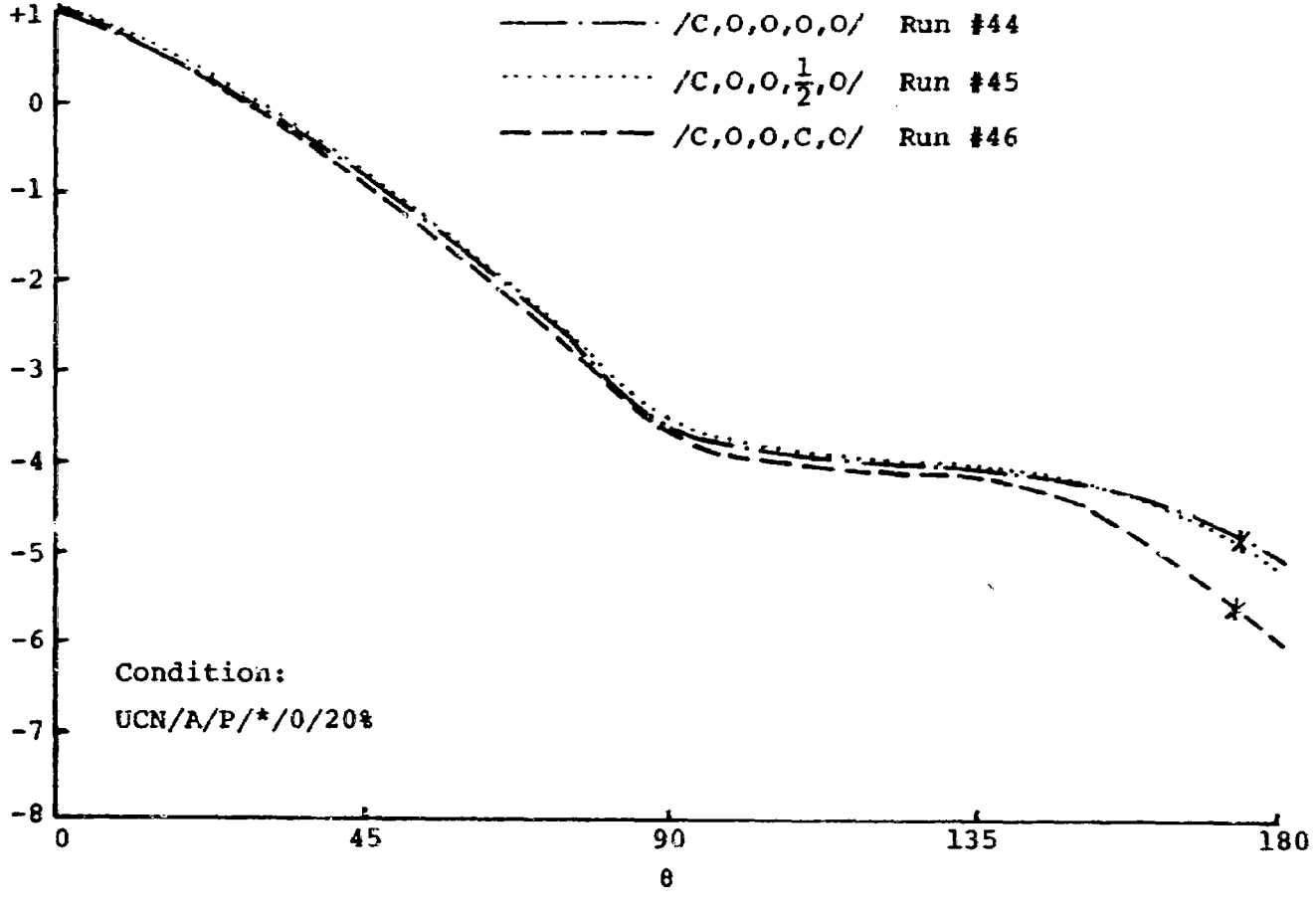

Figure 49. Cylindrical Pressure Distribution--
Effect of Throttle #4

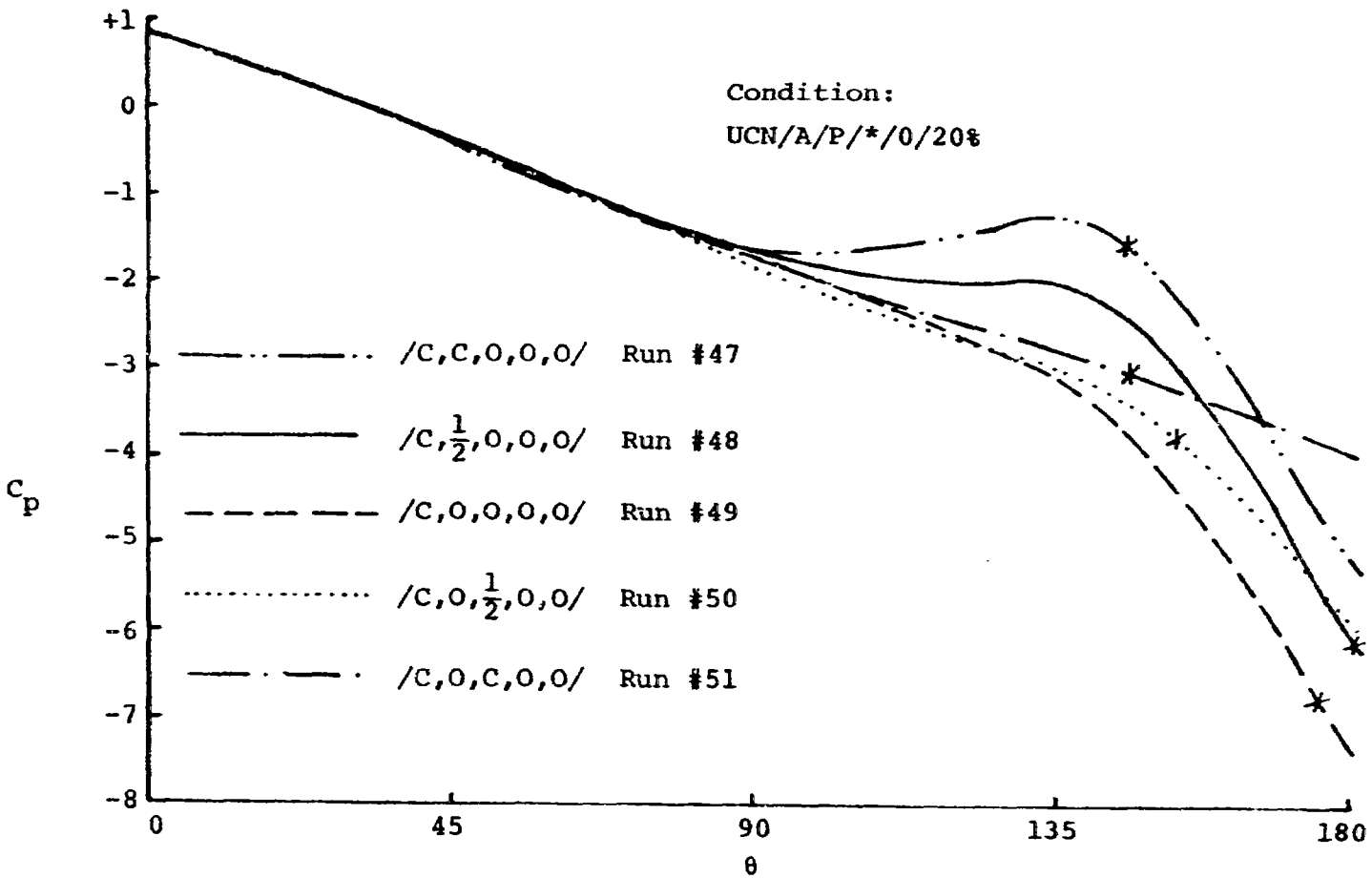

Figure 50. Spherical Pressure Distribution--
Effect of Throttles #2 and #3

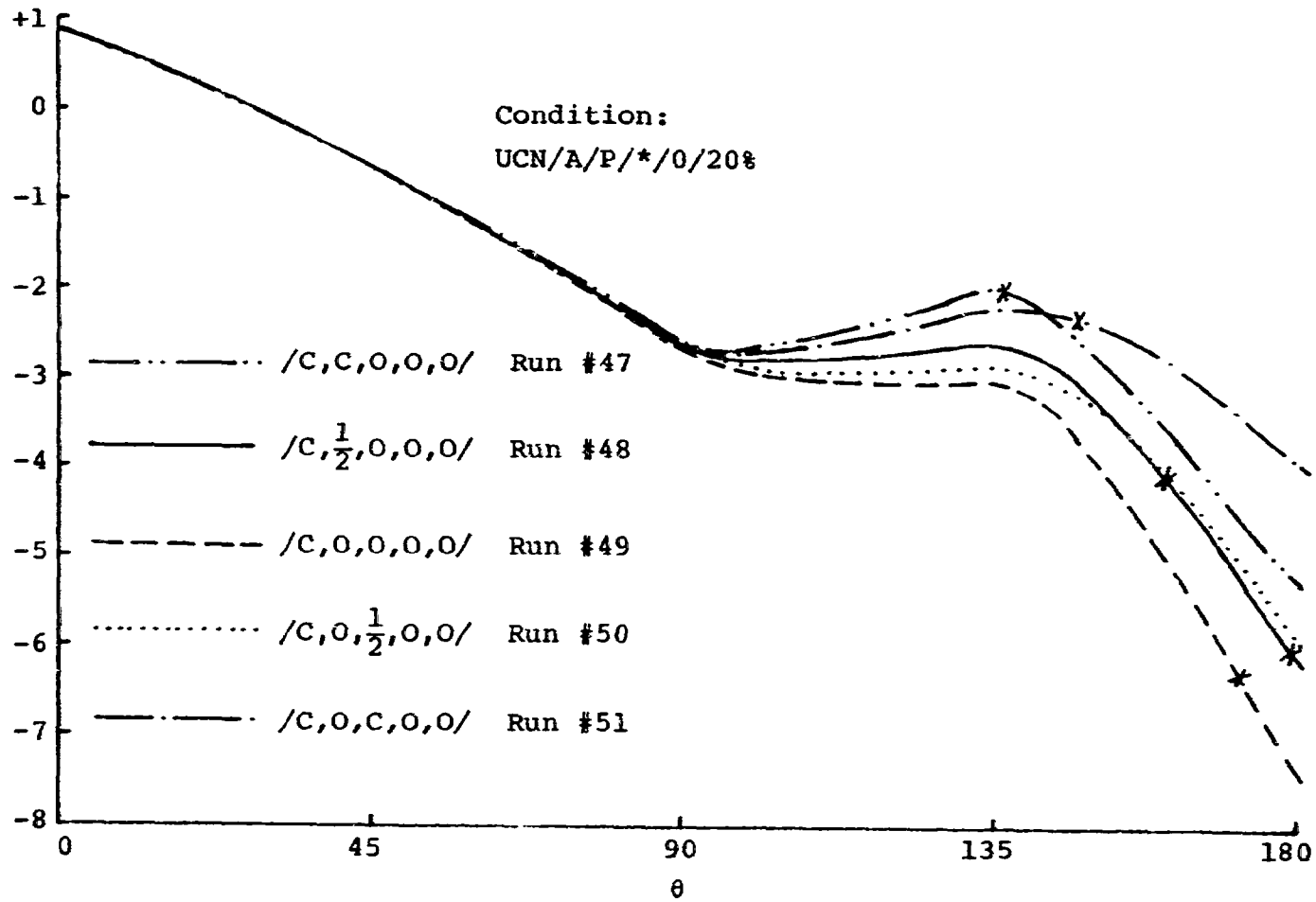

Figure 51. Cylindrical-Spherical Pressure Distribution--
Effect of Throttles #2 and #3

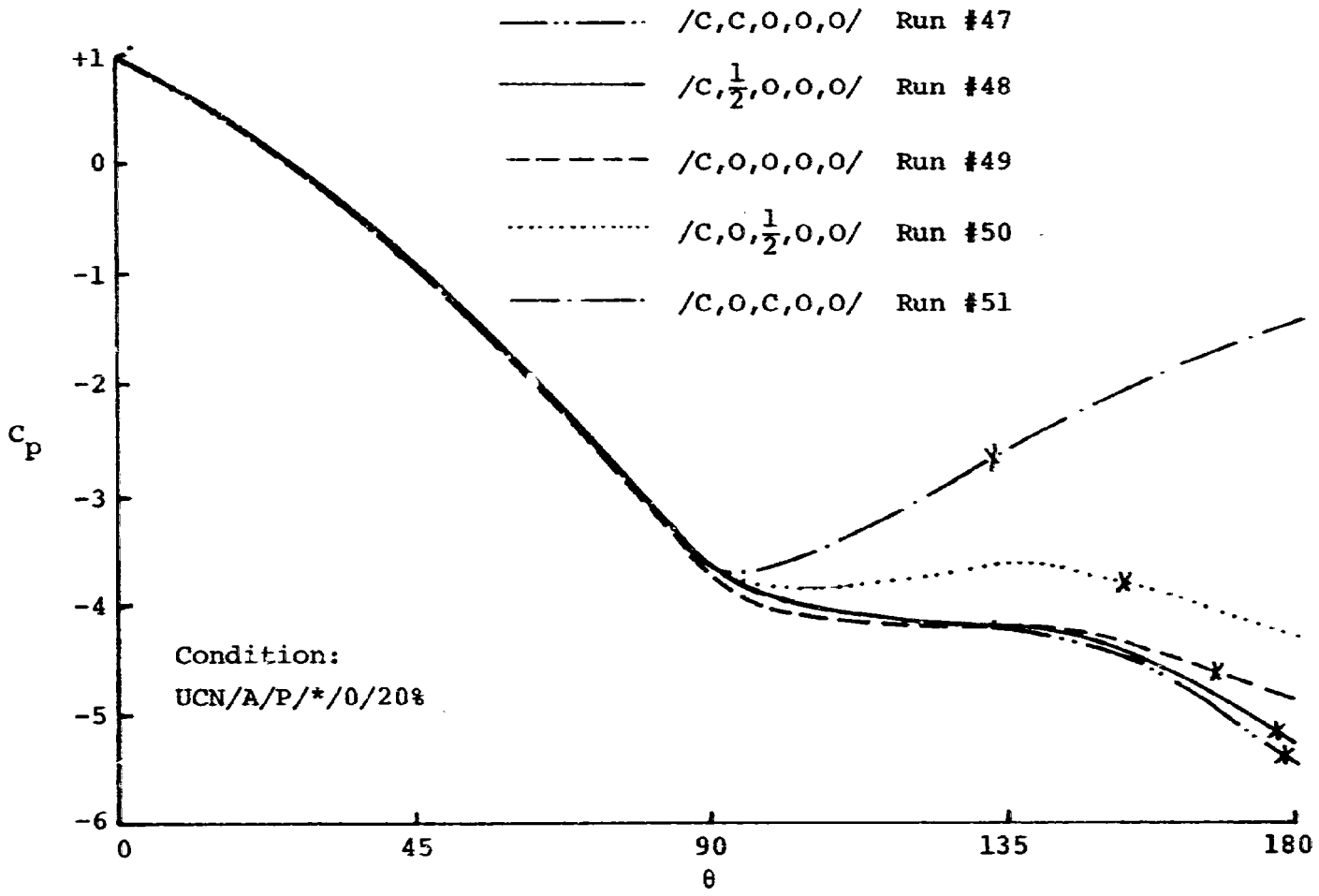

Figure 52. Cylindrical Pressure Distribution--
Effect of Throttles #2 and #3

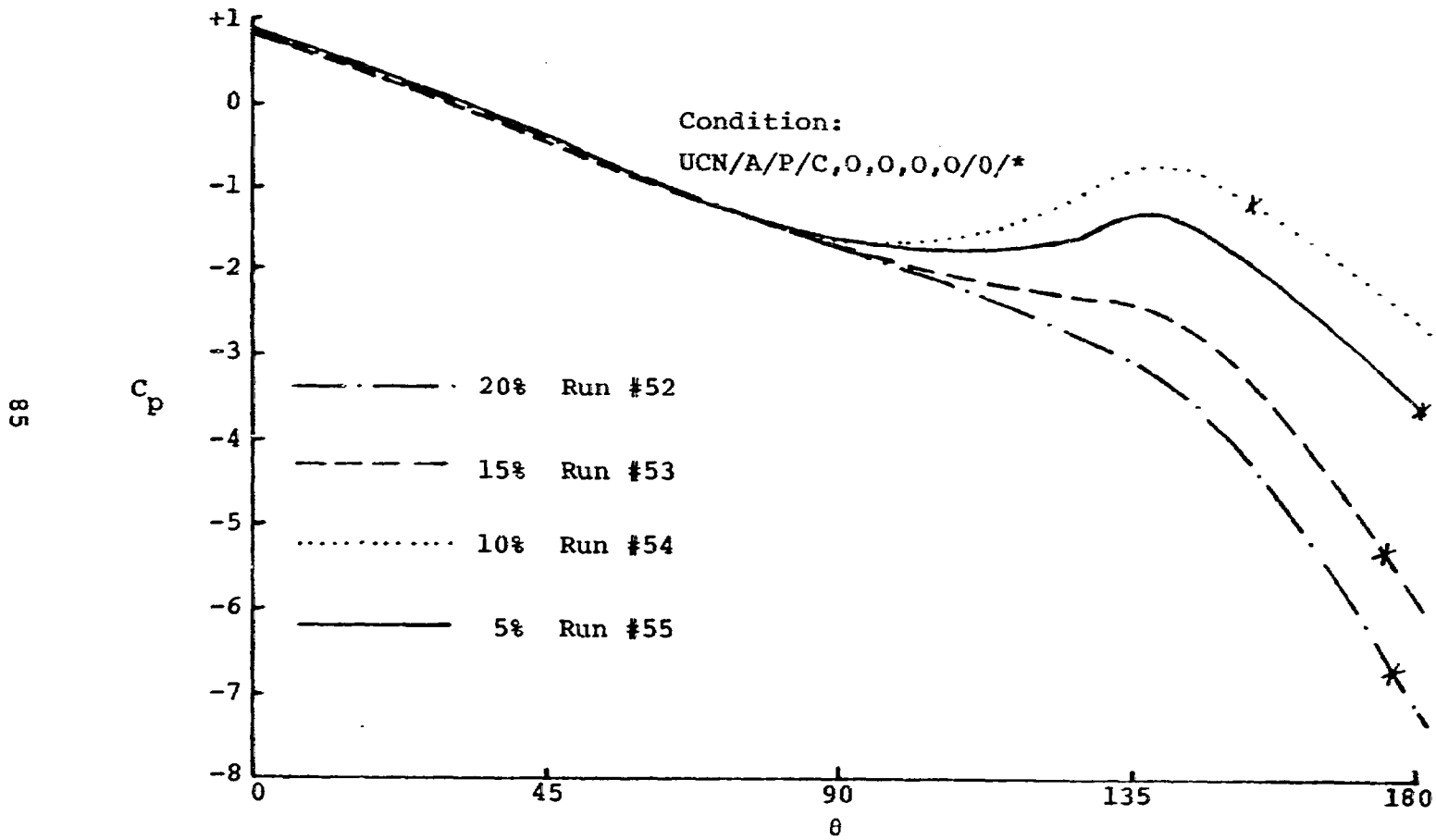

Figure 53. Spherical Pressure Distribution--
Effect of Blower Suction with
FBS Aft at 0 in. T-F Gap

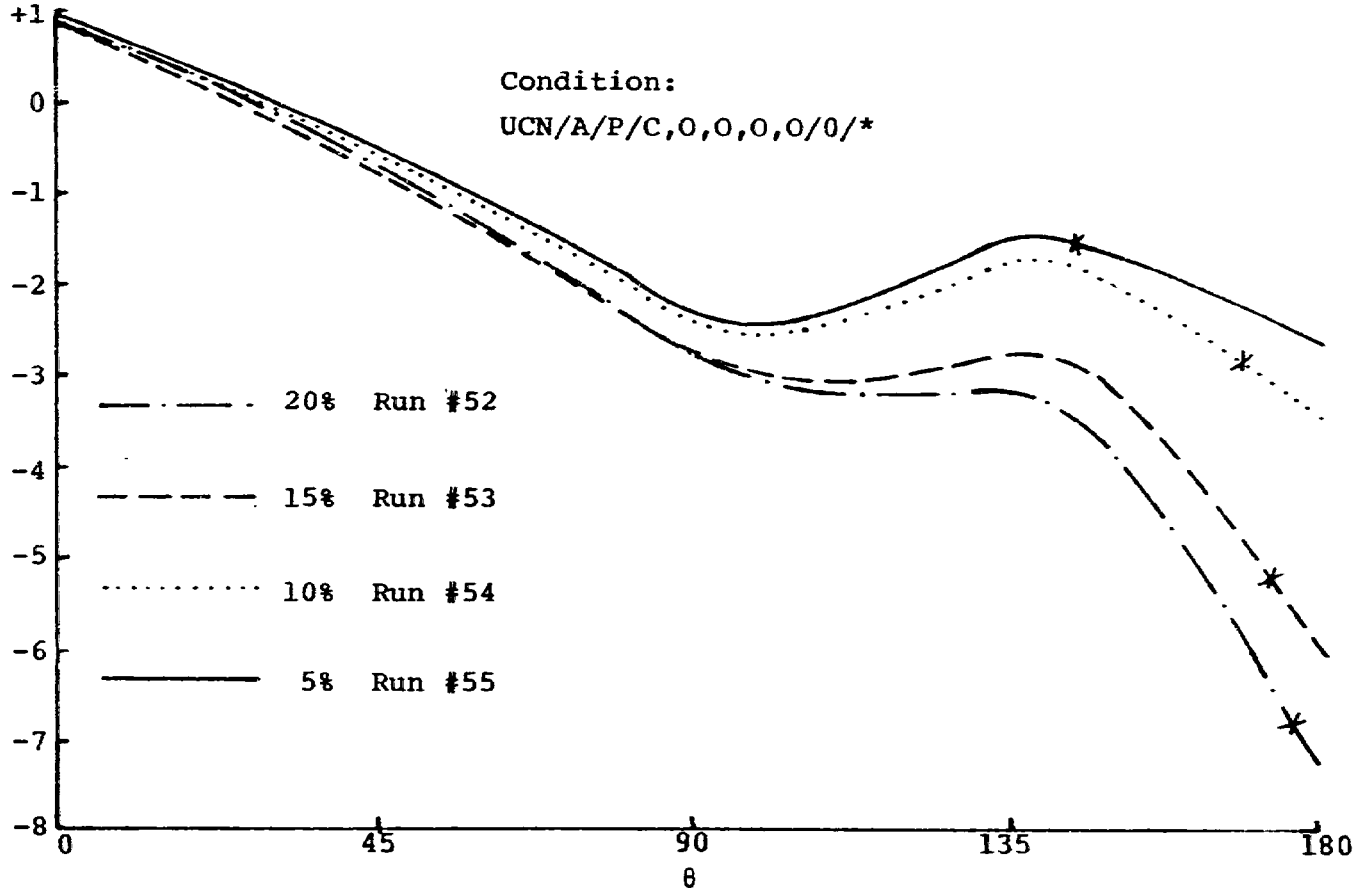

Figure 54. Cylindrical-Spherical Pressure Distribution--
Effect of Blower Suction with
FBS Aft at 0 in. T-F Gap

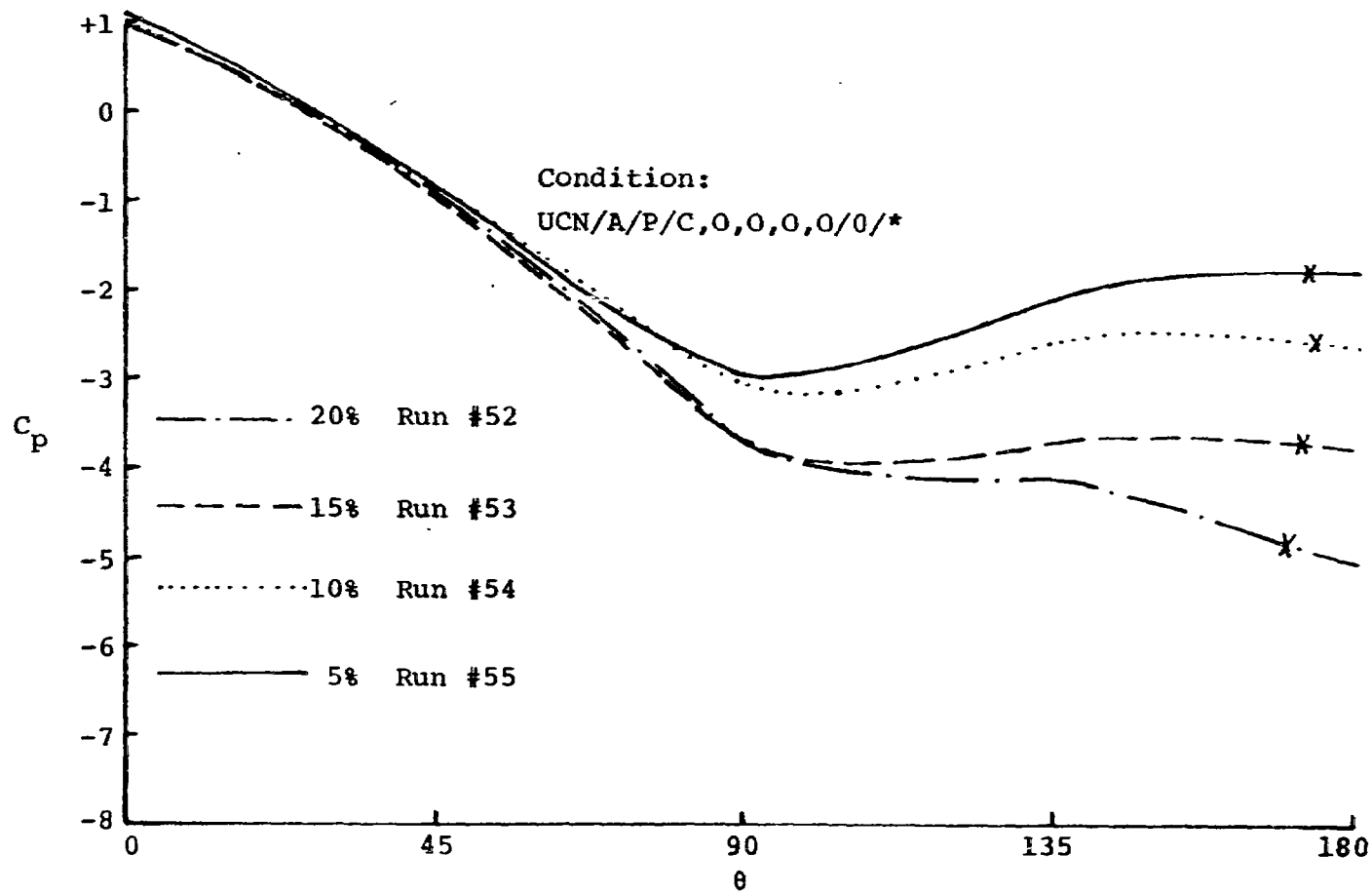

Figure 55. Cylindrical Pressure Distribution--
Effect of Blower Suction with
FBS Aft at 0 in. T-F Gap

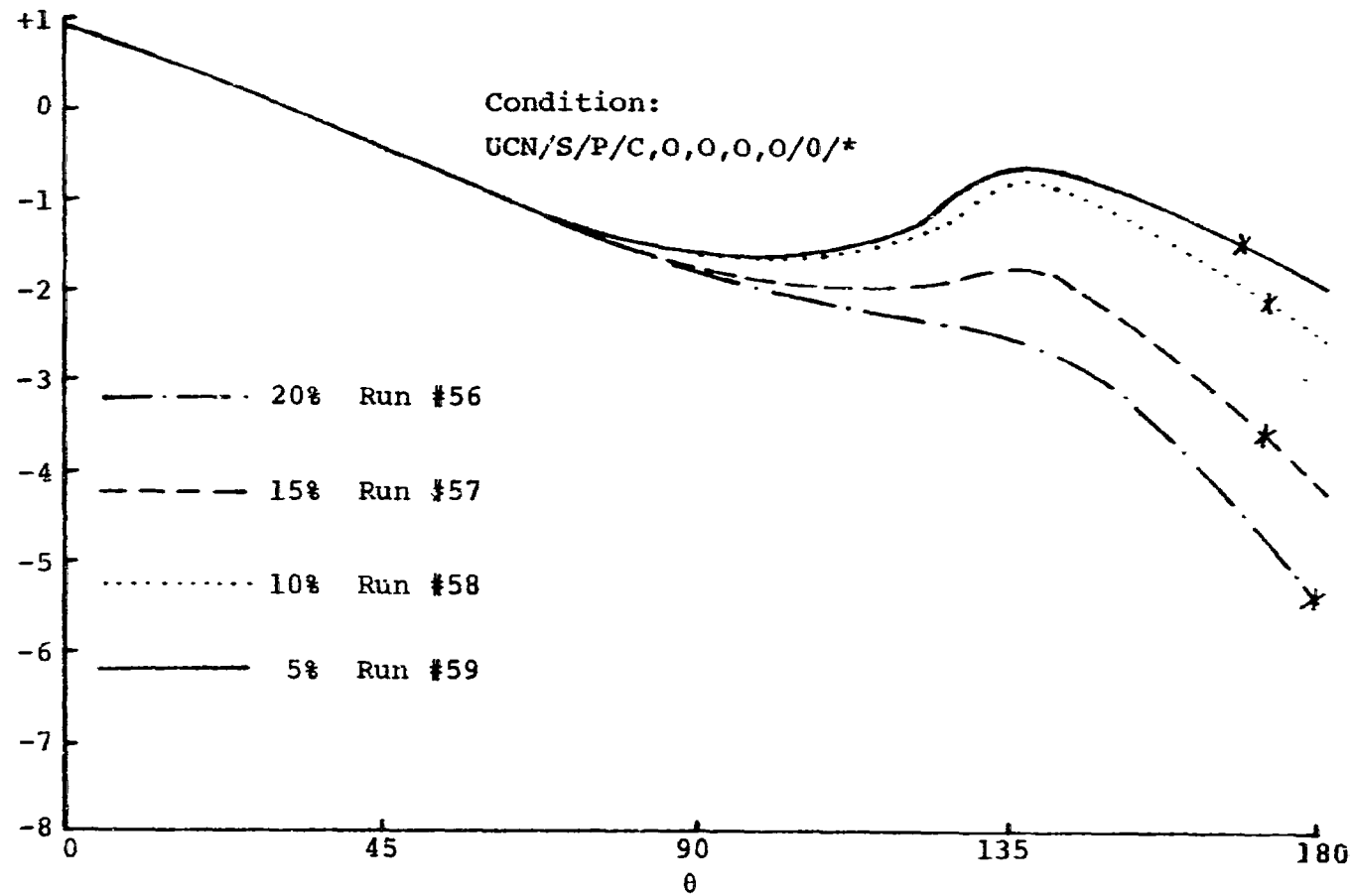

Figure 56. Spherical Pressure Distribution--
Effect of Blower Suction with
FBS Side at 0 in. T-F Gap

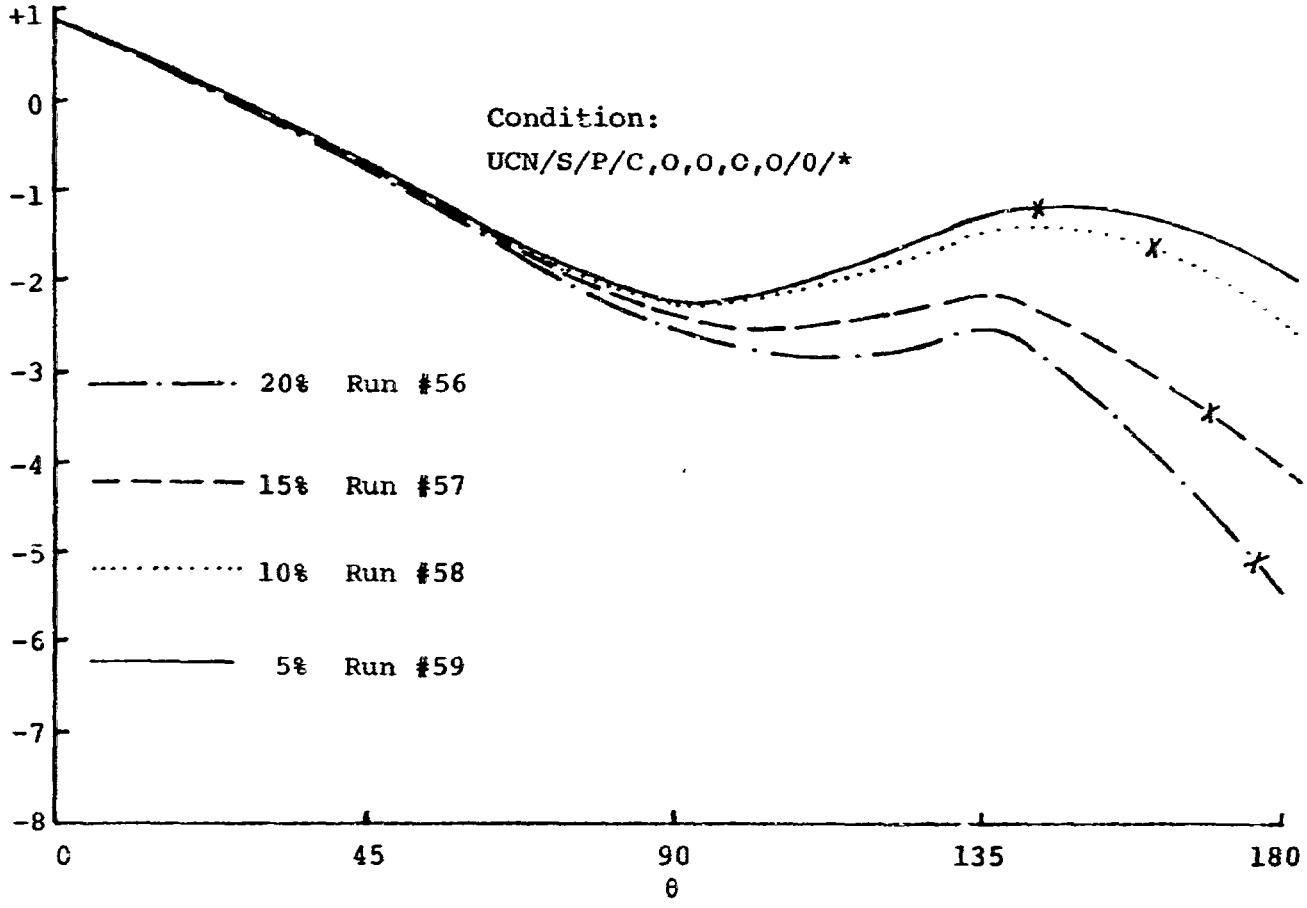

Figure 57. Cylindrical-Spherical Pressure Distribution--
Effect of Blower Suction with FBS Side at 0 in. T-F Gap

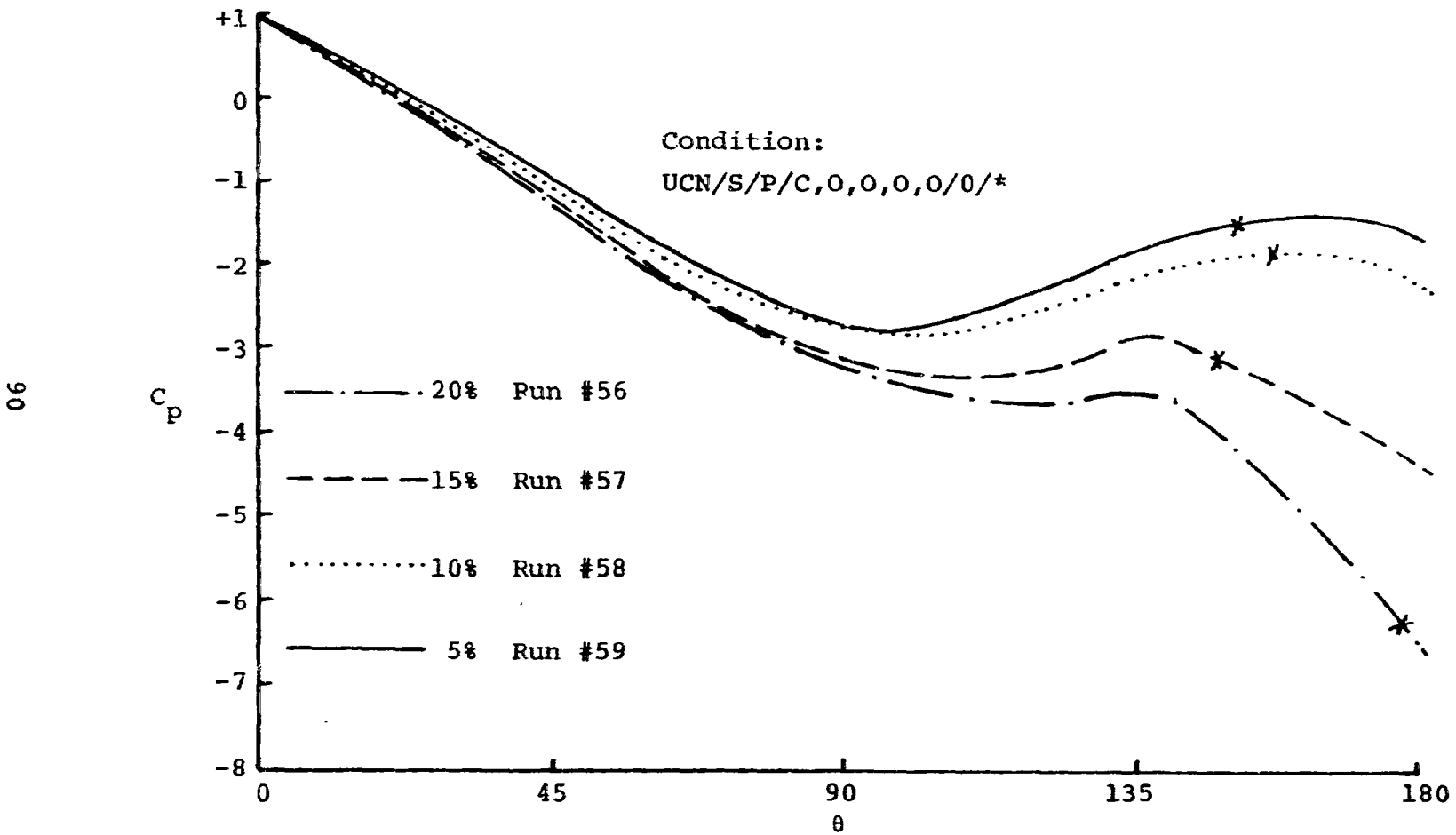

Figure 58. Cylindrical Pressure Distribution--
Effect of Blower Suction with
FBS Side at 0 in. T-F Gap

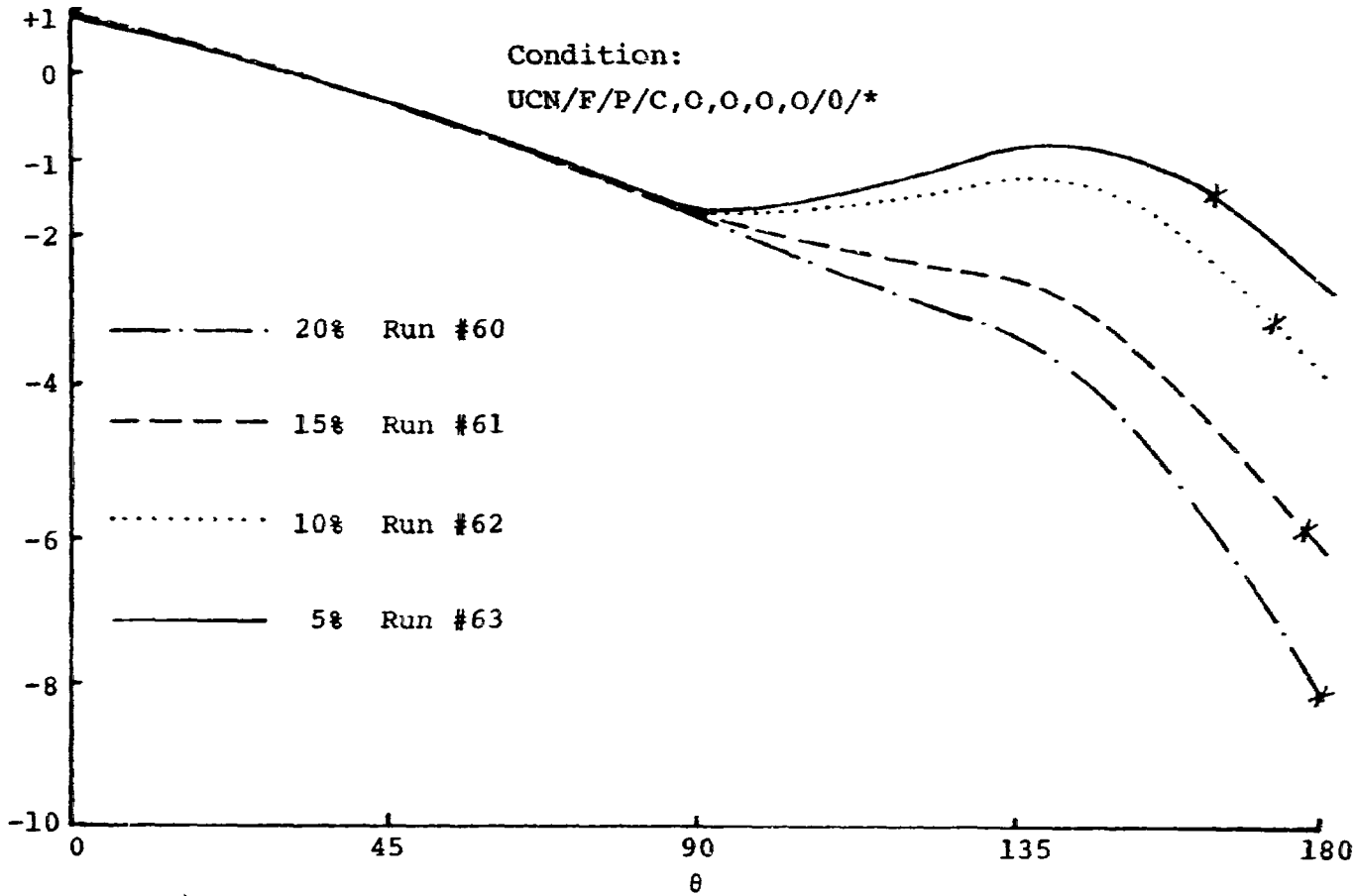

Figure 59. Spherical Pressure Distribution--
Effect of Blower Suction with FBS Forward

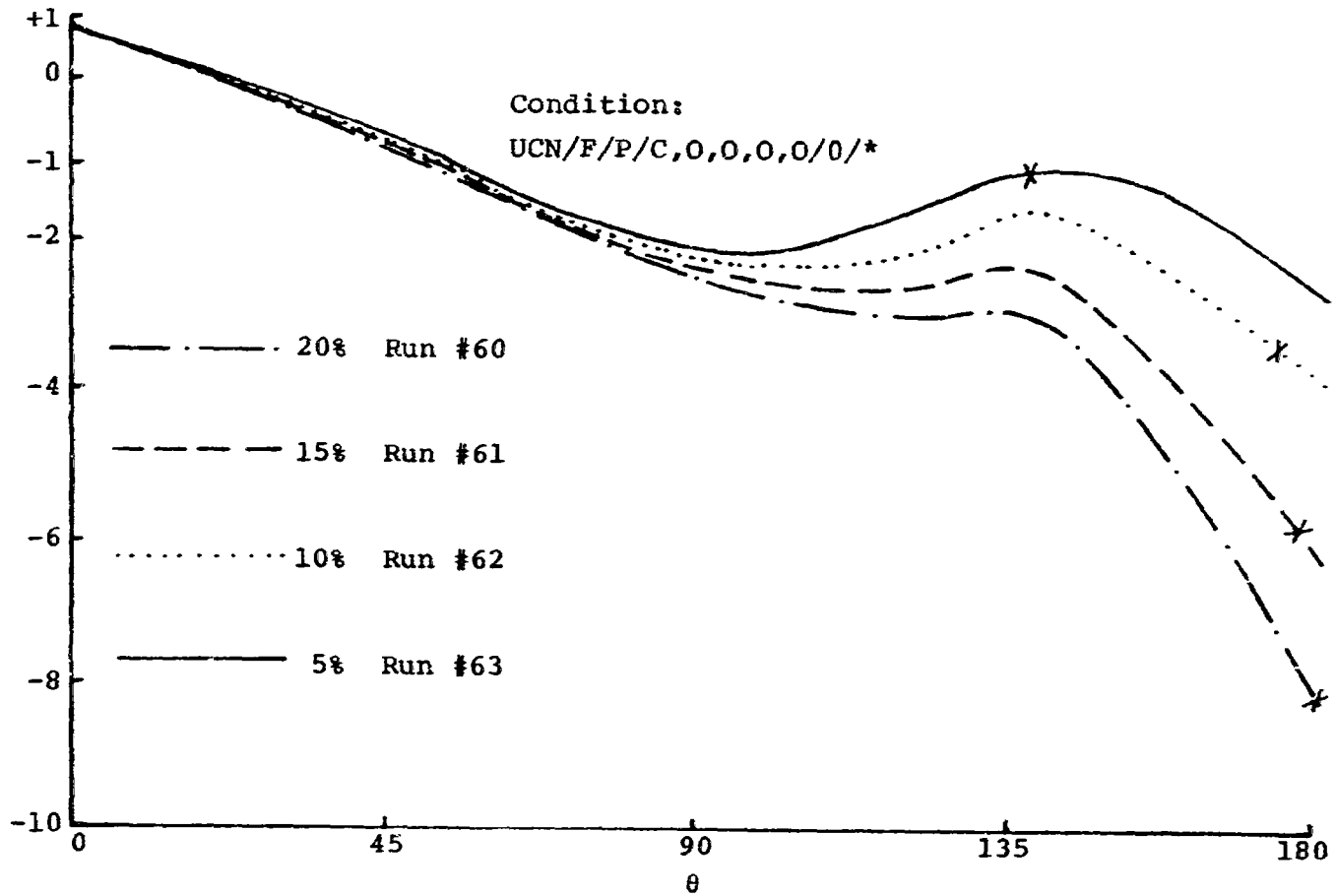

Figure 60. Cylindrical-Spherical Pressure Distribution--
Effect of Blower Suction with FBS Forward

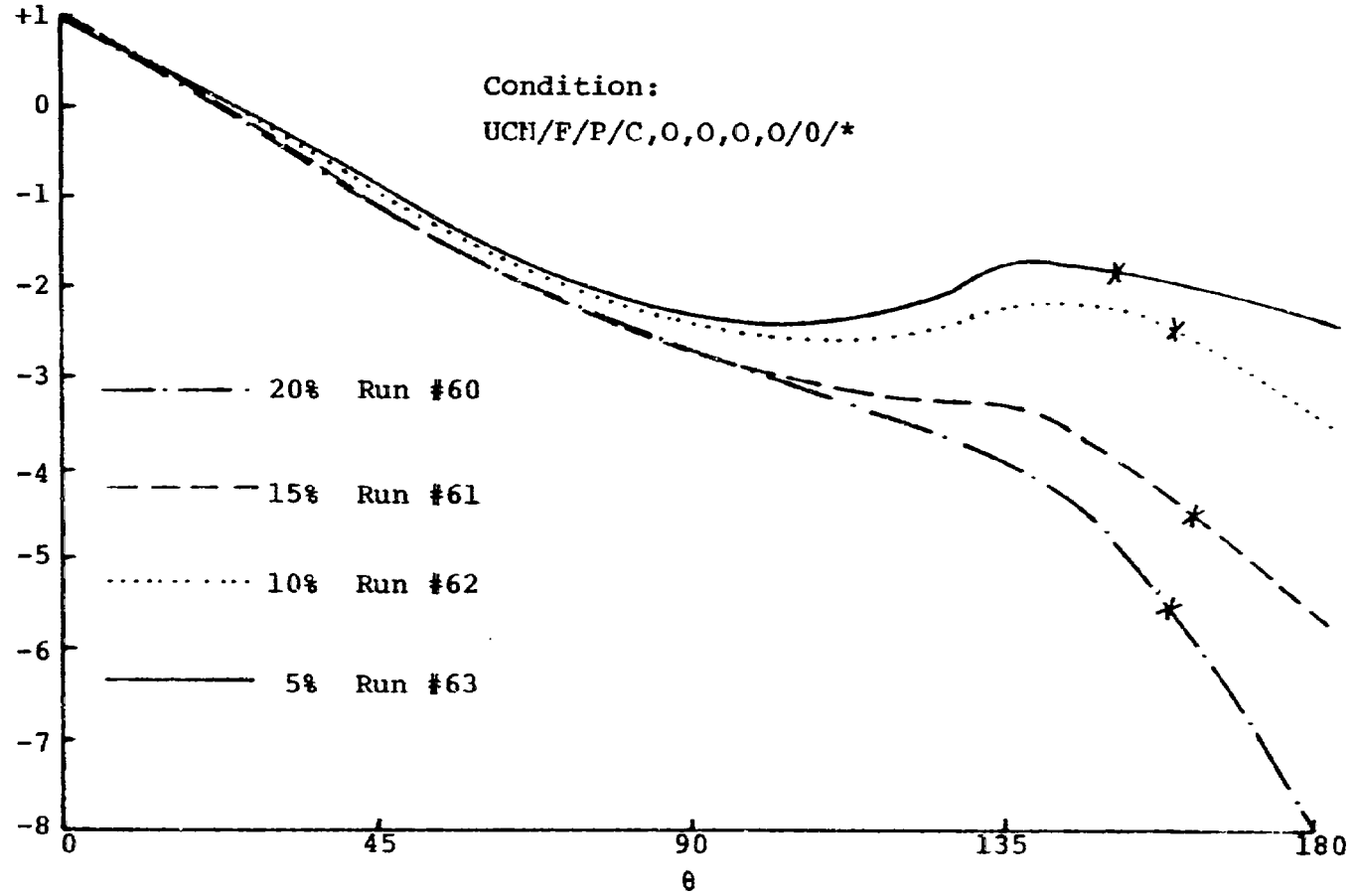

Figure 61. Cylindrical Pressure Distribution--
Effect of Blower Suction with FBS Forward

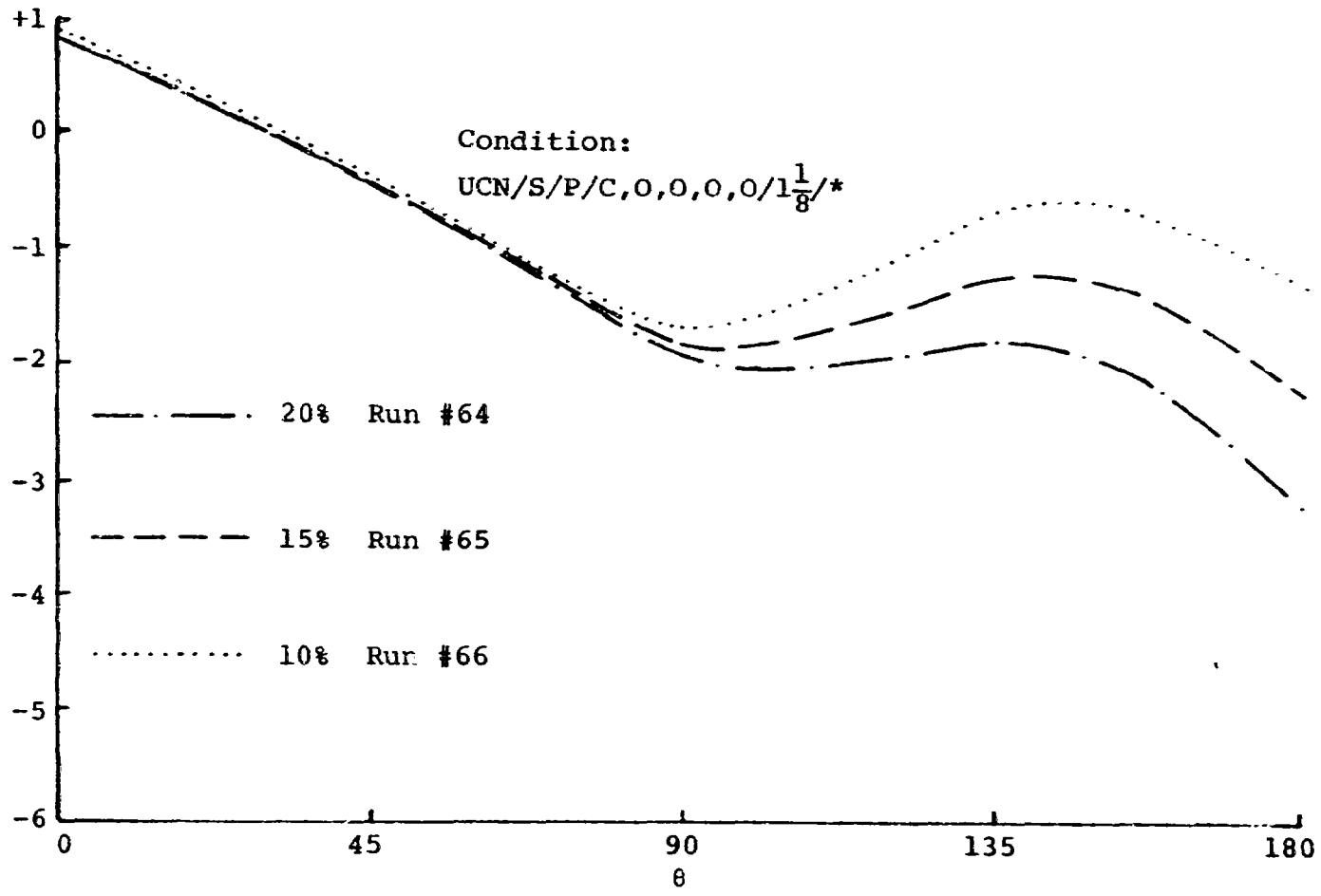

Figure 62. Spherical Pressure Distribution--
Effect of Blower Suction with
FBS Side at 1 1/8 in. T-F Gap

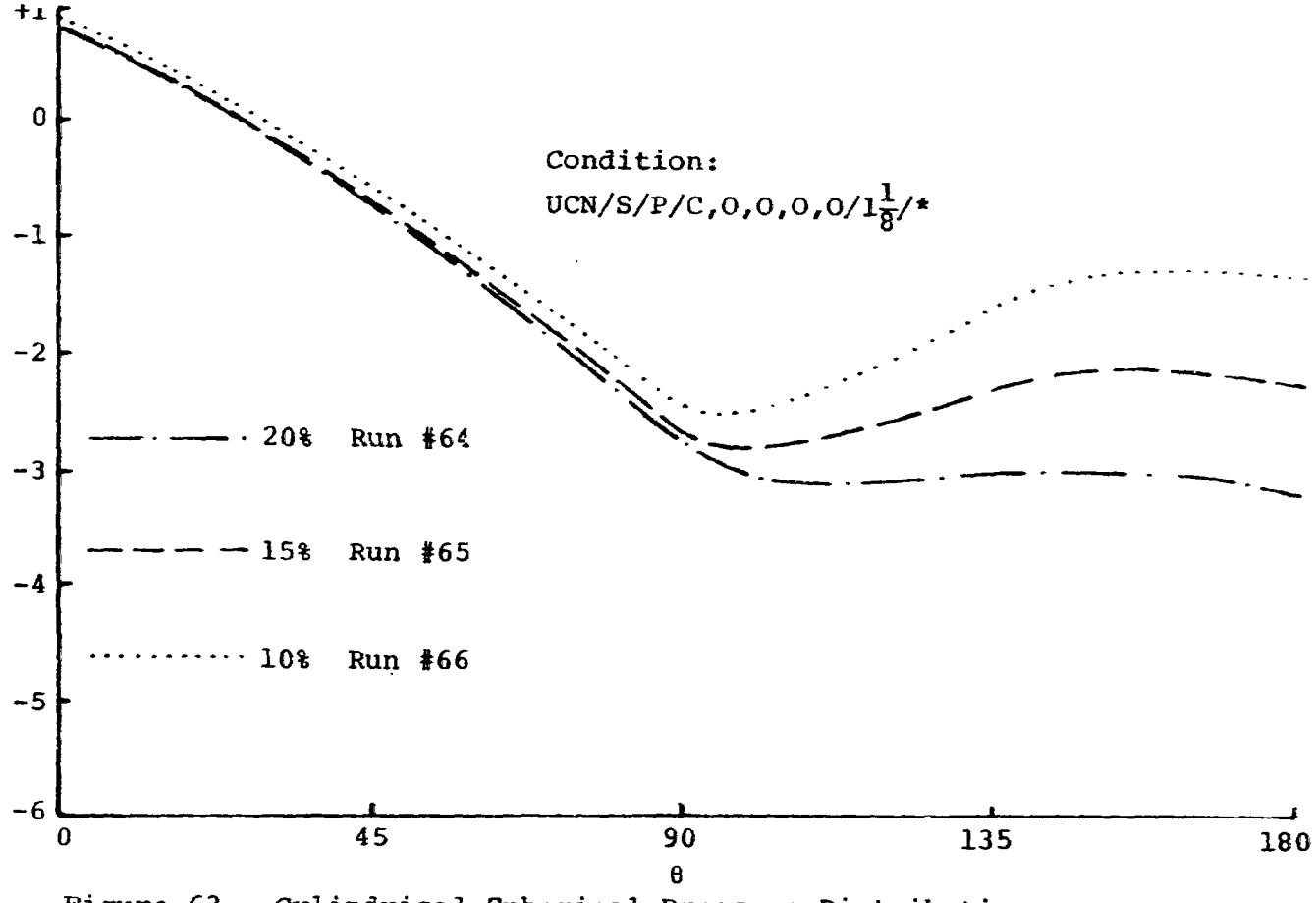

Figure 63. Cylindrical-Spherical Pressure Distribution--
Effect of Blower Suction with
FBS Side at 1 1/8 in. T-F Gap

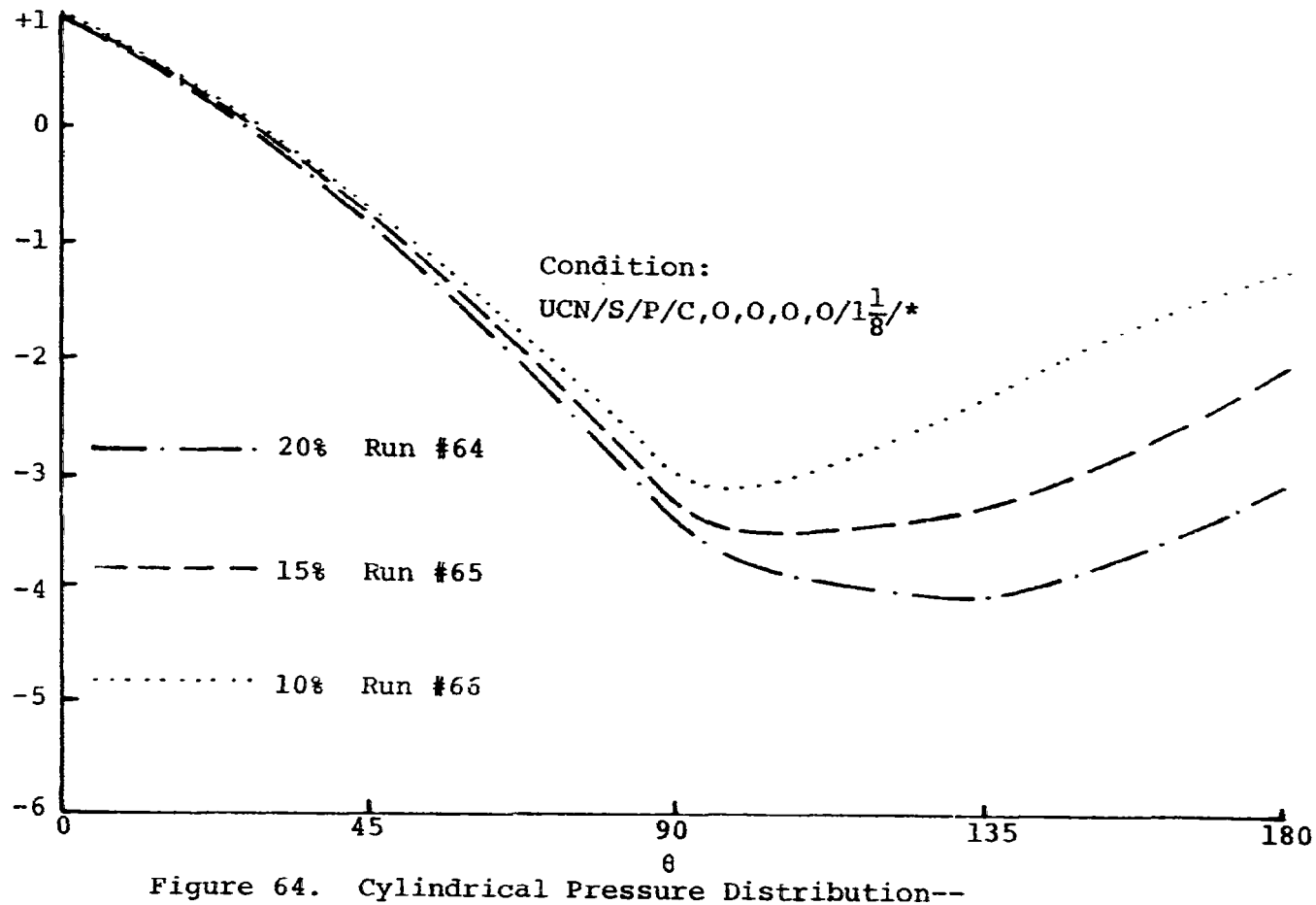

Figure 64. Cylindrical Pressure Distribution--
Effect of Blower Suction with
FBS Side at 1 1/8 in. T-F Gap

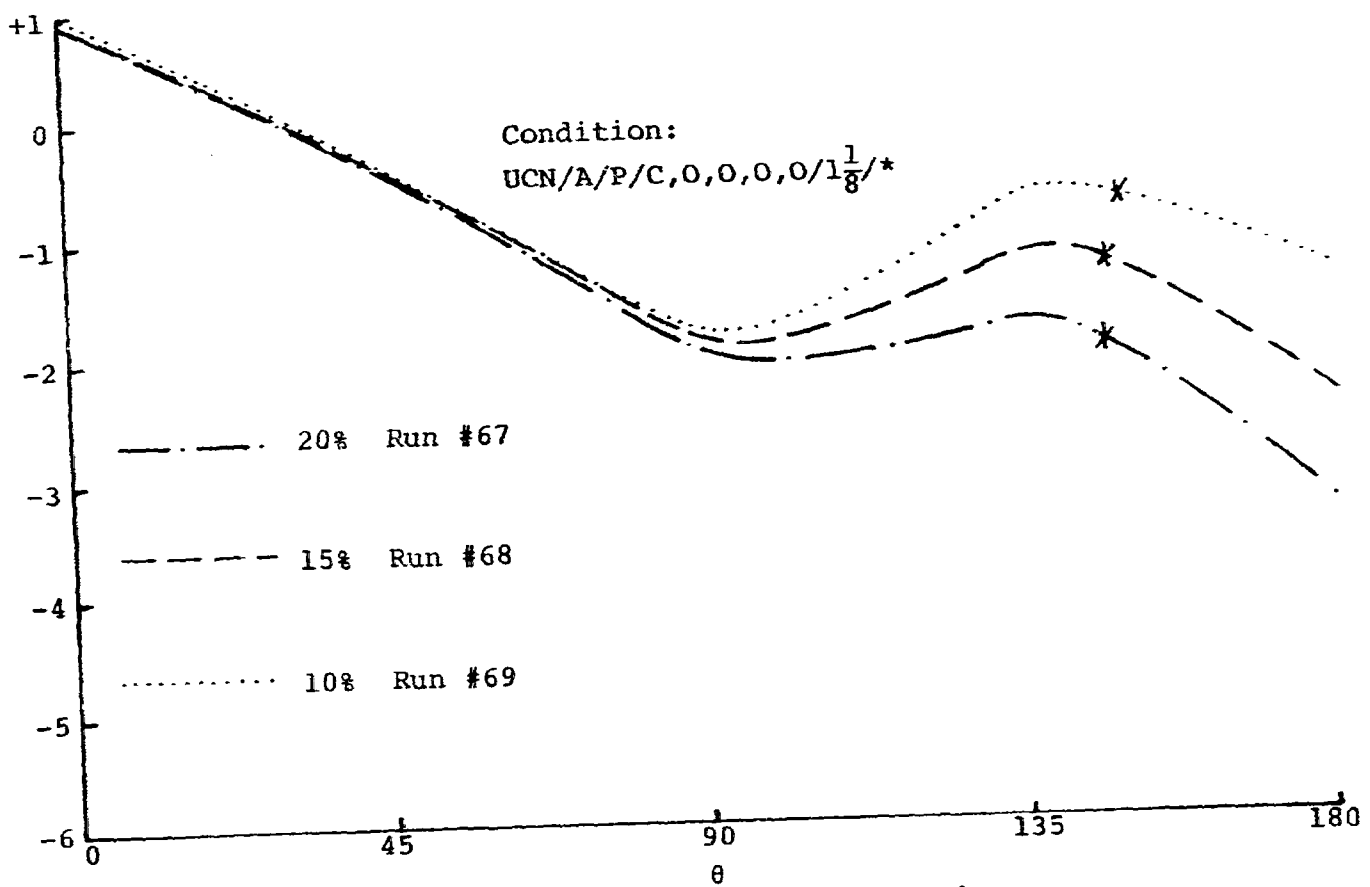

Figure 65. Spherical Pressure Distribution--
Effect of Blower Suction with
FBS Aft at 1 1/8 in. T-F Gap

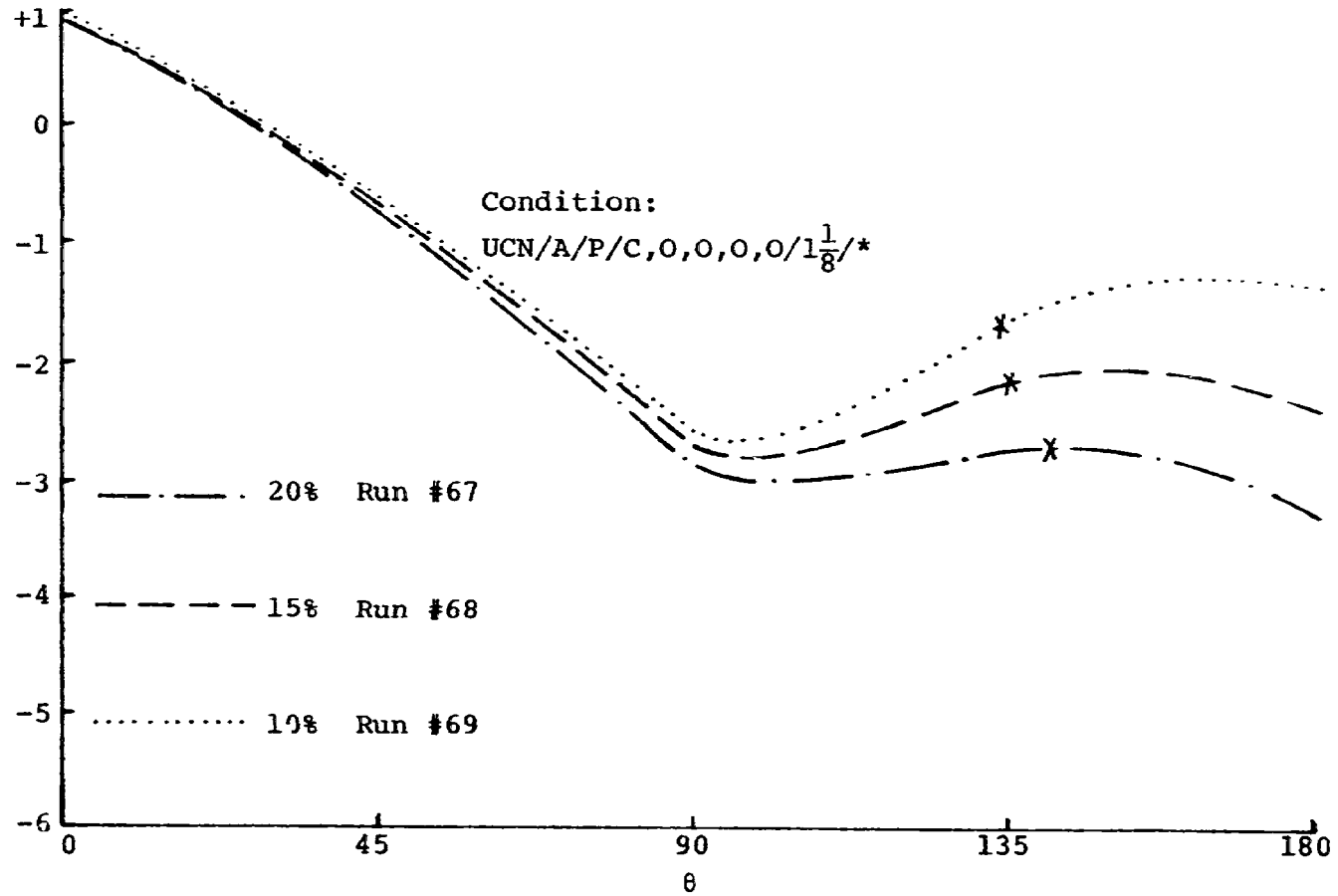

Figure 66. Cylindrical-Spherical Pressure Distribution--
Effect of Blower Suction with FBS Aft at 1 1/8 in. T-F Gap

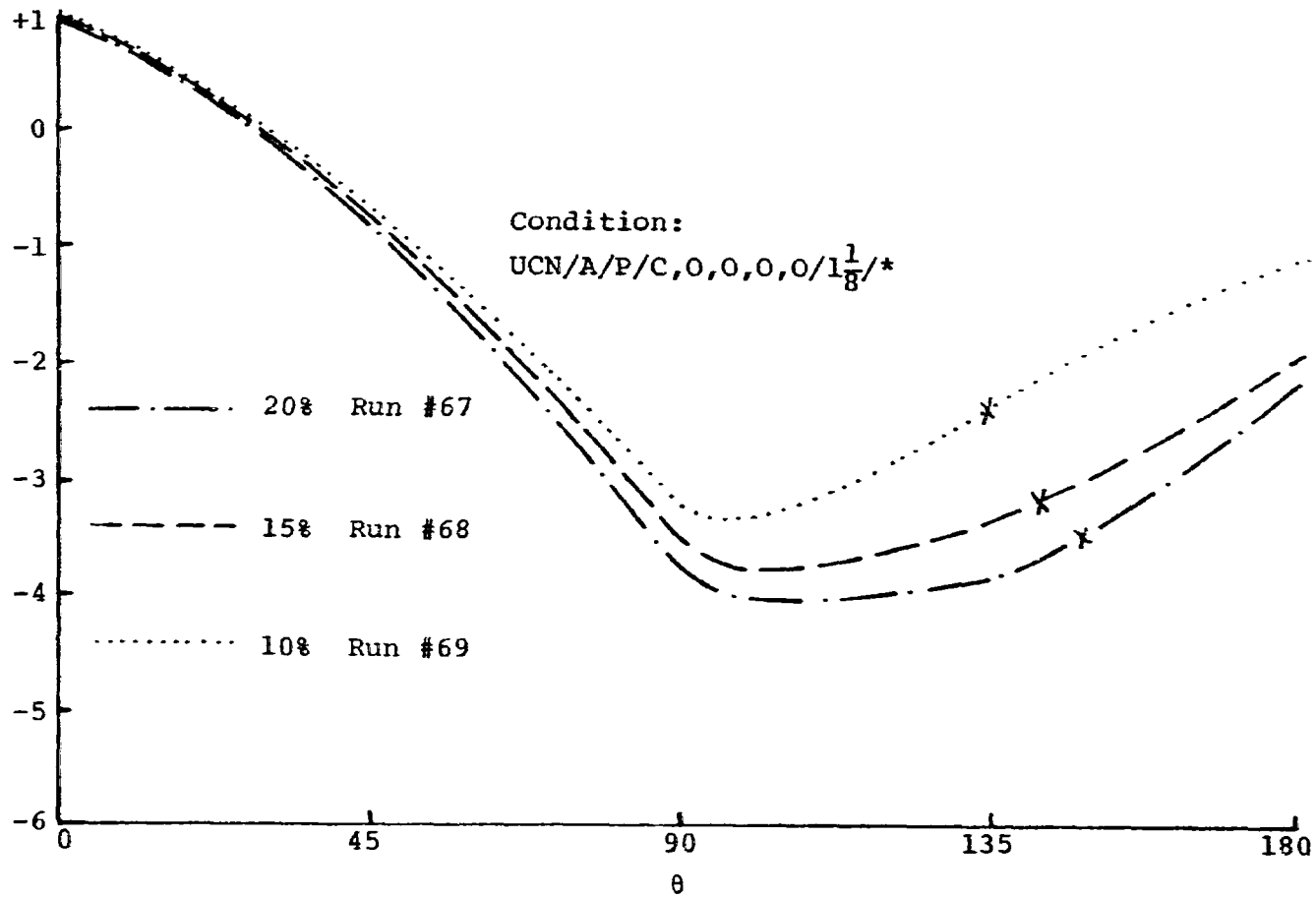

Figure 67. Cylindrical Pressure Distribution--
Effect of Blower Suction
with FBS Aft at 1 1/8 in. T-F Gap

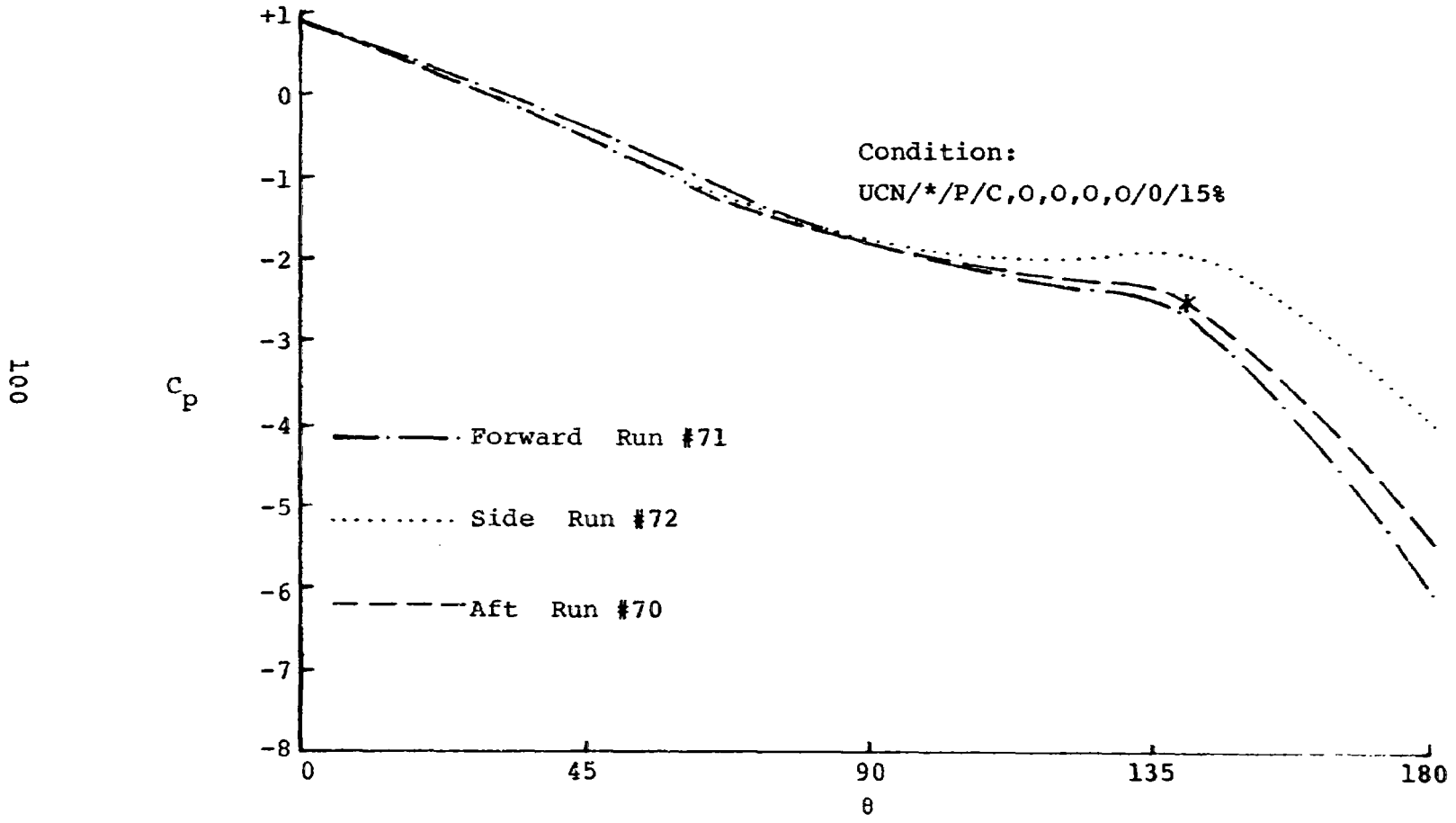

Figure 68. Spherical Pressure Distribution--
Effect of Fuselage Bleed Slot
Location at 15% Suction

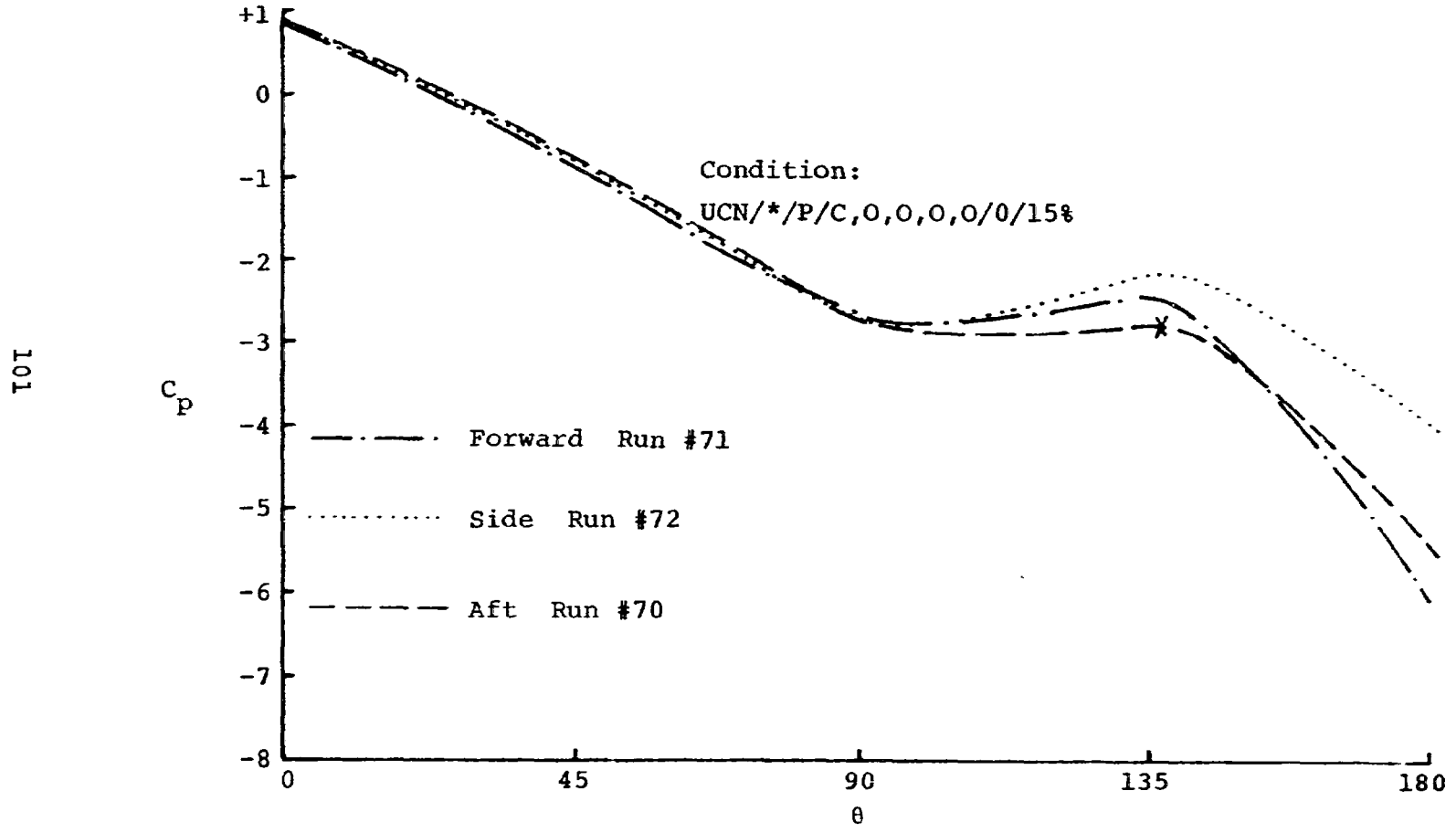

Figure 69. Spherical-Cylindrical Pressure Distribution--
Effect of Fuselage Bleed Slot Location at 15% Suction

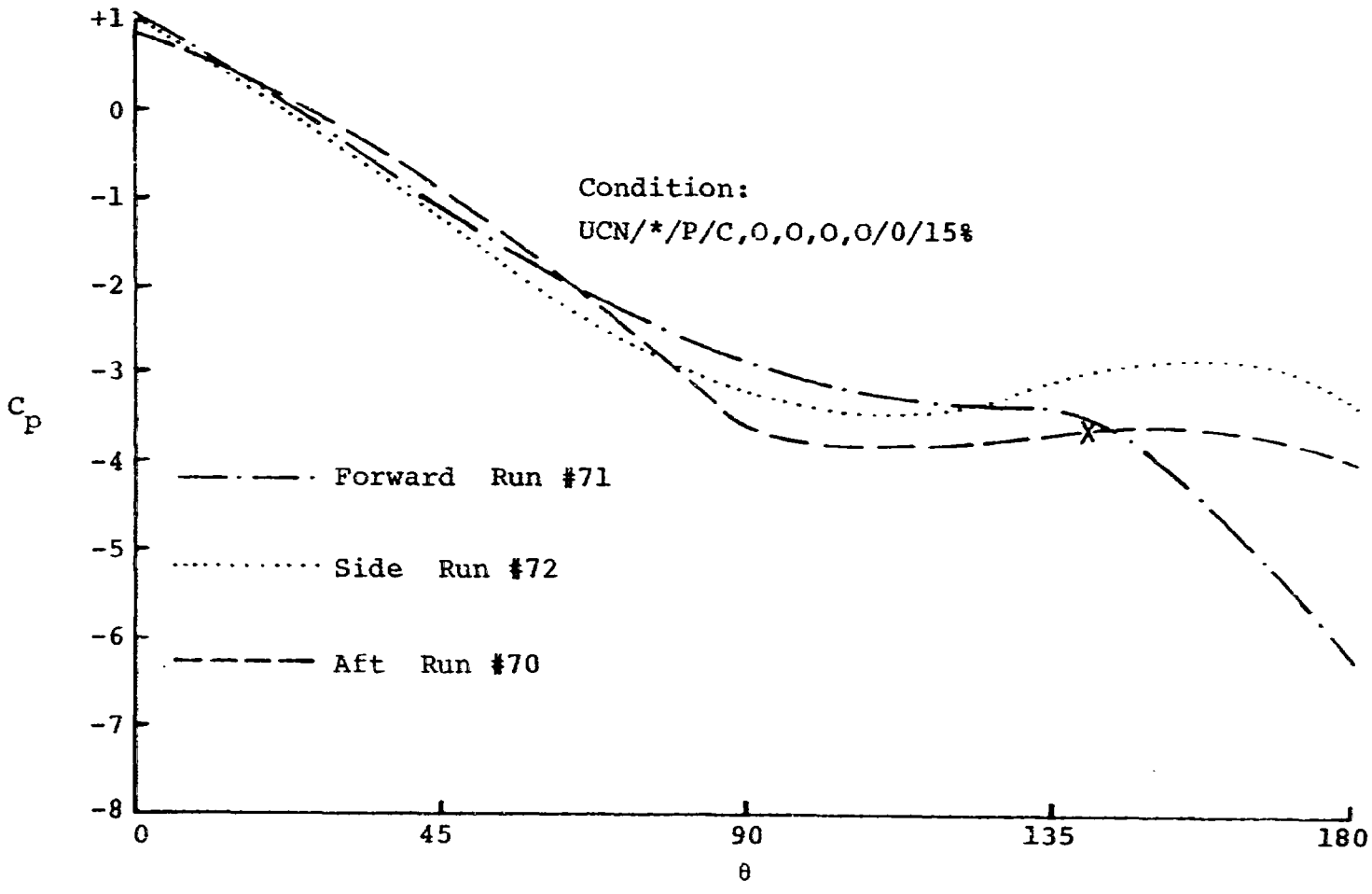

Figure 70. Cylindrical Pressure Distribution--
Effect of Fuselage Bleed Slot
Location at 15% Suction

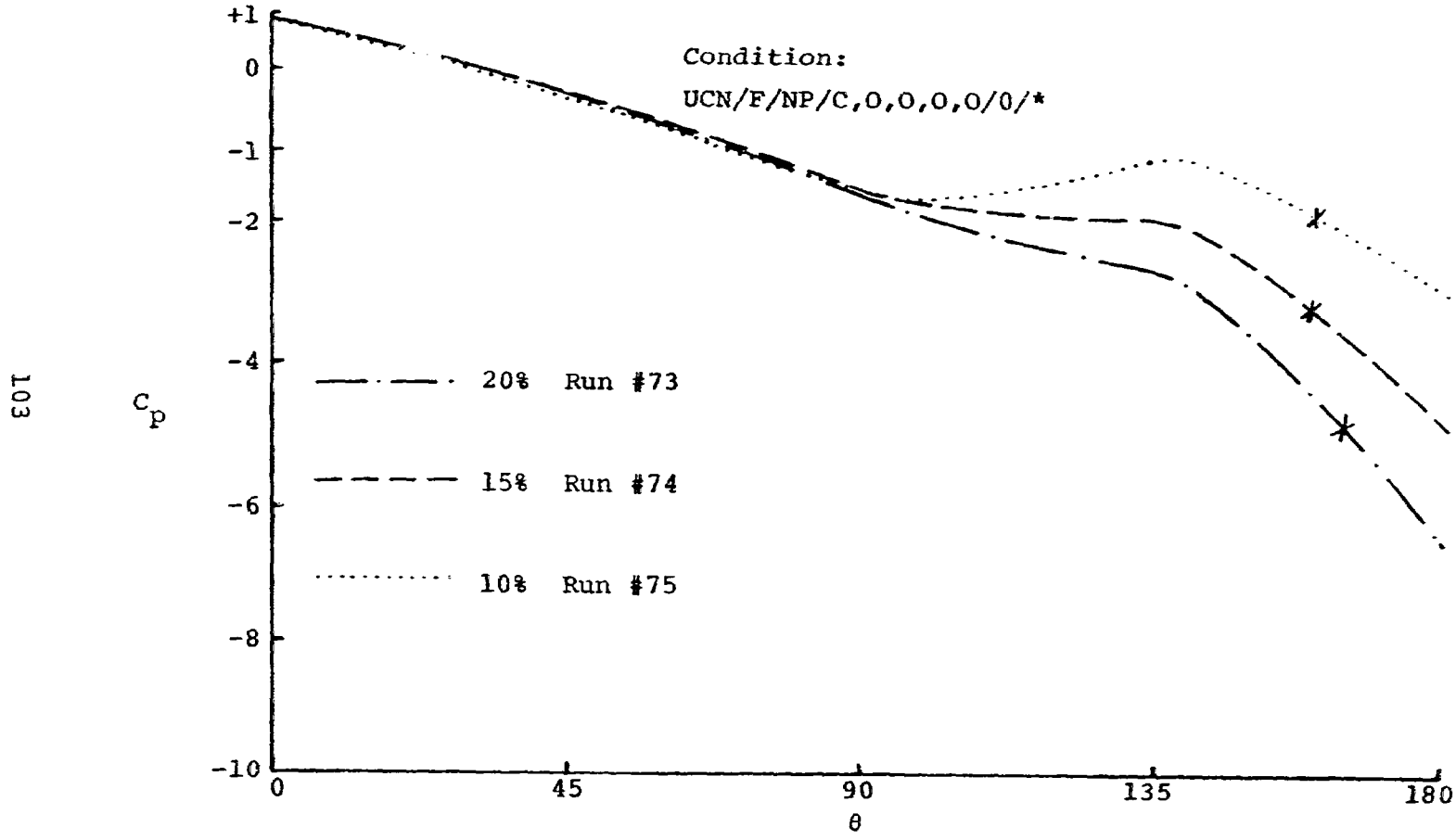

Figure 71. Spherical Pressure Distribution--
Effect of Blower Suction with
Non-Porous FBS Forward

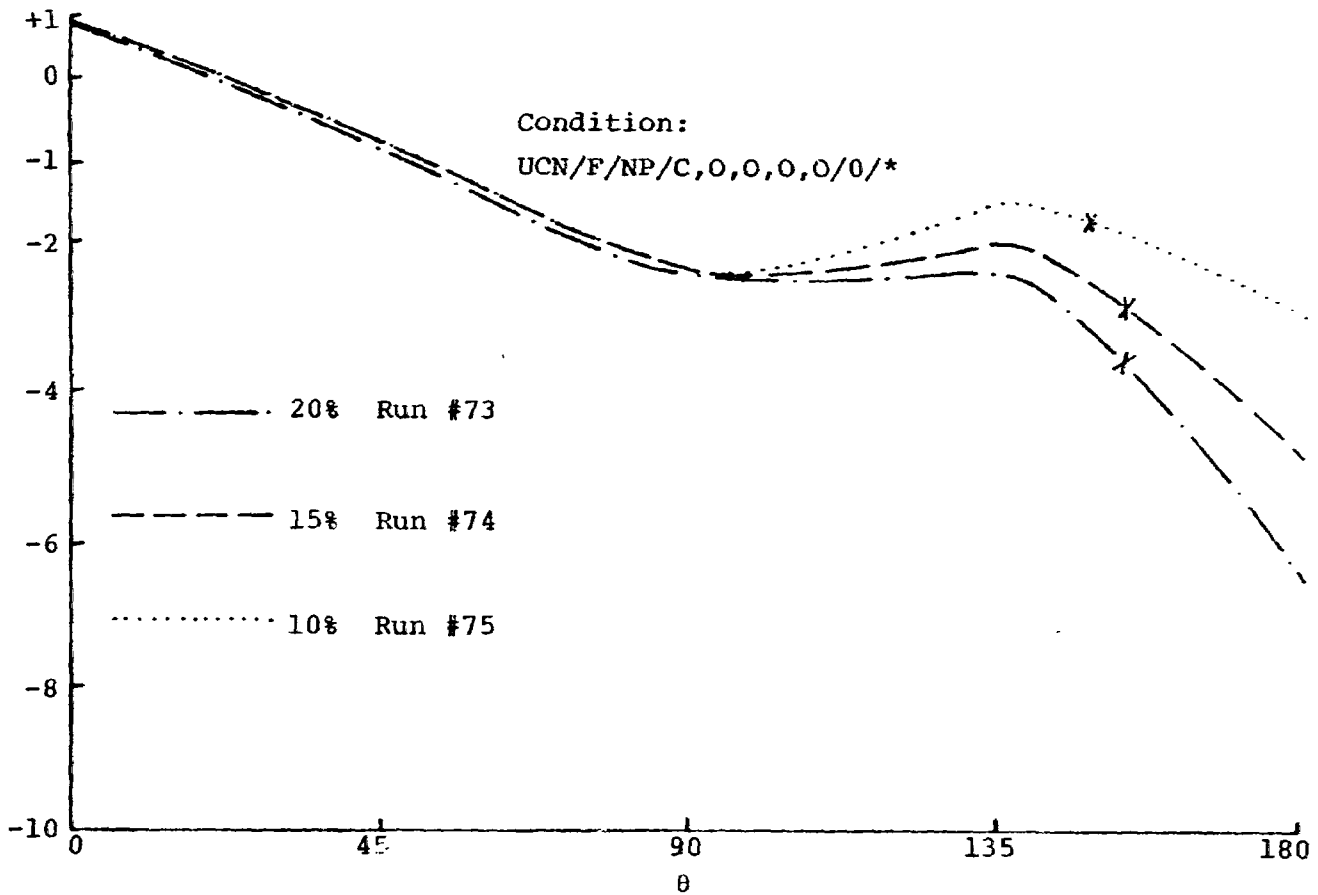

Figure 72. Cylindrical-Spherical Pressure Distribution--
Effect of Blower Suction with
Non-Porous FBS Forward

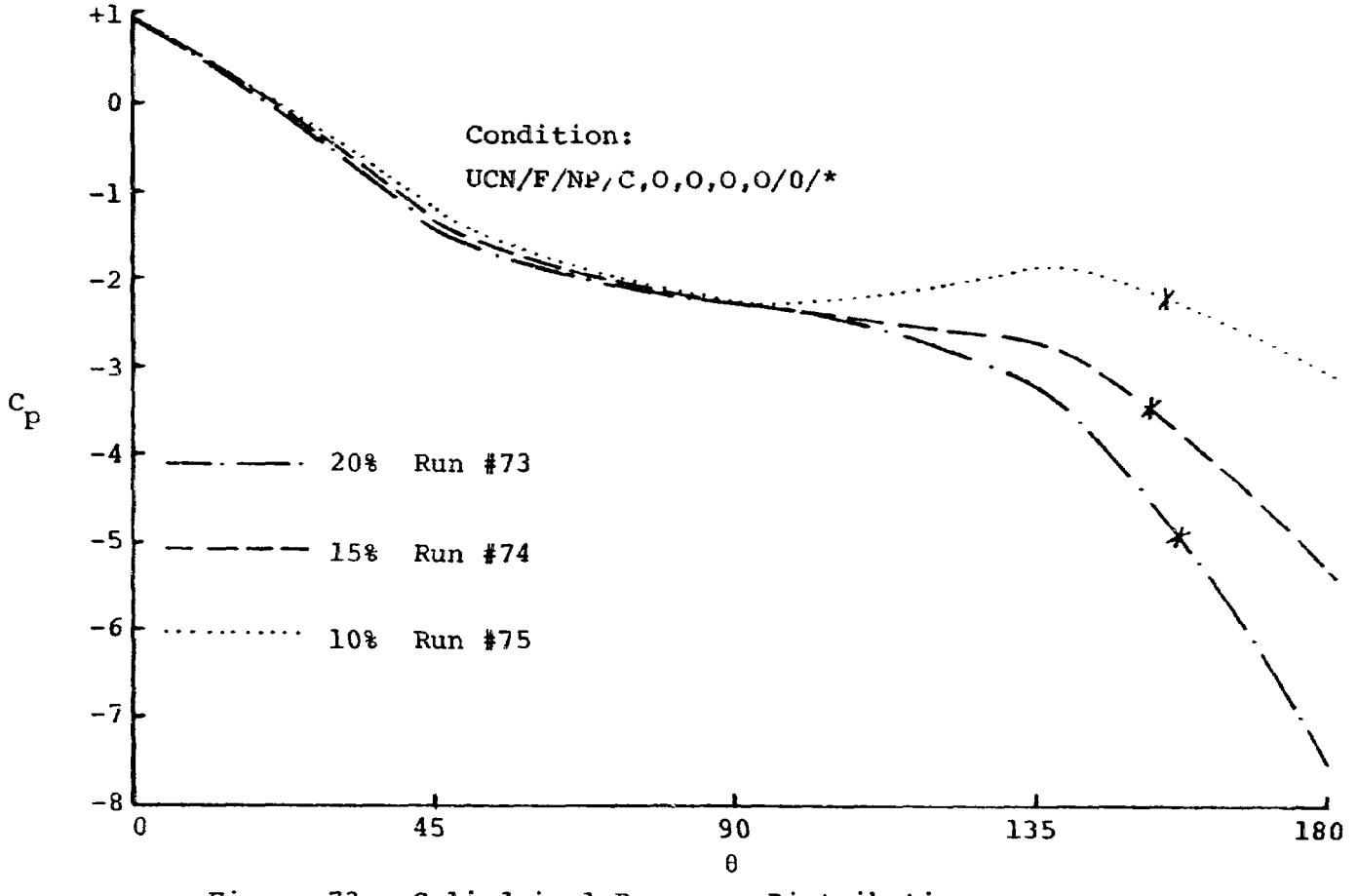

Figure 73. Cylindrical Pressure Distribution--
Effect of Blower Suction with
Non-Porous FBS Forward

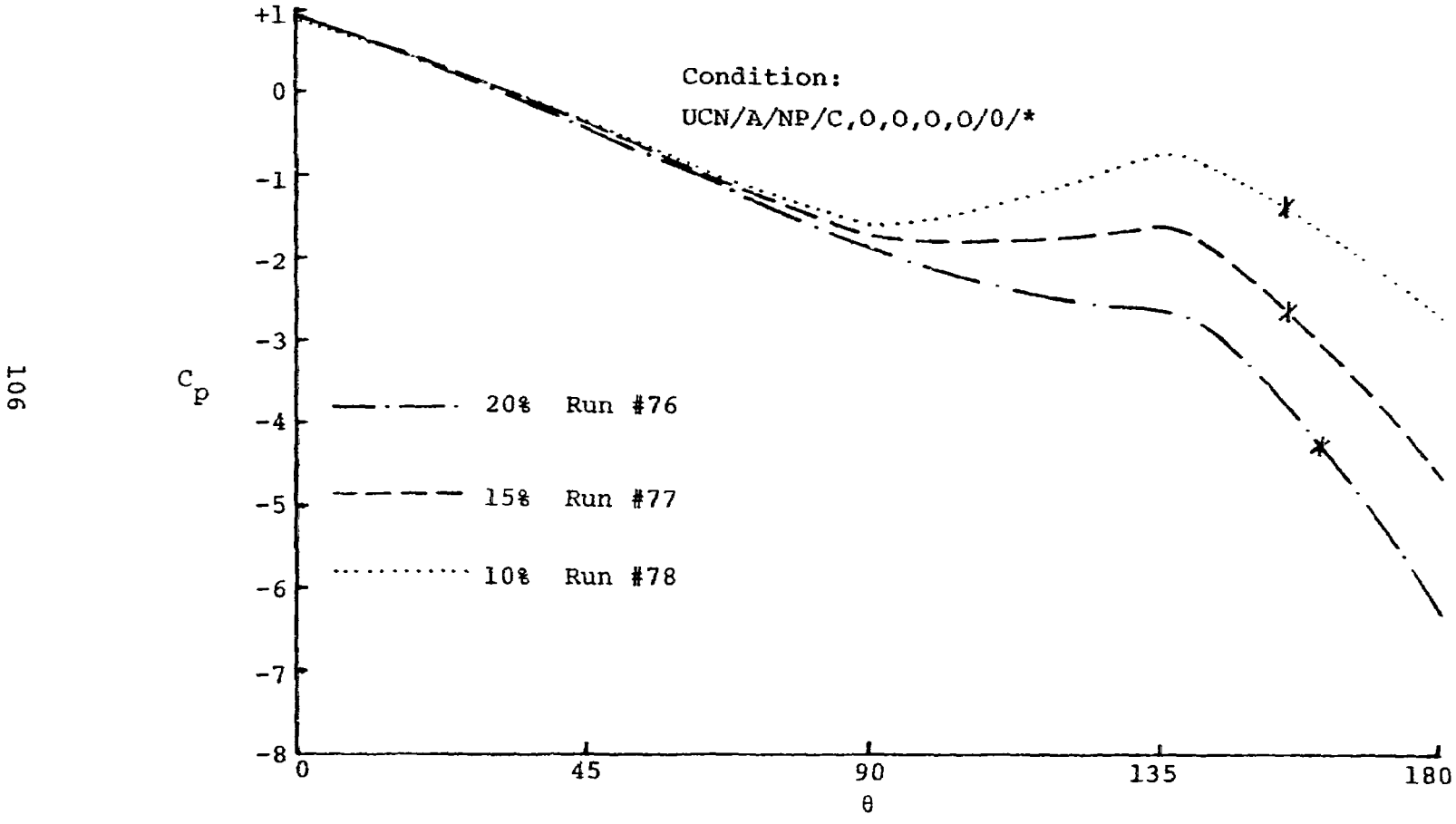

Figure 74. Spherical Pressure Distribution--
Effect of Blower Suction with
Non-Porous FBS Aft

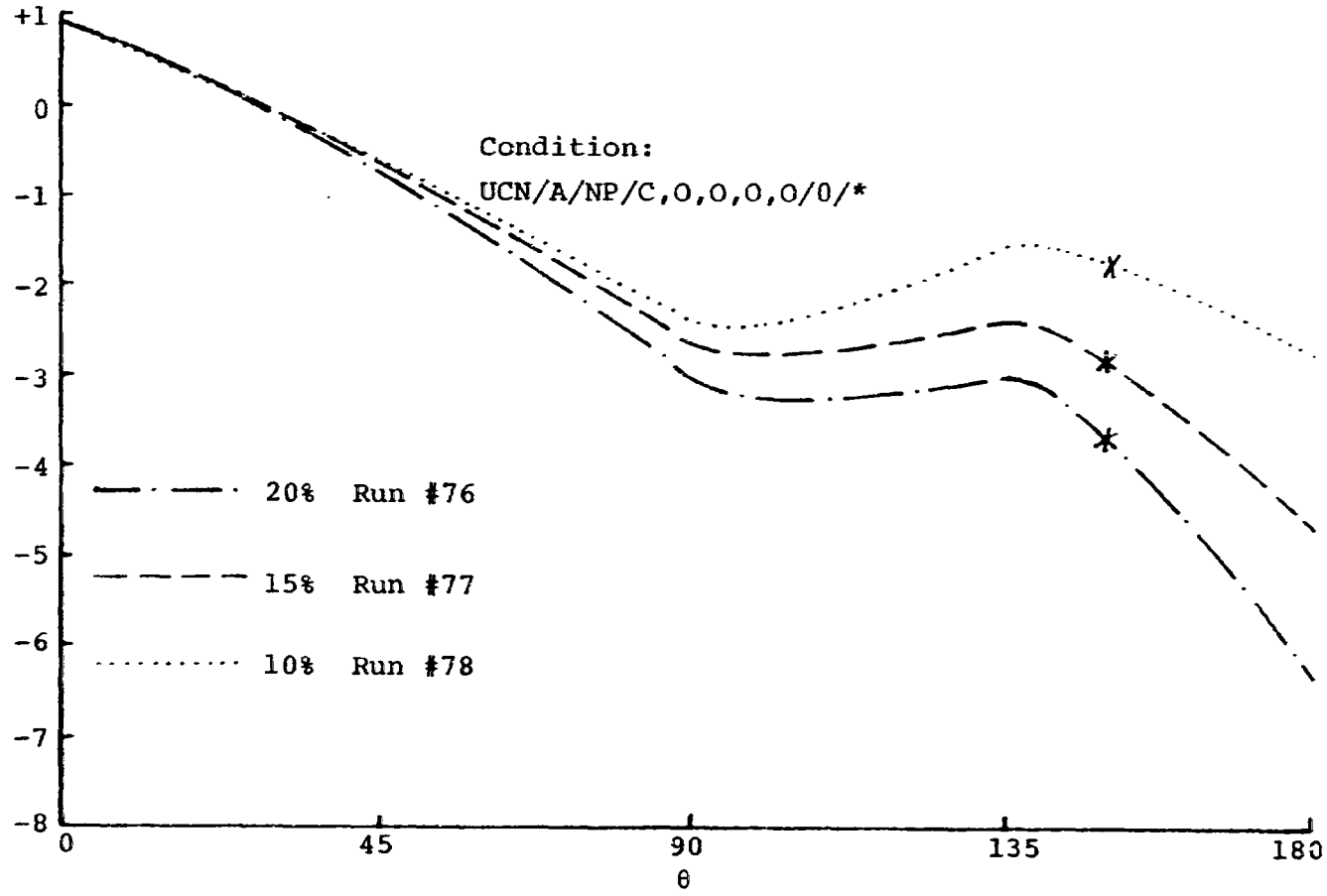

Figure 75. Cylindrical-Spherical Pressure Distribution--
Effect of Blower Suction with Non-Porous FBS Aft

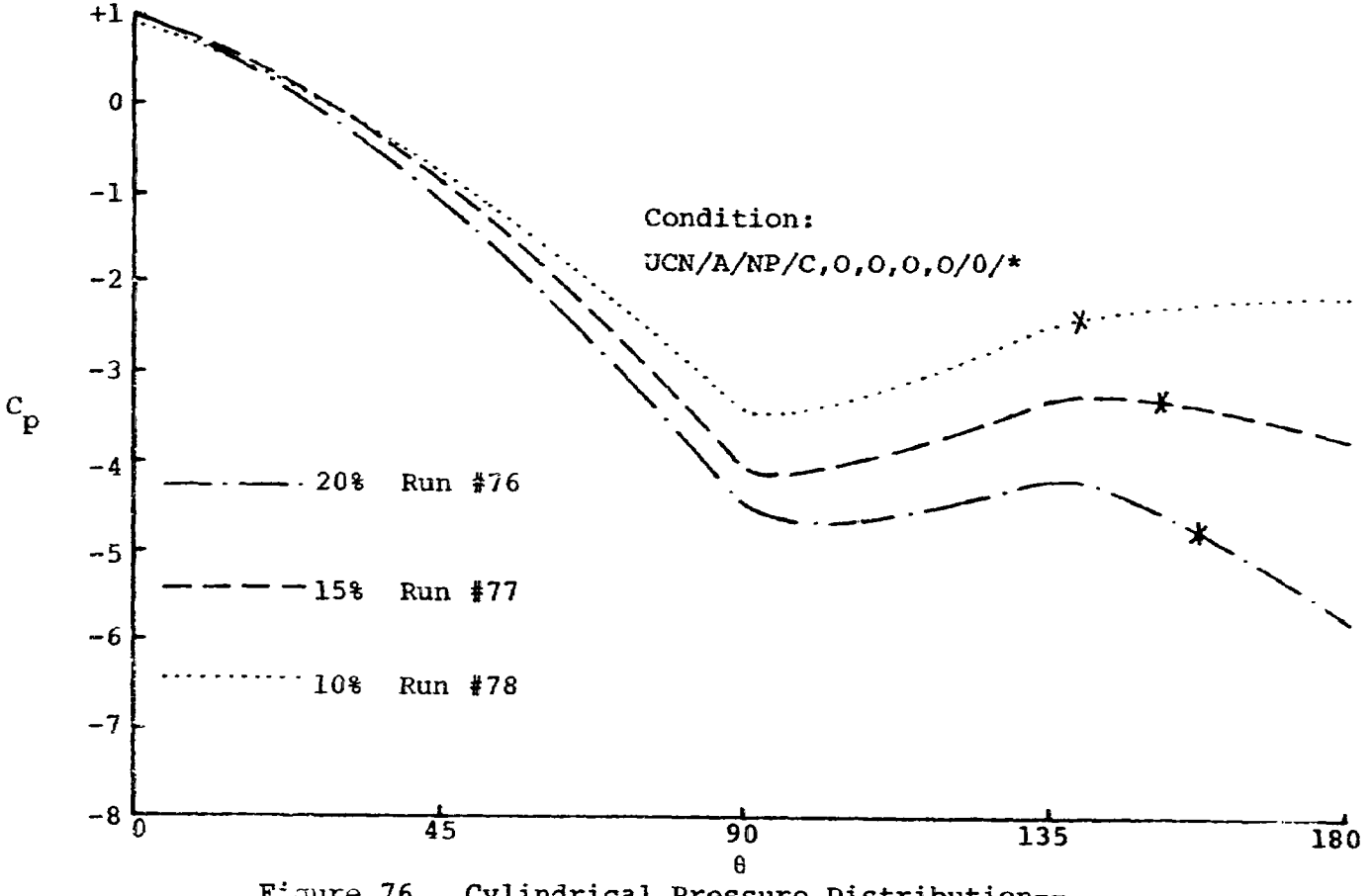

Figure 76. Cylindrical Pressure Distribution--
Effect of Blower Suction with
Non-Porous FBS Aft

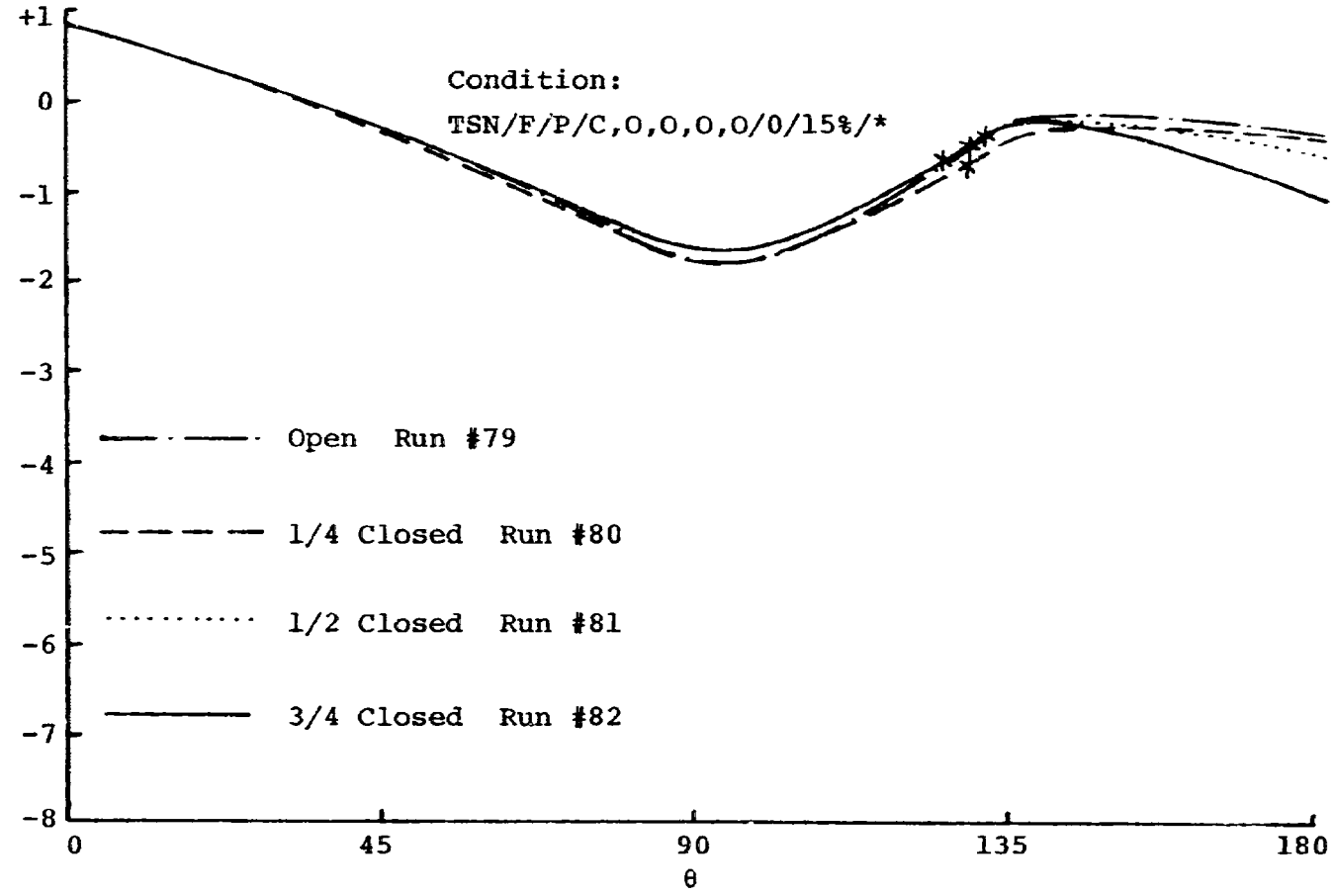

Figure 77. Spherical Pressure Distribution--
Effect of TSN Doors

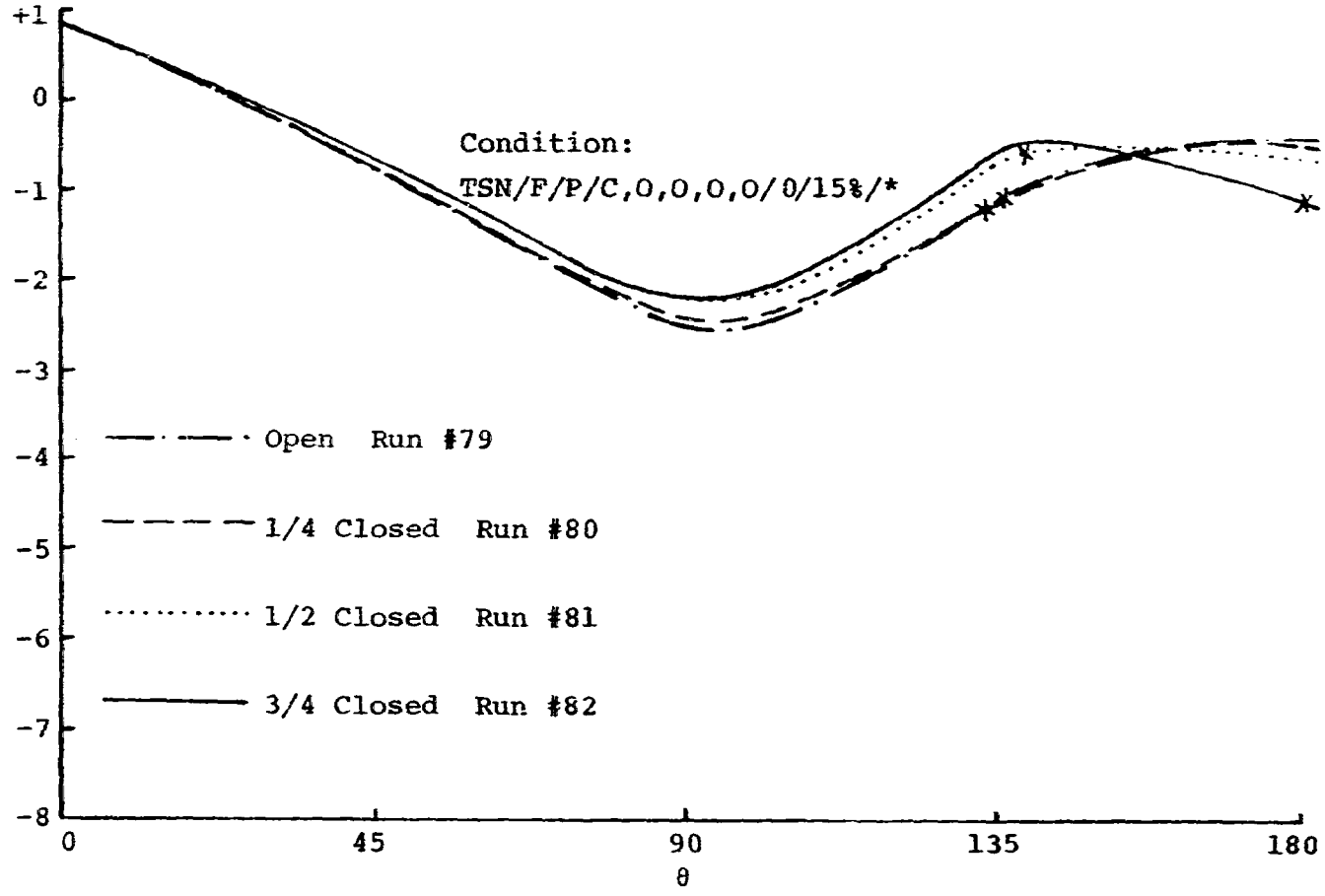

Figure 78. Cylindrical-Spherical Pressure Distribution--
Effect of TSN Doors

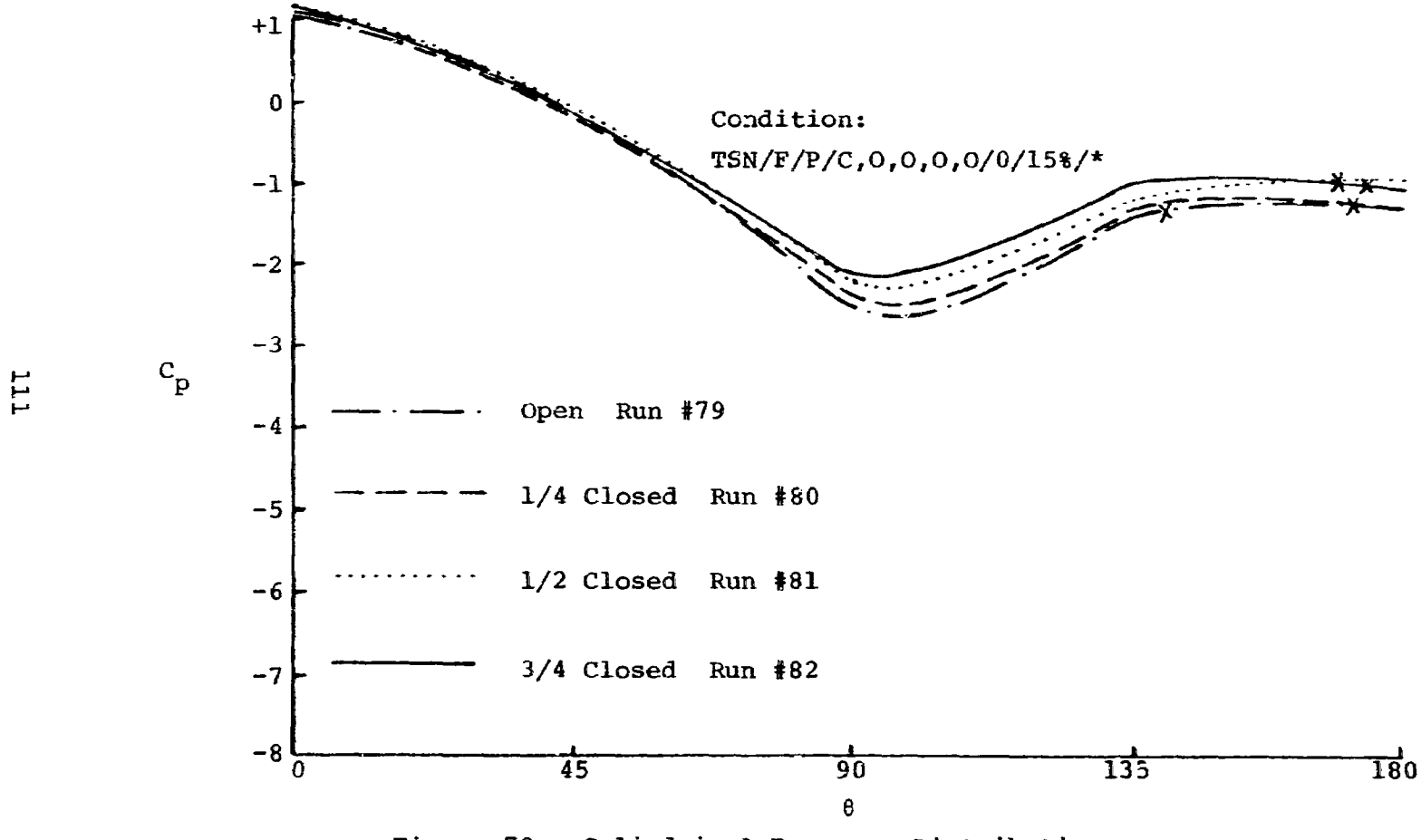

Figure 79. Cylindrical Pressure Distribution--
Effect of TSN Doors

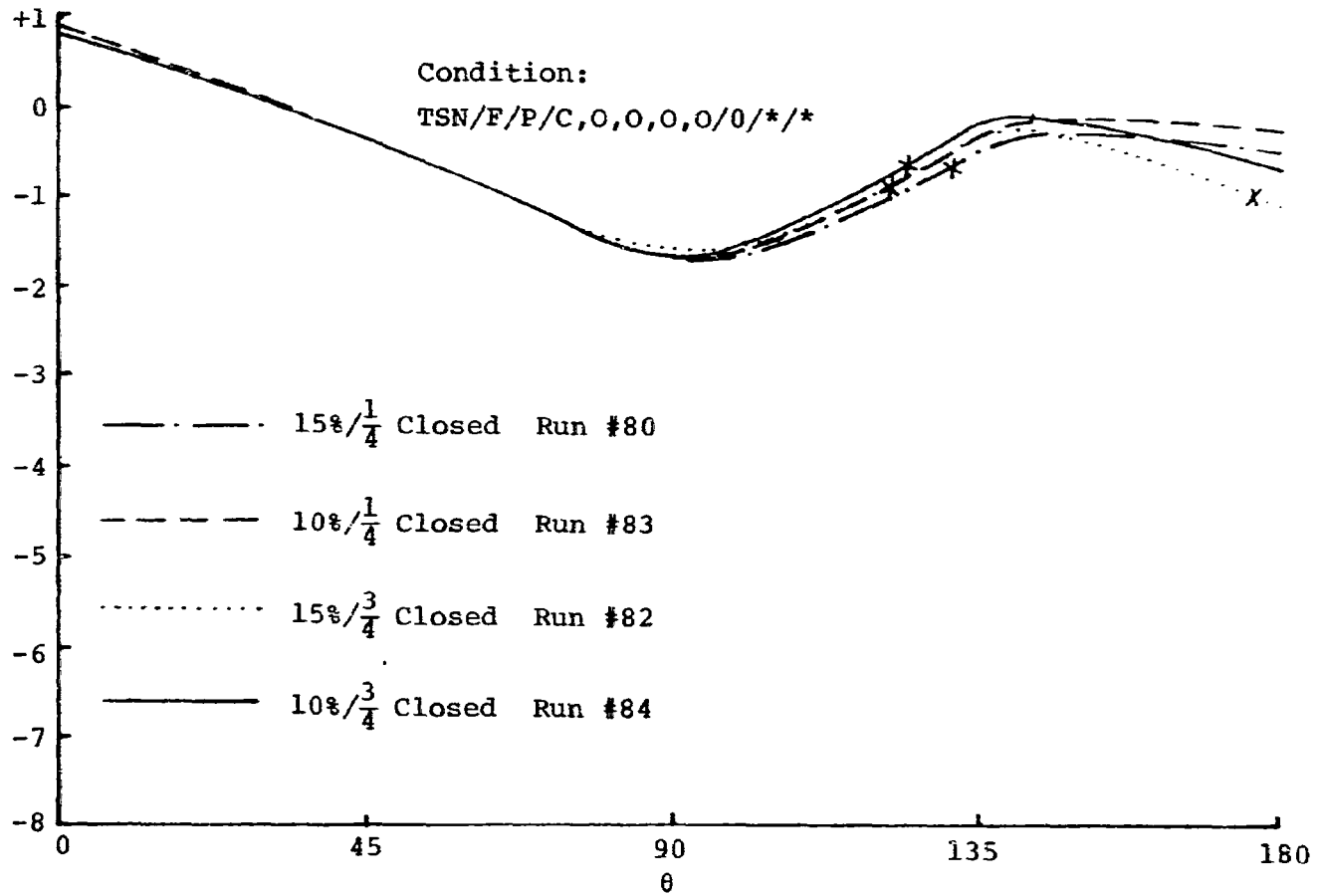

Figure 80. Spherical Pressure Distribution--
Effect of TSN Doors and Reduced Blower Suction

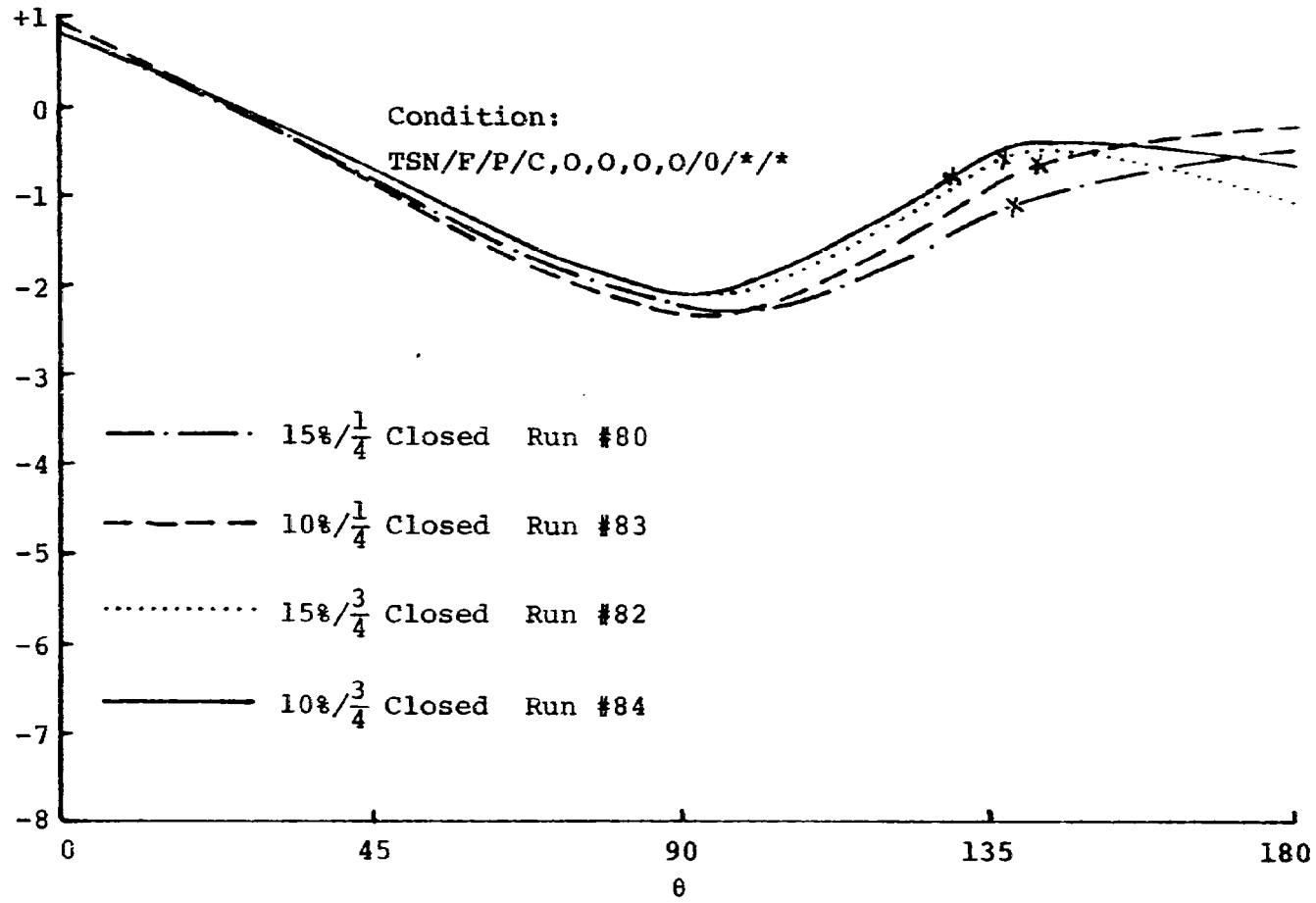

Figure 81. Cylindrical-Spherical Pressure Distribution--
Effect of TSN Doors and Reduced Blower Suction

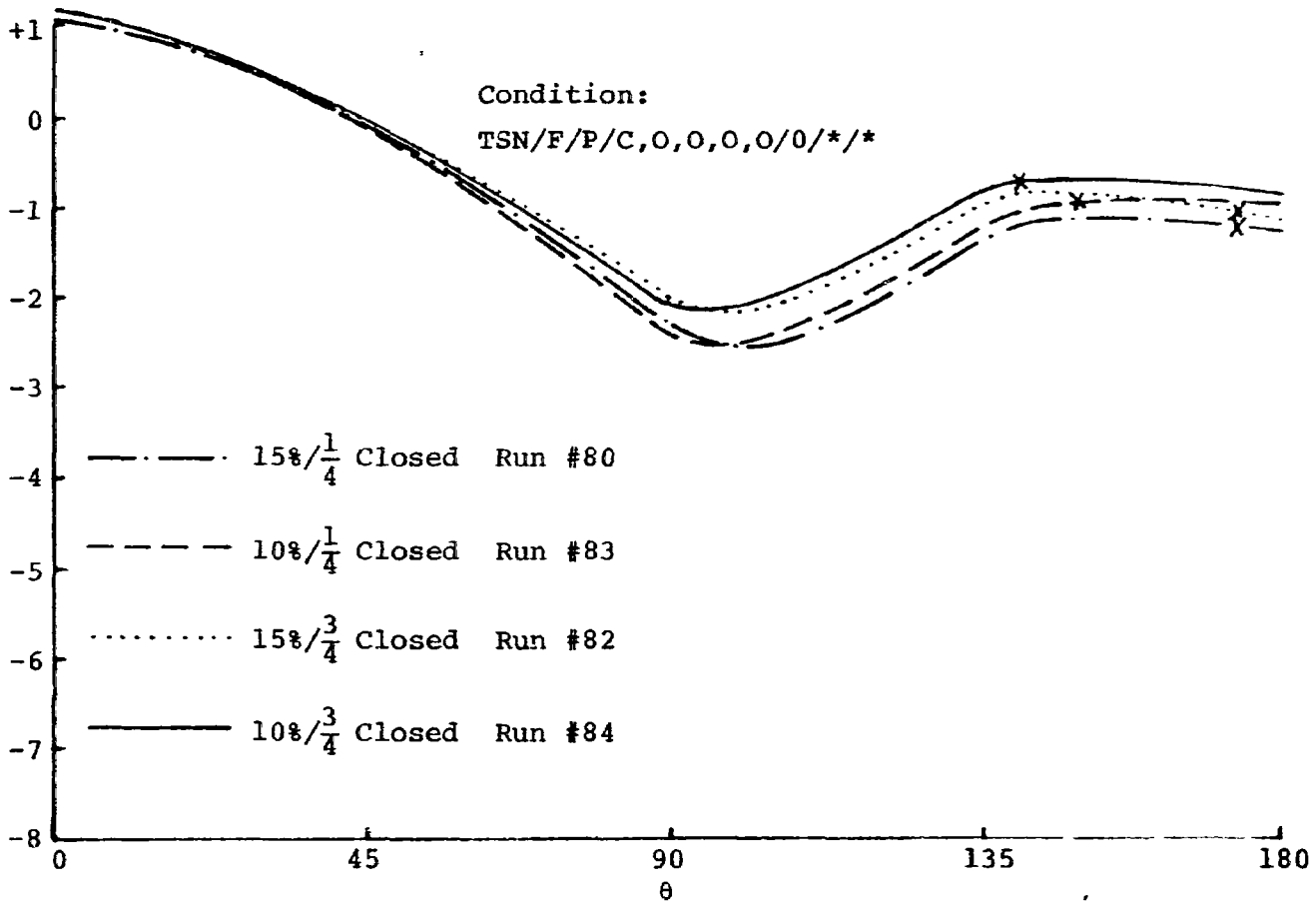

Figure 82. Cylindrical Pressure Distribution--
Effect of TSN Doors and Reduced Blower Suction

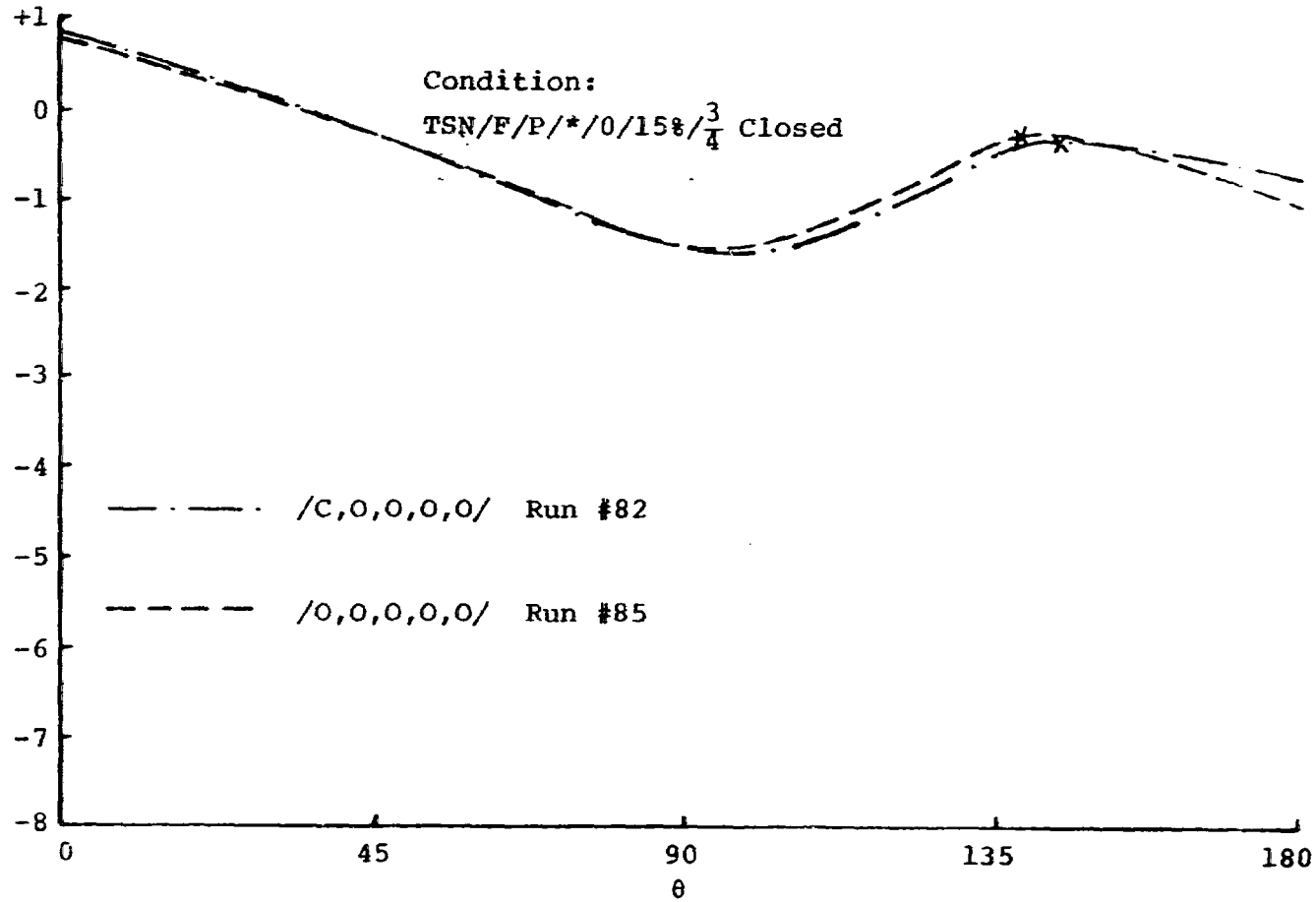

Figure 83. Spherical Pressure Distribution--
Effect of Suction Duct #1 with TSN

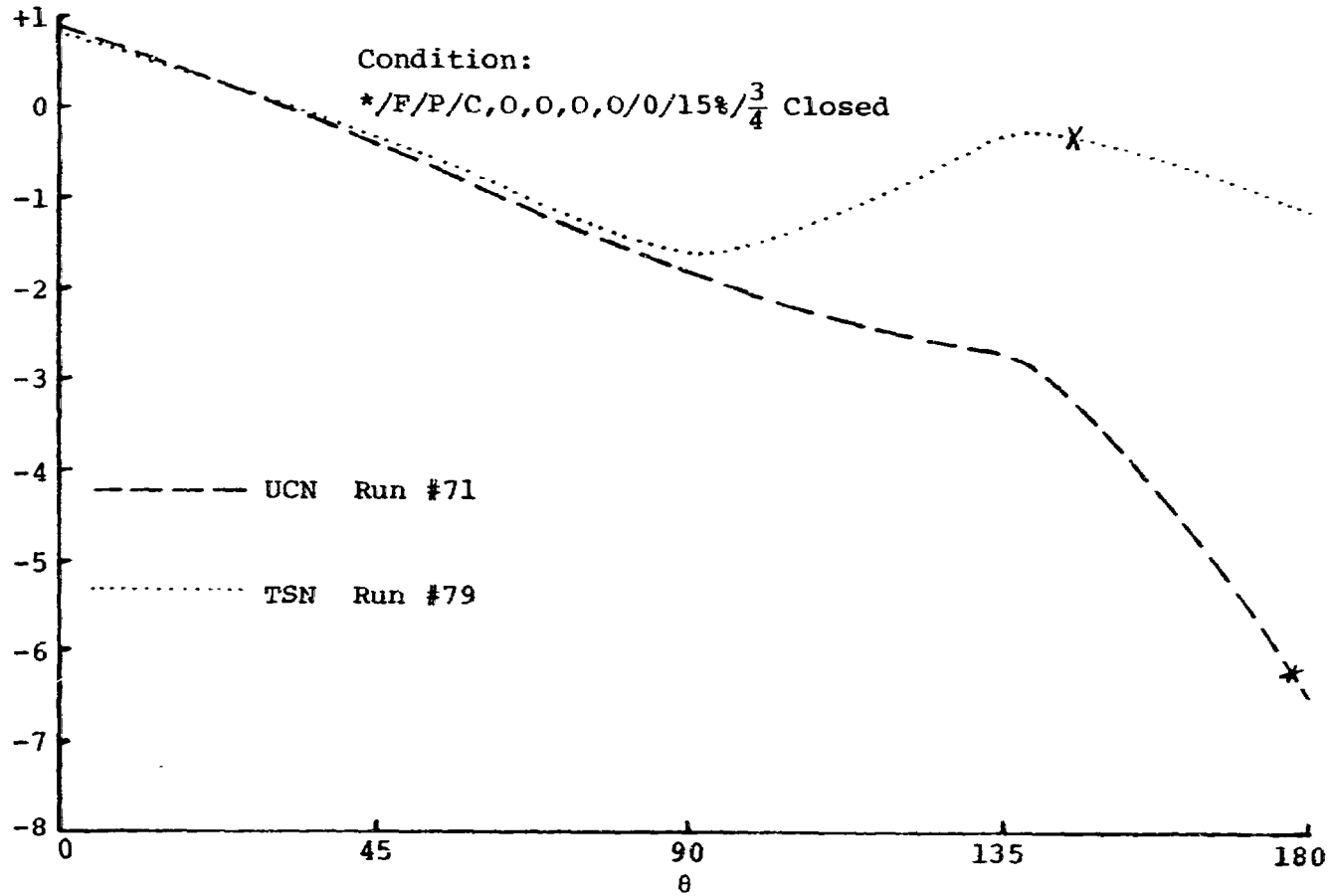

Figure 84. Spherical Pressure Distribution--
Effect of UCN and TSN at
Optimum Condition

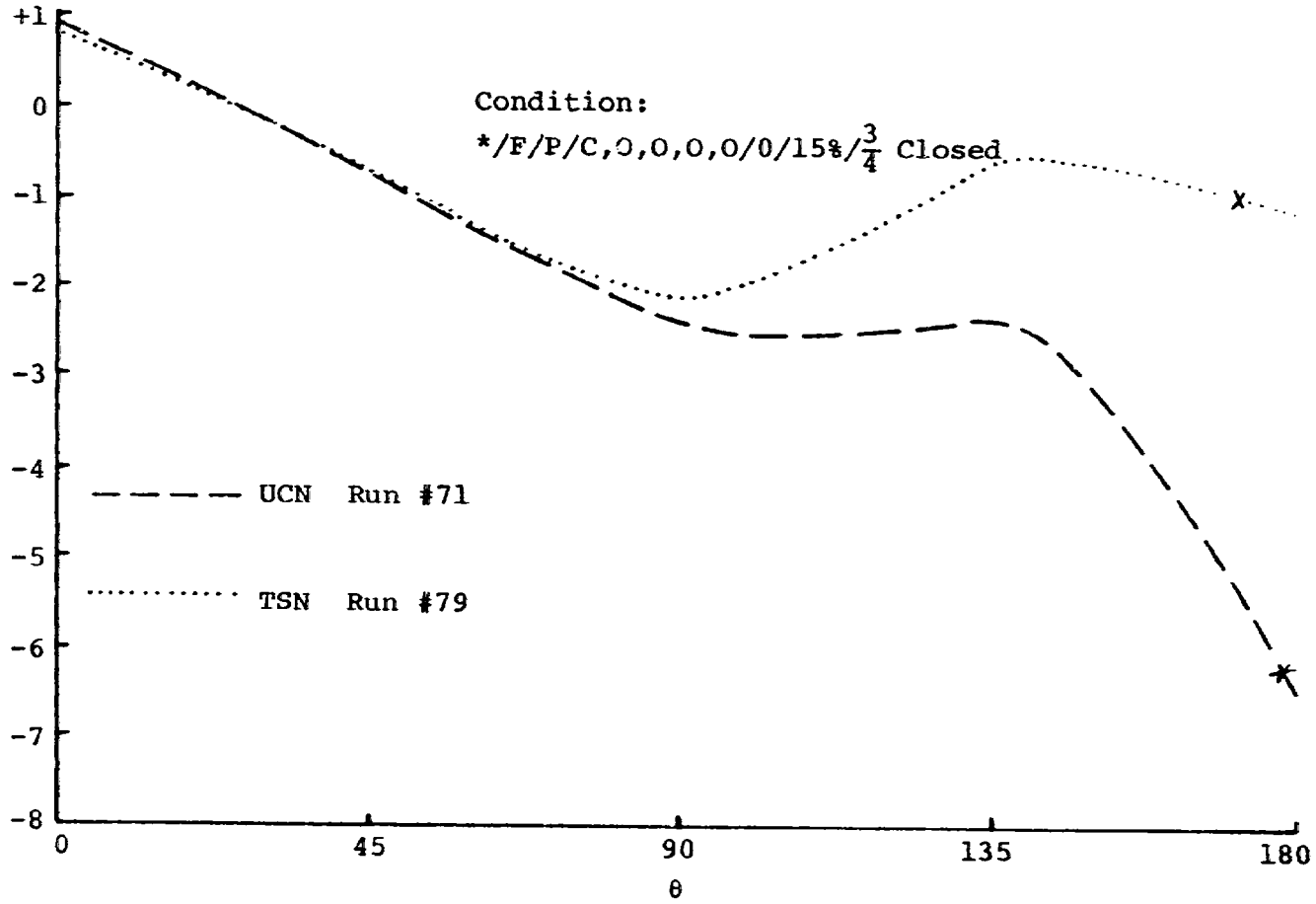

Figure 85. Cylindrical-Spherical Pressure Distribution--
Effect of UCN and TSN at Optimum Condition

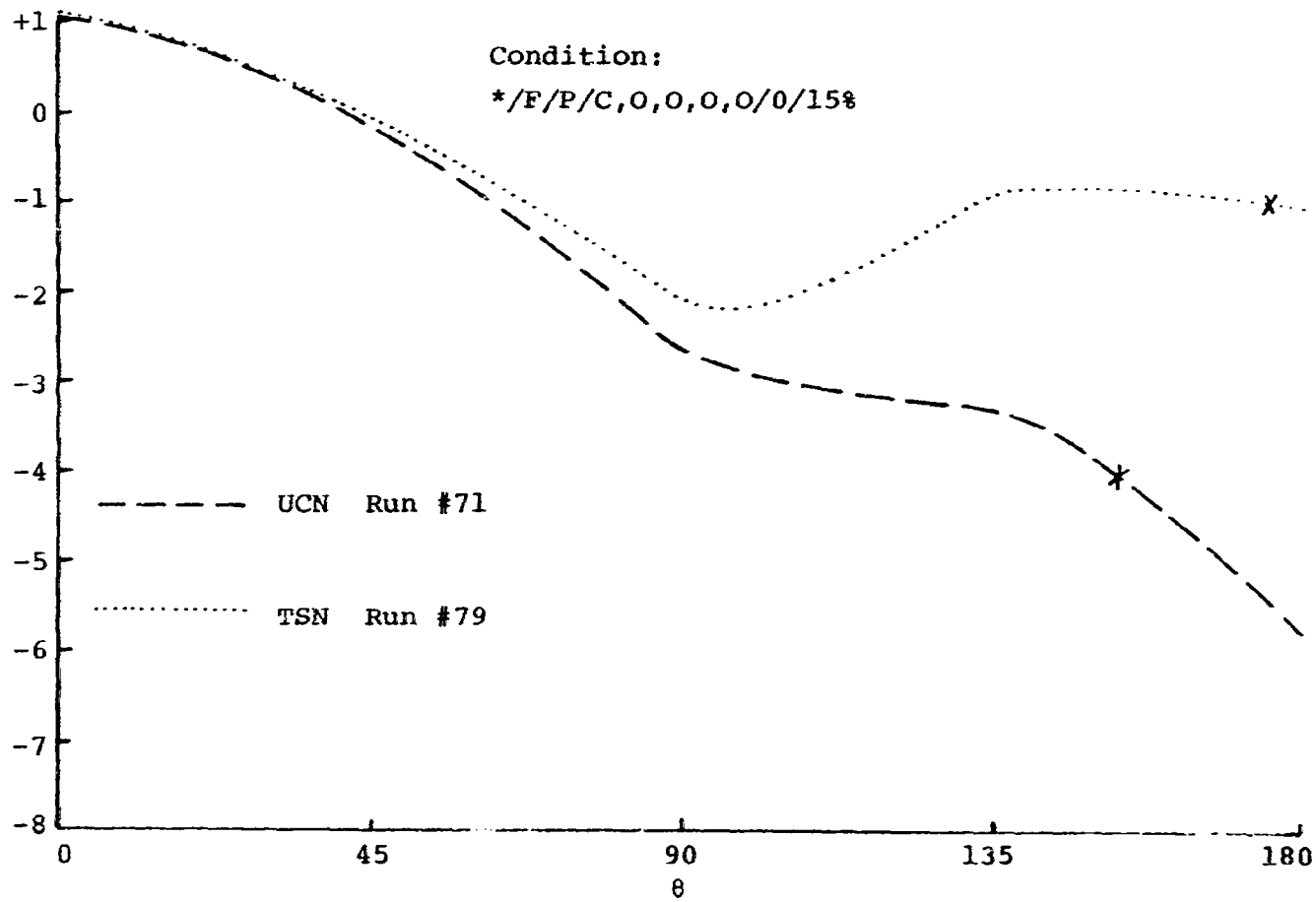

Figure 86. Cylindrical Pressure Distribution--
Effect of UCN and TSN at Optimum Condition

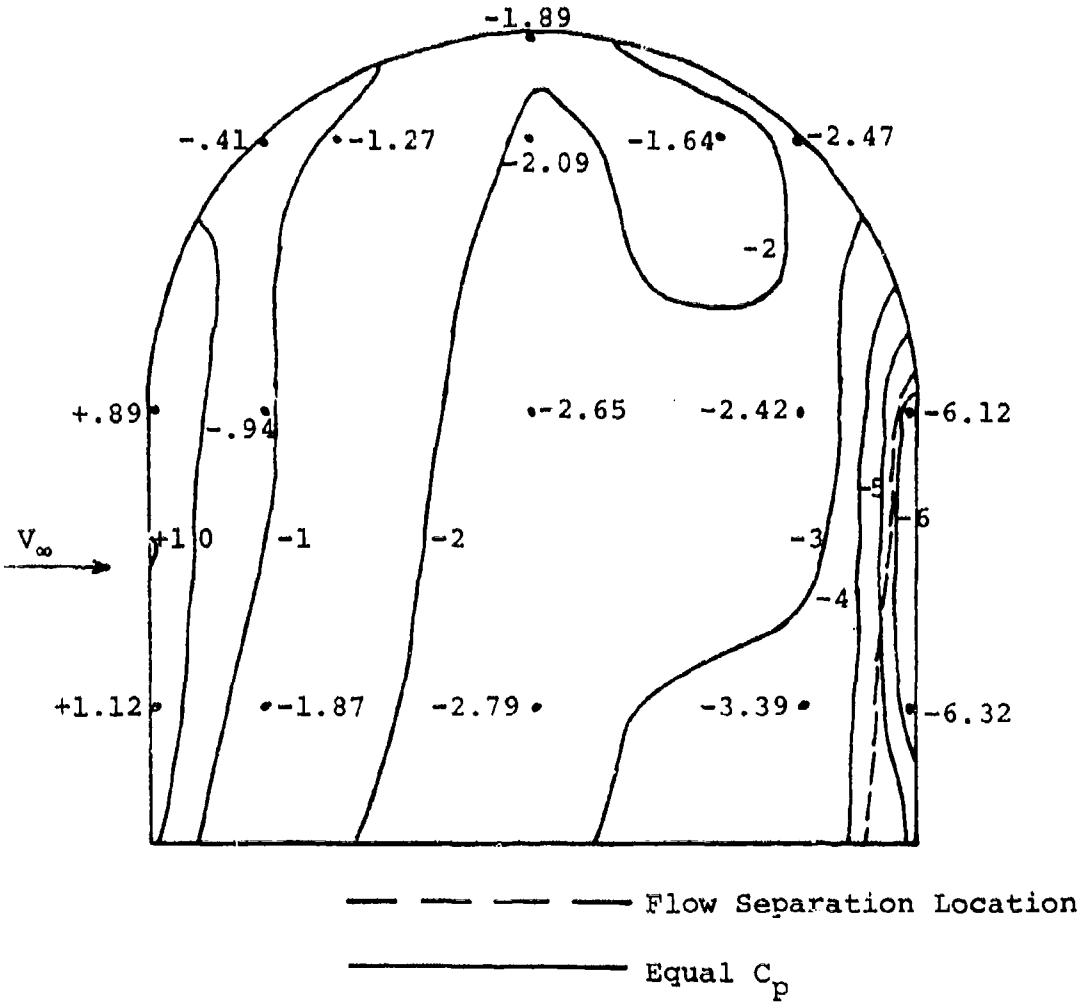

Figure 87. Turret Profile Pressure Distribution--
Run #71 Port Side

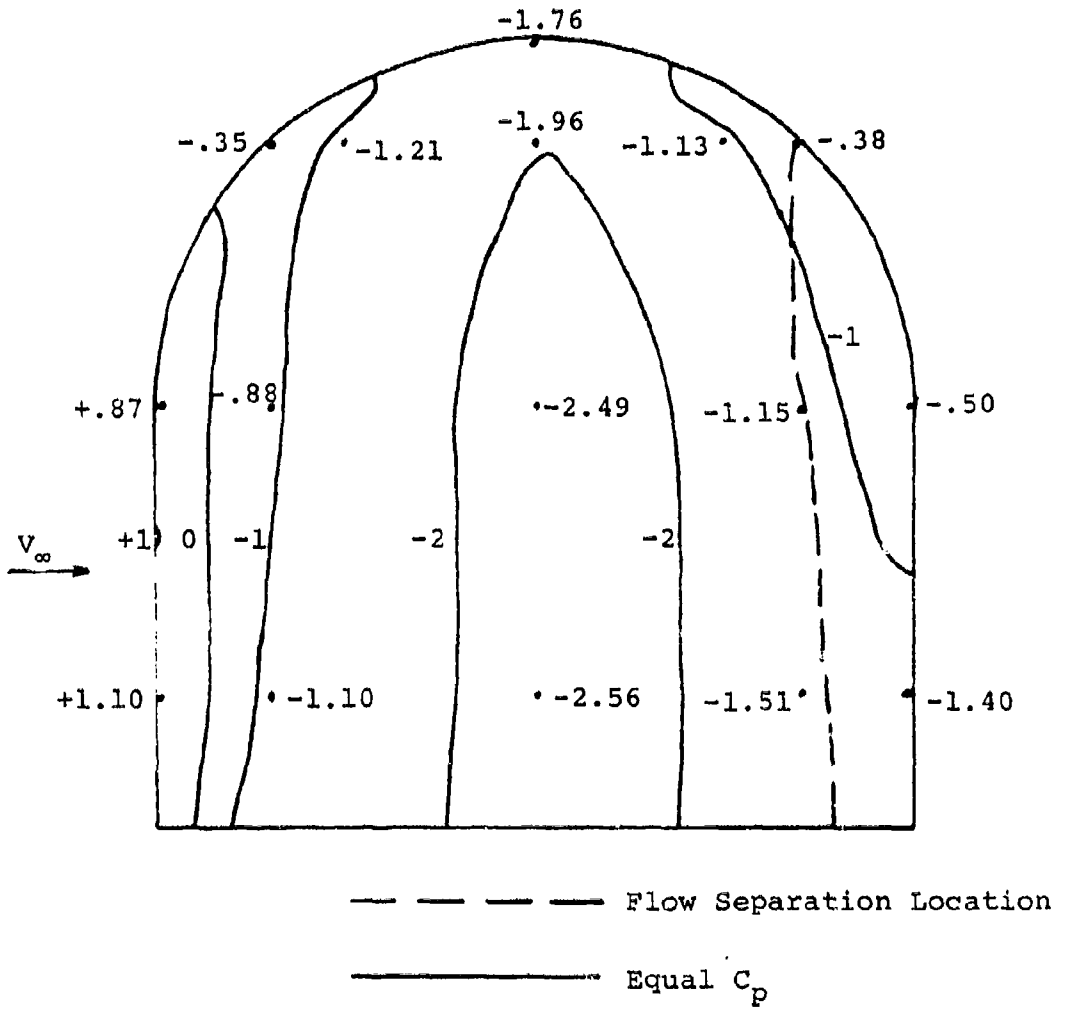

Figure 88. Turret Profile Pressure Distribution--
Run #79 Port Side

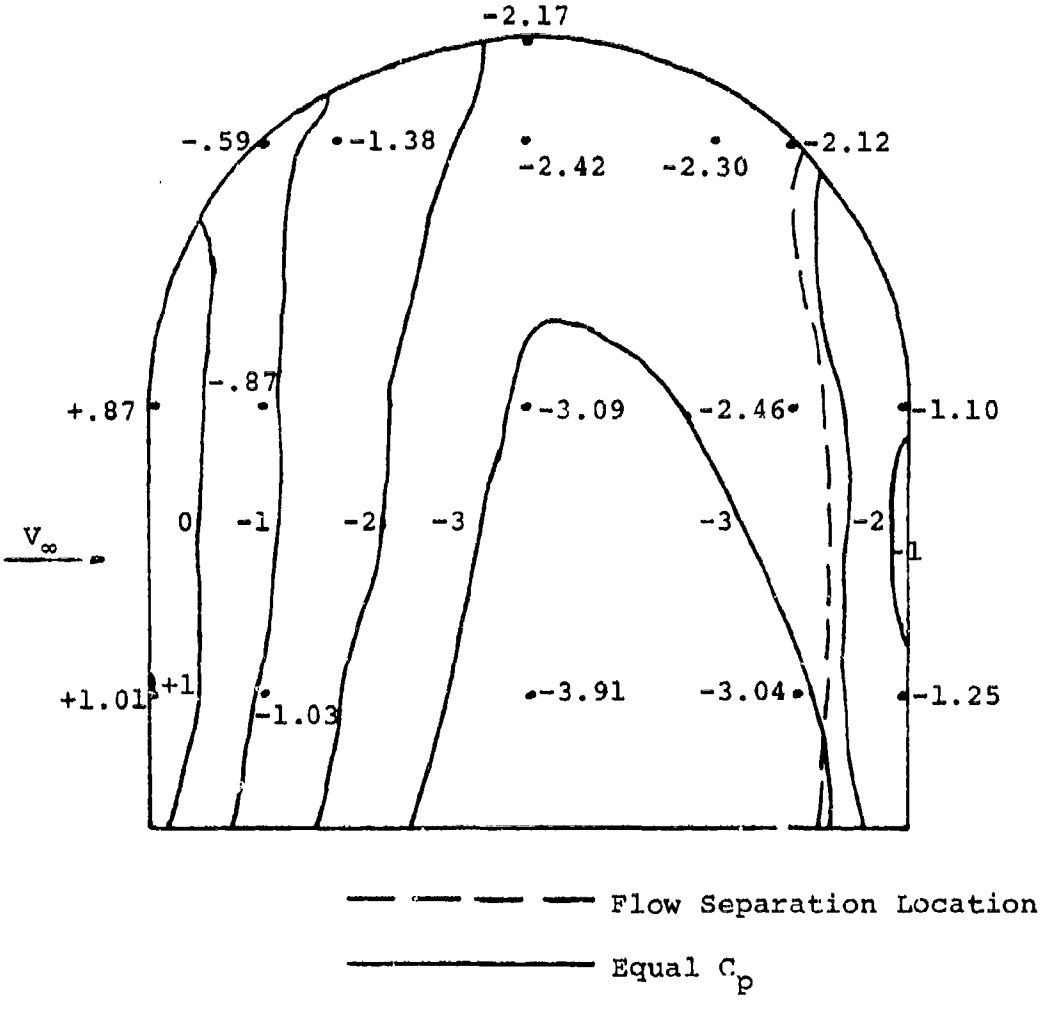

Figure 89. Turret Profile Pressure Distribution--
Run #18 Starboard Side

TABLE 1

PARAMETER VARIATIONS

PARAMETER	# OF SETTINGS	RANGES
Fairing Nosepieces	2	UCN, TSN
FBS Location	3	Forward, Side, Aft
FBS Condition	2	Porous, Non-Porous
Suction Duct Throttle Setting (5 ducts)	3	Open (O), Half-Open $\left(\frac{1}{2}\right)$, Closed (C)
Turret-Fairing Gap	3	0 in. - 2 1/4 in. by 1 1/8 in. increments
Blower Throttle Setting	20	0% - 100% by 5% increments
TSN Door Position	4	Open (O), One-Fourth Closed $\left(\frac{1}{4}C\right)$, One-Half Closed $\left(\frac{1}{2}C\right)$, Three-Fourths Closed $\left(\frac{3}{4}C\right)$

TABLE 2

PRESSURE TAP--SCANIVALVE PORT LOCATIONS

PORT #	LOCATION
1 - 11	Ambient Air
12	Tunnel Wall--Dynamic Probe
13	Tunnel Wall--Static (Fore)
14	Tunnel Wall--Static
15	Tunnel Wall--Static
16	Tunnel Wall--Static
17	Tunnel Wall--Static
18	Tunnel Wall--Static (Aft)
19	Turret Top
20	Turret Hemisphere $\theta = 0^{\circ}$, $\phi = 45^{\circ}$
21	Turret Hemisphere $\theta = 45^{\circ}$, $\phi = 45^{\circ}$
22	Turret Hemisphere $\theta = 90^{\circ}$, $\phi = 45^{\circ}$
23	Turret Hemisphere $\theta = 135^{\circ}$, $\phi = 45^{\circ}$
24	Turret Hemisphere $\theta = 180^{\circ}$, $\phi = 45^{\circ}$
25	Turret Hemisphere $\theta = 225^{\circ}$, $\phi = 45^{\circ}$
26	Turret Hemisphere $\theta = 270^{\circ}$, $\phi = 45^{\circ}$
27	Turret Hemisphere $\theta = 315^{\circ}$, $\phi = 45^{\circ}$
28	Turret Hemisphere $\theta = 0^{\circ}$, $\phi = 0^{\circ}$
29	Turret Hemisphere $\theta = 45^{\circ}$, $\phi = 0^{\circ}$
30	Turret Hemisphere $\theta = 90^{\circ}$, $\phi = 0^{\circ}$
31	Turret Hemisphere $\theta = 135^{\circ}$, $\phi = 0^{\circ}$
32	Turret Hemisphere $\theta = 180^{\circ}$, $\phi = 0^{\circ}$
33	Turret Hemisphere $\theta = 225^{\circ}$, $\phi = 0^{\circ}$
34	Turret Hemisphere $\theta = 270^{\circ}$, $\phi = 0^{\circ}$
35	Turret Hemisphere $\theta = 315^{\circ}$, $\phi = 0^{\circ}$
36	Turret Cylinder $\theta = 0^{\circ}$
37	Turret Cylinder $\theta = 45^{\circ}$
38	Turret Cylinder $\theta = 90^{\circ}$
39	Turret Cylinder $\theta = 135^{\circ}$
40	Turret Cylinder $\theta = 180^{\circ}$
41	Turret Cylinder $\theta = 225^{\circ}$
42	Turret Cylinder $\theta = 270^{\circ}$
43	Turret Cylinder $\theta = 315^{\circ}$
44	Ambient Air
45	Scanivalve Calibration
46 - 48	Ambient Air

TABLE 3

SAMPLE DATA--RUN #71 OPTIMUM CONDITIONS

PORT #	TRANSDUCER VOLTAGE	C_p	PORT #	TRANSDUCER VOLTAGE	C_p
11	-0.038		29	-0.318	-3.12
12	-0.046		30	-0.296	-2.79
13	-0.062		31	-0.166	-0.82
14	-0.112		32	-0.053	+0.89
15	-0.064		33	-0.174	-0.94
16	-0.074		34	-0.287	-2.65
17	-0.068		35	-0.272	-2.42
18	-0.110		36	-0.529	-6.32
19	-0.237	-1.89	37	-0.386	-4.15
20	-0.275	-2.47	38	-0.311	-3.02
21	-0.227	-1.74	39	-0.185	-1.11
22	-0.251	-2.11	40	-0.038	+1.12
23	-0.194	-1.24	41	-0.187	-1.14
24	-0.139	-0.41	42	-0.296	-2.79
25	-0.196	-1.27	43	-0.336	-3.39
26	-0.250	-2.09	44	-0.029	
27	-0.220	-1.64	45	-0.038	
28	-0.516	-6.12			

	1	2	3	4	5
Suction Duct Voltages	0	0.147	7.33	2.42	0.009
Suction Duct Velocities	0	36.79	47.48	15.93	10.87

Tunnel Velocity--40.8 ft/sec

TABLE 4

SAMPLE DATA--RUN #82

PORT #	TRANSDUCER VOLTAGE	C_p	PORT #	TRANSDUCER VOLTAGE	C_p
11	-0.031		29	-0.160	-0.78
12	-0.037		30	-0.252	-2.12
13	-0.055		31	-0.148	-0.61
14	-0.106		32	-0.047	+0.86
15	-0.057		33	-0.163	-0.83
16	-0.068		34	-0.257	-2.19
17	-0.063		35	-0.156	-0.72
18	-0.103		36	-0.187	-1.17
19	-0.219	-1.64	37	-0.165	-0.86
20	-0.129	-0.33	38	-0.253	-2.13
21	-0.174	-0.99	39	-0.175	-1.00
22	-0.232	-1.83	40	-0.032	+1.07
23	-0.179	-1.06	41	-0.182	-1.10
24	-0.130	-0.35	42	-0.256	-2.17
25	-0.184	-1.13	43	-0.174	-0.99
26	-0.229	-1.78	44	-0.025	
27	-0.163	-0.83	45	+0.006	
28	-0.188	-1.19			

	1	2	3	4	5
Suction Duct Voltages	0	0.078	3.23	5.10	0.047
Suction Duct Velocities	0	23.46	23.65	27.89	21.94

Tunnel Velocity--41.7 ft/sec

TABLE 5

TRIAL SUMMARY

Run Number	Conditions	Duct Velocities (ft/sec)	Duct Mass Flow Rate (lbm/sec)
1	UCN/A/P/O,O,O,O,O/O/O		
2	TSN/A/P/O,O,O,O,O/O/O/O		
3	UCN/A/P/O,O,O,O,O/O/25%	56.1/51.6/39.9/9.0/35.4	1.77/1.04/2.11/0.11/2.25
4	UCN/F/P/O,O,O,O,O/O/25%	55.8/52.1/43.8/7.4/17.3	1.76/1.05/2.32/0.09/1.10
5	UCN/S/P/O,O,O,O,O/O/25%	54.7/53.4/43.5/5.2/30.6	1.72/1.08/2.31/0.07/1.95
6	UCN/S/NP/O,O,O,O,O/O/25%	53.0/42.8/41.6/0/29.8	1.67/0.86/2.20/0/1.90
7	UCN/F/NP/O,O,O,O,O/O/25%	55.0/39.3/42.7/0/38.2	1.73/0.79/2.26/0/2.43
8	UCN/A/NP/O,O,O,O,O/O/25%	52.2/35.6/34.7/0/35.4	1.64/0.72/1.84/0/2.25
9	UCN/A/NP/O,O,O,O,O/O/20%	44.8/30.5/28.7/0/33.3	1.41/0.62/1.52/0/2.12
10	UCN/F/NP/O,O,O,O,O/O/20%	46.0/33.5/35.1/0/30.0	1.45/0.68/1.86/0/1.91
11	UCN/S/NP/O,O,O,O,O/O/20%	45.3/36.0/35.1/0/12.8	1.43/0.73/1.86/0/0.82
12	UCN/A/P/O,O,O,O,O/O/20%	46.9/32.6/34.8/0/18.4	1.48/0.66/1.84/0/1.17
13	UCN/F/P/O,O,O,O,O/O/20%	48.6/33.7/38.5/0/10.2	1.53/0.68/2.04/0/0.65
14	UCN/S/P/O,O,O,O,O/O/20%	47.6/34.2/36.5/0/12.5	1.50/0.69/1.93/0/0.80

Run Number	Conditions	Duct Velocities (ft/sec)	Duct Mass Flow Rate (lbm/sec)
15	UCN/A/P/O,O,O,O,O/O/$1\frac{1}{8}$/20%	47.4/39.6/36.9/9.7/23.5	1.49/0.80/1.96/0.12/1.50
16	UCN/A/P/O,O,O,O,O/O/$2\frac{1}{4}$/20%	47.6/41.5/37.5/11.2/24.7	1.50/0.84/1.99/0.14/1.57
17	UCN/A/NP/O,O,O,O,O/O/$1\frac{1}{8}$/20%	44.1/36.3/32.6/0/25.0	1.39/0.73/1.73/0/1.59
18	UCN/A/NP/O,O,O,O,O/O/$2\frac{1}{4}$/20%	43.9/38.1/34.3/8.8/36.1	1.38/0.77/1.82/0.11/2.30
19	UCN/A/P/O,O,O,O,C/O/20%	50.7/36.8/41.2/18.8/0	1.60/0.74/2.18/0.24/0
20	UCN/A/P/C,C,C,C,O/O/20%	8.1/0/0/0/42.5	0.26/0/0/0/2.71
21	UCN/A/P/C,O,C,O,C/O/20%	6.7/87.6/0/50.2/9.9	0.21/1.77/0/0.63/0.63
22	UCN/A/P/O,C,O,C,O/O/20%	53.0/5.5/40.5/0/19.2	1.67/0.11/2.15/0/1.22
23	UCN/A/P/$\frac{1}{2},\frac{1}{2},\frac{1}{2},\frac{1}{2},\frac{1}{2}$/O/20%	26.7/27.7/33.2/19.9/20.9	0.84/0.56/1.76/0.25/1.33
24	UCN/A/P/$\frac{1}{2},\frac{1}{2},\frac{1}{2},\frac{1}{2}$,O/O/20%	25.4/25.0/29.6/17.0/26.9	0.80/0.50/1.57/0.21/1.71
25	UCN/A/P/O,O,O,O,$\frac{1}{2}$/O/20%	48.0/33.3/36.3/9.9/11.8	1.51/0.67/1.92/0.12/0.75
26	UCN/A/P/O,O,O,O,C/O/20%	43.6/30.5/40.6/20.1/0	1.37/0.62/2.15/0.25/0
27	UCN/A/P/O,O,O,C,O/O/20%	47.4/27.3/36.3/0/18.4	1.49/0.55/1.92/0/1.17
28	UCN/A/P/O,O,C,O,O/O/20%	55.6/42.1/0/19.9/25.2	1.75/0.85/0/0.25/1.61
29	UCN/A/P/O,C,O,O,O/O/20%	53.5/0/39.0/0/23.5	1.69/0/2.07/0/1.50
30	UCN/A/P/C,O,O,O,O/O/20%	0/40.8/46.8/12.5/25.5	0/0.82/2.48/0.16/1.62
31	UCN/A/P/$\frac{1}{2}$,O,O,O,O/O/20%	17.1/41.4/43.8/11.0/27.8	0.54/0.84/2.32/0.14/1.77

Run Number	Conditions	Duct Velocities (ft/sec)	Duct Mass Flow Rate (lbm/sec)
32	UCN/A/P/O,$\frac{1}{2}$,O,O,O/0/20%	42.6/14.8/36.7/0/21.4	1.34/0.30/1.94/0/1.36
33	UCN/A/P/O,O,$\frac{1}{2}$,O,O/0/20%	42.3/35.4/21.2/10.6/20.6	1.33/0.71/1.12/0.13/1.31
34	UCN/A/P/O,O,O,$\frac{1}{2}$,O/0/20%	47.0/26.9/34.8/0/19.2	1.48/0.54/1.84/0/1.22
35	UCN/A/P/O,O,O,O,$\frac{1}{2}$/0/20%	47.6/26.9/35.7/8.1/12.5	1.50/0.54/1.89/0.10/0.80
36	UCN/A/P/C,C,O,O,O/0/20%	0/0/48.3/18.6/30.0	0/0/2.56/0.23/1.91
37	UCN/A/P/O,C,C,O,O/0/20%	60.8/0/0/23.0/28.7	1.92/0/0/0.29/1.83
38	UCN/A/P/O,O,C,C,O/0/20%	57.2/44.8/0/0/25.9	1.80/0.90/0/0/1.65
39	UCN/A/P/O,O,O,C,C/0/20%	52.0/33.0/44.4/0/0	1.64/0.67/2.35/0/0
40	UCN/A/P/$\frac{1}{2}$,$\frac{1}{2}$,O,O,O/0/20%	23.7/18.2/44.2/12.5/24.7	0.75/0.37/2.34/0.16/1.57
41	UCN/A/P/O,$\frac{1}{2}$,$\frac{1}{2}$,O,O/0/20%	55.0/15.3/25.3/11.6/21.2	1.73/0.31/1.34/0.15/1.35
42	UCN/A/P/O,O,$\frac{1}{2}$,$\frac{1}{2}$,O/0/20%	49.6/34.9/23.2/0/19.2	1.56/0.70/1.23/0/1.22
43	UCN/A/P/O,O,O,$\frac{1}{2}$,$\frac{1}{2}$/0/20%	47.4/28.1/35.9/0/15.8	1.49/0.57/1.90/0/1.00
44	UCN/A/P/C,O,O,O,O/0/20%	0/41.7/46.5/12.2/25.0	0/0.84/2.46/0.15/1.59
45	UCN/A/P/C,O,O,$\frac{1}{2}$,O/0/20%	0/41.5/47.8/0/24.5	0/0.84/2.53/0/1.56
46	UCN/A/P/C,O,O,C,O/0/20%	0/42.1/49.7/0/23.7	0/0.85/2.63/0/1.51
47	UCN/A/P/C,C,O,O,O/0/20%	0/0/48.4/19.5/27.1	0/0/2.56/0.25/1.73
48	UCN/A/P/C,$\frac{1}{2}$,O,O,O/0/20%	0/15.8/48.5/16.4/25.9	0/0.32/2.57/0.21/1.65

Run Number	Conditions	Duct Velocities (ft/sec)	Duct Mass Flow Rate (lbm/sec)
49	UCN/A/P/C,O,O,O,O/0/20%	0/42.0/46.4/12.0/25.7	0/0.85/2.46/0.15/1.64
50	UCN/A/P/C,O,$\frac{1}{2}$,O,O/0/20%	0/50.9/31.3/22.6/25.9	0/1.03/1.66/0.29/1.65
51	UCN/A/P/C,O,C,O,O/0/20%	0/51.7/0/26.0/29.1	0/1.04/0/0.33/1.85
52	UCN/A/P/C,O,O,O,O/0/20%	0/41.5/46.2/12.3/25.7	0/0.84/2.44/0.16/1.64
53	UCN/A/P/C,O,O,O,O/0/15%	0/37.1/42.1/0/22.7	0/0.75/2.23/0/1.45
54	UCN/A/P/C,O,O,O,O/0/10%	0/30.1/36.2/0/17.6	0/0.61/1.92/0/1.12
55	UCN/A/P/C,O,O,O,O/0/5%	0/21.9/30.8/0/14.6	0/0.44/1.63/0/0.93
56	UCN/S/P/C,O,O,O,O/0/20%	0/45.7/51.6/12.5/16.7	0/0.92/2.73/0.16/1.06
57	UCN/S/P/C,O,O,O,O/0/15%	0/42.0/46.4/11.6/14.6	0/0.85/2.46/0.15/0.93
58	UCN/S/P/C,O,O,O,O/0/10%	0/30.7/37.0/0/9.9	0/0.62/1.96/0/0.63
59	UCN/S/P/C,O,O,O,O/0/5%	0/26.3/33.2/0/10.2	0/0.53/1.76/0/0.65
60	UCN/F/P/C,O,O,O,O/0/20%	0/42.9/52.8/12.4/14.0	0/0.87/2.80/0.16/0.89
61	UCN/F/P/C,O,O,O,O/0/15%	0/37.9/47.5/12.2/11.5	0/0.77/2.52/0.15/0.73
62	UCN/F/P/C,O,O,O,O/0/10%	0/26.9/38.0/0/10.2	0/0.54/2.01/0/0.65
63	UCN/F/P/C,O,O,O,O/0/5%	0/20.5/32.2/0/9.6	0/0.41/1.71/0/0.61
64	UCN/S/P/C,O,O,O,O/1$\frac{1}{8}$/20%	0/39.3/52.5/20.9/18.1	0/0.79/2.78/0.26/1.15
65	UCN/S/P/C,O,O,O,O/1$\frac{1}{8}$/15%	0/45.9/46.2/18.6/14.9	0/0.93/2.45/0.23/0.95

Run Number	Conditions	Duct Velocities (ft/sec)	Duct Mass Flow Rate (lbm/sec)
66	UCN/S/P/C,0,0,0,0/0/1$\frac{1}{8}$/10%	0/39.9/38.5/13.3/13.1	0/0.81/2.04/0.17/0.83
67	UCN/A/P/C,0,0,0,0/0/1$\frac{1}{8}$/20%	0/48.3/49.1/15.3/23.2	0/0.98/2.60/0.19/1.48
68	UCN/A/P/C,0,0,0,0/0/1$\frac{1}{8}$/15%	0/44.9/43.4/14.6/16.1	0/0.91/2.30/0.18/1.03
69	UCN/A/P/C,0,0,0,0/0/1$\frac{1}{8}$/10%	0/37.6/36.6/12.3/15.2	0/0.76/1.94/0.16/0.97
70	UCN/A/P/C,0,0,0,0/0/0/15%	0/36.0/41.8/7.8/21.2	0/0.73/2.21/0.10/1.35
71	UCN/F/P/C,0,0,0,0/0/0/15%	0/36.8/47.5/15.9/10.9	0/0.74/2.52/0.20/0.69
72	UCN/S/P/C,0,0,0,0/0/0/15%	0/40.1/45.5/11.2/13.1	0/0.81/2.41/0.14/0.83
73	UCN/F/NP/C,0,0,0,0/0/0/20%	0/38.6/48.7/10.4/35.9	0/0.78/2.58/0.13/2.29
74	UCN/F/NP/C,0,0,0,0/0/0/15%	0/33.3/43.8/9.0/32.0	0/0.67/2.32/0.11/2.04
75	UCN/F/NP/C,0,0,0,0/0/0/10%	0/22.6/35.2/0/23.7	0/0.46/1.87/0/1.51
76	UCN/A/NP/C,0,0,0,0/0/0/20%	0/37.0/38.8/0/32.8	0/0.75/2.06/0/2.09
77	UCN/A/NP/C,0,0,0,0/0/0/15%	0/30.7/34.7/0/17.6	0/0.62/1.84/0/1.12
78	UCN/A/NP/C,0,0,0,0/0/0/10%	0/21.9/28.7/0/14.0	0/0.44/1.52/0/0.89
79	TSN/F/P/C,0,0,0,0/0/0/15%/0	0/25.2/37.8/23.6/14.3	0/0.51/2.00/0.30/0.91
80	TSN/F/P/C,0,0,0,0/0/0/15%/$\frac{1}{4}$C	0/23.2/36.0/26.4/16.4	0/0.47/1.91/0.33/1.04
81	TSN/F/P/C,0,0,0,0/0/0/15%/$\frac{1}{2}$C	0/19.4/35.7/29.1/19.5	0/0.39/1.89/0.37/1.24
82	TSN/F/P/C,0,0,0,0/0/0/15%/$\frac{3}{4}$C	0/23.5/23.7/27.9/21.4	0/0.47/1.26/0.35/1.36

Run Number	Conditions	Duct Velocities (ft/sec)	Duct Mass Flow Rate (lbm/sec)
83	TSN/F/P/C,O,O,O,O/O/10%/$\frac{1}{4}$C	0/18.2/31.0/23.2/12.5	0/0.37/1.64/0.29/0.80
84	TSN/F/P/C,O,O,O,O/O/10%/$\frac{3}{4}$C	0/17.7/19.1/25.2/14.9	0/0.36/1.01/0.32/0.95
85	TSN/F/P/O,O,O,O,O/O/15%/$\frac{3}{4}$C	10.4/10.9/21.8/27.5/20.9	0.33/0.22/1.16/0.35/1.33

TABLE 6

POROUS/NON-POROUS CONCLUSIONS

FIGURES	and	FIGURES	CONCLUSION
12, 13		14, 15	Porous better SPH and CYL
16, 17, 18		19, 20, 21	Porous better SPH and CYL
22, 23, 24		25, 26, 27	Porous better SPH, CYL-SPH and CYL
59, 60, 61		71, 72, 73	Porous better SPH, CYL-SPH and CYL
53, 54, 55		74, 75, 76	Porous better SPH, CYL-SPH and CYL

TABLE 7

TURRET-FAIRING GAP CONCLUSIONS

FIGURES	and	FIGURES	CONCLUSION
22, 23, 24			0 in. gap better SPH, CYL-SPH and CYL
25, 26, 27			0 in. gap better SPH, CYL-SPH and CYL
56, 57, 58		62, 63, 64	0 in. gap better SPH, CYL-SPH and CYL
53, 54, 55		65, 66, 67	0 in. gap better SPH, CYL-SPH and CYL

TABLE 8

FUSELAGE BLEED SLOT LOCATION CONCLUSIONS

FIGURES	and	FIGURES	CONCLUSION
12, 13			Forward better SPH Aft better CYL
14, 15			Inconclusive SPH Forward Better CYL
16, 17, 18			Aft better SPH Aft better CYL-SPH Side better CYL
19, 20, 21			Inconclusive SPH Aft better CYL-SPH Forward better CYL
68, 69, 70			Forward better SPH Inconclusive CYL-SPH Forward better CYL Side worst of the three
53, 54, 55		59, 60, 61	Forward better SPH Inconclusive CYL-SPH Forward better CYL

TABLE 9

SUCTION DUCT THROTTLE CONCLUSIONS

FIGURES	and	FIGURES	CONCLUSION
28, 29, 30			Combination of both fairing and FBS needed
31, 32			Alternate throttle closing inconclusive
22, 23, 24		33, 34, 35	All throttles open slightly better than all throttles half closed
36, 37, 38		39, 40, 41	#1 closed produced better SPH, CYL-SPH and CYL; #1 closed slightly better than #1 half closed
36, 37, 38		42, 43, 44	#1 and #2 closed produced best SPH, CYL-SPH and CYL of any two adjacent throttles closed; not as good as only #1 closed
42, 43, 44		45, 46, 47	#1 and #2 half closed produced best SPH, CYL-SPH and CYL of any two adjacent throttles half-closed; slightly better SPH and CYL-SPH than #1 and #2 closed
48, 49			#4 position insignificant
50, 51, 52			#2 and #3 open produced better SPH, CYL-SPH and CYL with #1 closed

TABLE 10

BLOWER SUCTION CONCLUSIONS

FIGURES	CONCLUSION
53, 54, 55	15% MIN for SPH and CYL 20% MIN for CYL-SPH
56, 57, 58	20% MIN for SPH and CYL > 20% MIN for CYL-SPH
59, 60, 61	15% MIN for SPH and CYL 20% MIN for CYL-SPH
62, 63, 64	> 20% MIN for SPH and CYL 20% MIN for CYL-SPH
65, 66, 67	> 20% MIN for SPH, CYL-SPH and CYL
71, 72, 73	15% MIN for SPH and CYL 20% MIN for CYL-SPH
74, 75, 76	20% MIN for SPH > 20% MIN for CYL-SPH and CYL

TABLE 11

FAIRING NOSEPIECE CONCLUSIONS

FIGURES	CONCLUSION
77, 78, 79, 80, 81, 82, 83	TSN door position had insignificant effect on SPH, CYL-SPH and CYL
84, 85, 86	UCN better SPH, CYL-SPH and CYL

APPENDIX A

SUCTION DUCT VOLTAGE-TO-VELOCITY CONVERSION EQUATIONS

Second degree curve-fit equations were used to convert the propeller anemometer voltage into velocity in each suction duct. Note: X represents voltage in volts or millivolts and Y represents duct velocity in ft/sec.

Duct #1: $Y = -0.0806 \cdot X^2 + 6.9037 \cdot X + 2.4016$ (X in volts)

Duct #2: $Y = -3.9687E\text{-}04 \cdot X^2 + 2.8239E\text{-}01 \cdot X + 3.8530$ (X in mV)

Duct #3: $Y = -0.1146 \cdot X^2 + 7.0215 \cdot X + 2.1691$ (X in volts)

Duct #4: $Y = -0.1476 \cdot X^2 + 5.5755 \cdot X + 3.2969$ (X in volts)

Duct #5: $Y = -7.6316E\text{-}04 \cdot X^2 + 0.3341 \cdot X + 7.9236$ (X in mV)

APPENDIX B

PRESSURE COEFFICIENT CALCULATION

By definition the pressure coefficient C_p is

$$C_p = \frac{\Delta P}{q} = \frac{P - P_\infty}{q} ,$$

where P is the static pressure at the station in question, P_∞ is freestream static pressure and q is freestream dynamic pressure. Furthermore, $q = P_{impact} - P_\infty$ where P_{impact} is the freestream total pressure. Relating these to scanivalve port locations we have:

$$C_p = \frac{P - P_{14}}{P_{12} - P_{14}} .$$

For example, from Table 3 (Run #71) C_p at Port #19 (or the turret top) the pressure coefficient is

$$C_p = \frac{P_{19} - P_{14}}{P_{12} - P_{14}} = \frac{(-0.237) - (-0.112)}{(-0.046) - (-0.112)} = -1.89$$

It should be noted that the scanivalve output voltages contain a linear conversion factor which cancels, and hence the raw transducer voltages can be used to calculate C_p as illustrated.

LIST OF REFERENCES

1. Burd, James, Boundary Layer Control of a High Energy Laser Turret Using Suction of Trapped Vortices, M.S. Thesis, Naval Postgraduate School, Monterey, California, 1981.

2. Schonberger, James, Flow Control About an Airborne Laser Turret, M.S. Thesis, Naval Postgraduate School, Monterey, California, 1980.

3. Mandigo, Alan, Control of Airflow About a High Energy Laser Turret, M.S. Thesis, Naval Postgraduate School, Monterey, California, 1980.

4. Schlichting, Hermann, Boundary Layer Theory, 6th Edition, McGraw-Hill, 1968.

INITIAL DISTRIBUTION LIST

		No. Copies
1.	Defense Technical Information Center Cameron Station Alexandria, Virginia 22314	2
2.	Library, Code 0142 Naval Postgraduate School Monterey, California 93940	2
3.	Department Chairman, Code 67 Department of Aeronautics Naval Postgraduate School Monterey, California 93940	1
4.	Professor Allen E. Fuhs, Code 67Fu Department of Aeronautics Naval Postgraduate School Monterey, California 93940	4
5.	Lcdr. David A. Rippel 1302 - 39th St., N.W. Canton, Ohio 44709	2
6.	Lt. James E. Burd 3926 Corral Canyon Road Bonita, California 92002	1
7.	Capt. Richard deJonckheere AFWL/ARLB Kirtland Air Force Base Albuquerque, New Mexico 87177	10
8.	Lt. James Schonberger 1920 Catherine Drive Bismarck, North Dakota 58501	1
9.	Lt. Alan M. Mandigo 208 Dunning Drive Camillus, New York 13031	1
10.	Mr. Ralph Haslund M/S 8H-29 Boeing Aerospace Company P.O. Box 3999 Seattle, Washington 98124	1